HAL open science

Nature and coordination geometry of geologically relevant aqueous Uranium(VI) complexes up to 400 ºC: A review and new data

Alexander Kalintsev, Qiushi Guan, Joël Brugger, Artas Migdisov, Barbara Etschmann, Rahul Ram, Weihua Liu, Yuan Mei, Denis Testemale, Hongwu Xu

To cite this version:

Alexander Kalintsev, Qiushi Guan, Joël Brugger, Artas Migdisov, Barbara Etschmann, et al.. Nature and coordination geometry of geologically relevant aqueous Uranium(VI) complexes up to 400 ºC: A review and new data. Journal of Hazardous Materials, 2023, 452, pp.131309. 10.1016/j.jhazmat.2023.131309 . hal-04239591

HAL Id: hal-04239591

https://hal.science/hal-04239591v1

Submitted on 12 Oct 2023

HAL is a multi-disciplinary open access archive for the deposit and dissemination of scientific research documents, whether they are published or not. The documents may come from teaching and research institutions in France or abroad, or from public or private research centers.

L'archive ouverte pluridisciplinaire **HAL**, est destinée au dépôt et à la diffusion de documents scientifiques de niveau recherche, publiés ou non, émanant des établissements d'enseignement et de recherche français ou étrangers, des laboratoires publics ou privés.

Distributed under a Creative Commons Attribution - NonCommercial - NoDerivatives 4.0 International License

Journal of Hazardous Materials 452 (2023) 131309

Contents lists available at ScienceDirect

Journal of Hazardous Materials

journal homepage: www.elsevier.com/locate/jhazmat

Review

Nature and coordination geometry of geologically relevant aqueous Uranium(VI) complexes up to 400 °C: A review and new data

Alexander Kalintsev [a,b,*], Qiushi Guan [c], Joël Brugger [a], Artas Migdisov [b], Barbara Etschmann [a], Rahul Ram [a], Weihua Liu [c], Yuan Mei [c], Denis Testemale [d], Hongwu Xu [b]

[a] School of Earth, Atmosphere and Environment, Monash University, 9 Rainforest Walk, VIC 3800, Australia
[b] Los Alamos National Laboratory, Earth & Environmental Division, Los Alamos, NM, USA
[c] CSIRO Mineral Resources, Kensington, WA 6151, Australia
[d] CNRS, Université Grenoble Alpes, Institut NEEL, Grenoble F-38000, France

HIGHLIGHTS

- The first detailed review of uranium complex structure work has been conducted.
- Up to now, very little work has been conducted at temperatures above 25 °C.
- Overall coordination systematically decreases with temperature.
- Uranyl complexes exhibit no major structural changes up to 400 °C.
- We have verified recently derived thermodynamic data for uranyl complexes.

GRAPHICAL ABSTRACT

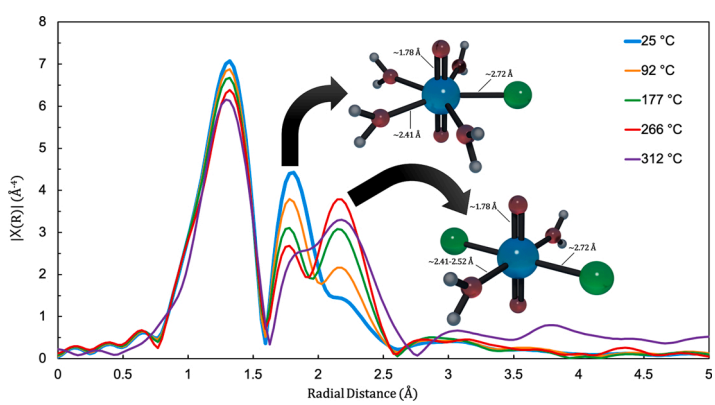

ARTICLE INFO

Editor: <Edward Burton>

Keywords:
Hydrothermal geochemistry
Aqueous uranium complexes
Nuclear waste
Chemical thermodynamics
X-ray absorption spectroscopy
EXAFS

ABSTRACT

The structure of the uranyl aqua ion (UO_2^{2+}) and a number of its inorganic complexes (specifically, UO_2Cl^+, $UO_2Cl_2^0$, $UO_2SO_4^0$, $UO_2(SO_4)_2^{2-}$, $UO_2(CO_3)_3^{4-}$ and $UO_2(OH)_4^{2-}$) have been characterised using X-Ray absorption spectroscopy/extended X-Ray absorption fine structure (XAS/EXAFS) at temperatures ranging from 25 to 326 °C. Results of ab initio molecular dynamics (MD) calculations are also reported for uranyl in chloride and sulfate-bearing fluids from 25 to 400 °C and 600 bar to 20 kilobar (kb). These results are reported alongside a comprehensive review of prior structural characterisation work with particular focus given to EXAFS works to provide a consistent and up-to-date view of the structure of these complexes under conditions relevant to U mobility in ore-forming systems and around high-grade nuclear waste repositories. Regarding reported EXAFS results, average equatorial coordination was found to decrease in uranyl and its sulfate and chloride complexes as temperature rose – the extent of this decrease differed between species and solution compositions but typically resulted in an equatorial coordination number of ~3–4 at temperatures above 200 °C. The $UO_2(CO_3)_3^{4-}$ complex was observed at temperatures from 25 to 247 °C and exhibited no major structural changes over this temperature

* Corresponding author at: School of Earth, Atmosphere and Environment, Monash University, 9 Rainforest Walk, VIC 3800, Australia.
E-mail address: alexander.kalintsev@monash.edu (A. Kalintsev).

https://doi.org/10.1016/j.jhazmat.2023.131309
Received 22 January 2023; Received in revised form 23 March 2023; Accepted 26 March 2023
Available online 28 March 2023
0304-3894/© 2023 The Author(s). Published by Elsevier B.V. This is an open access article under the CC BY-NC-ND license (http://creativecommons.org/licenses/by-nc-nd/4.0/).

range. $UO_2(OH)_4^{2-}$ exhibited only minor structural changes over a temperature range from 88 to 326 ºC and was suggested to manifest fivefold coordination with four hydroxyl molecules and one water molecule around its equator. Average coordination values derived from fits of the reported EXAFS data were compared to average coordination values calculated using the experimentally derived thermodynamic data for chloride complexes reported by Dargent et al. (2013) and Migdisov et al. (2018b), and for sulfate complexes reported by Alcorn et al. (2019) and Kalintsev et al. (2019). Sulfate EXAFS data were well described by available thermodynamic data, and chloride EXAFS data were described well by the thermodynamic data of Migdisov et al. (2018b), but not by the data of Dargent et al. (2013). The ab initio molecular dynamics calculations confirmed the trends in equatorial coordination observed with EXAFS and were also able to provide an insight into the effect of pressure in equatorial water coordination – for a given temperature, higher pressures appear to lead to a greater number of equatorially bound waters counteracting the temperature effect.

1. Introduction

Hydrothermal transport of uranium is a key process in the formation of a wide range of uranium ore deposits [12,145,32] and is also a concern when assessing the long-term environmental impact of containment breaches in geological nuclear waste repositories. Both of these environments form the bookends of the nuclear fuel cycle and as such are very much worth considering in a world seeking to move away from hydrocarbon-based energy infrastructure. Fluid temperatures in these systems generally range from 150 to 400 ºC. Although most repository designs are not expected to reach local rock temperatures above 100 ºC [103,130,65,80], models suggest that a few may exhibit local rock temperatures in excess of 200 ºC [107,168,23,54,64,65].

In hydrothermal systems uranium is at its most mobile in its hexavalent oxidation state – in this state U(VI) almost invariably covalently bonds with two oxygen atoms forming the uranyl (UO_2^{2+}) ion. The uranyl ion in turn may form a large variety of complexes with both organic and inorganic ligands, with chloride (Cl^-), sulfate (SO_4^{2-}), carbonate (CO_3^{2-}) and hydroxyl (OH^-) being among the most important in geological hydrothermal systems.

Thermodynamic modelling is an important tool for predicting the mode and efficiency of aqueous metal transport and deposition in complex ore-forming environments, or the magnitude of long-term environmental risks associated with radioactive waste repositories [130,138,31,66]. To model such systems accurately high-temperature thermodynamic properties (Gibbs free energies, entropies, enthalpies etc.) are required. Theoretically, these can be derived from extrapolations of room temperature properties e.g. Plyasunov, Grenthe ($year$) [128,141,142,150] but the accuracy of such extrapolations can be questionable as explored in Kalintsev et al. [82] and Kalintsev et al. [81]. Experimentally derived, molal properties for uranyl sulfate and chloride complexes have recently been reported for temperatures up to 250–350 ºC [112,2,34,82]. While data for uranyl sulfate complexes appear to be well constrained between [82] and [2], there exists significant disagreement regarding values for uranyl chloride complexes [111,33,34].

While recent advances have been made in experimentally determining above ambient temperature uranyl complex molal properties, very little recent work has been conducted to characterise the structures of these complexes at elevated temperatures. This is in stark contrast with the vast swathe of data available for ambient conditions obtained via numerous studies using a variety of analytical techniques such as ^{13}C and ^{17}O Nuclear Magnetic Resonance (NMR), High Energy X-Ray Scattering (HEXS), and X-Ray Absorption Spectroscopy (XAS) with XAS being the most widely used. Numerous computational works (typically Density functional theory (DFT) based) have also been conducted, often in support of experiments and often to constrain complex geometry. However, even among these computational efforts there is a generally paucity of work dedicated to temperatures beyond ambient.

Such studies are important to conduct as changes in metal complex structure can lead to somewhat unintuitive changes in speciation with temperature. Example cases of such behaviour are the chloride complexes of iron, manganese and cobalt where rising temperatures lead to their tetrahedrally coordinated tri- or tetra-chloride species superseding their octahedral monochloride species with the intermediate species predominating only under very specific conditions [154,157,16,99]. Such a 'skipping' behaviour can be difficult to recognise with Raman or UV-Vis potentially leading to erroneous elevated-temperature speciation models. Furthermore, standard thermodynamic property extrapolation models such as the Modified Ryzhenko Brzygalin (MRB) [133,143] or Helgeson-Kirkham-Flowers (HKF) [67,142] models are contingent upon the structural consistency of a given complex. A given complex will be defined by a set number of ligands and inner-shell water molecules (e.g. the uranyl ion UO_2^{2+} at room temperature may be more completely written as $UO_2(H_2O)_5^{2+}$ hence accounting for its five inner-shell equatorially bound waters) but if the number or arrangement of these inner shell molecules changes drastically enough then these extrapolation models cannot be used with confidence. Instead, these different 'isoligand complexes' have to be treated separately for the purposes of these models which necessitates the derivation of separate properties for each, which in turn presents experimental challenges.

Thus, when verifying molal properties derived for a particular complex over a range of temperatures and given the mutability of complex hydration with temperature it is wise to verify that no drastic changes occur in hydration as temperature rises to provide assurance that a given set of properties are valid for the temperature range they were collected for.

Coordination changes can also underpin the solubility characteristics of metals and their solids as in the case of the strongly retrograde solubility of zircon in fluoride-bearing fluids which is associated with a shift from octahedral to tetrahedral coordination [16,113]. With in situ experimental techniques such as XAS (coupled with appropriate spectroscopic cells) it is possible to clearly identify what species are controlling metal solubility at elevated temperatures and thus verify/inform the speciation models used by other techniques such as Raman or UV-Vis which are less suited to metal complex identification and structural characterisation. It should be noted that XAS has its weaknesses. The process of fitting data generally results in large (~10–20%) uncertainties in the number (coordination) of first shell atoms (i.e. the atoms of bonded ligands) and there is always a further measure of uncertainty in these values due to correlations between Debye Waller (DW) factors (a measure of thermal and structural disorder) and coordination numbers. However, this is why individual fitting parameter results are not interpreted in a vacuum. Major coordination changes are generally accompanied by significant bond length changes the precision of which is typically very high (generally on the order of 0.01–0.03 Å or ~<1%) in XAS data fits. Large coordination changes are also often associated with significant changes in the XANES region of XAS spectra. And further, even though the precision of coordination values may be low the trends identified as functions of temperature or solution composition are still valid and provide useful information. XAS data interpretations may further be augmented with computational work which all together help to clarify what at first may seem an unclear picture presented by the low precision of coordination numbers [83].

Table 1
Summary of experimental investigations on the structure of the hydrated uranyl ion. Debye Waller factors (σ2) are given for works using EXAFS. (f) denotes if parameters were fixed during fitting. The number of axial oxygen atoms was fixed in all fits to 2. All experiments were conducted at room temperature. The confidence of reported uncertainties is typically not discussed at all but can generally be assumed to be 1σ unless otherwise stated (C.I. – confidence interval).

Publication	Technique (s) used	Equatorial oxygen coordination	Distances (Å), σ^2 (Å^2)	Other notes
Aberg et al. [1]	X-Ray Diffraction ^{1}H NMR	4.9–4.3 ± 0.2	AxO - 1.702 ± 0.005 EqO - 2.421 ± 0.005	Investigation conducted on 1.014, 2.222 and 2.945 M $UO_2(HClO_4)_2$ solutions.
Allen et al. [4]	EXAFS	5.3 ± 0.3 (95% C.I.)	AxO – 1.76 ± 0.006 σ^2 = 0.0018 EqO – 2.41 ± 0.012 σ^2 = 0.0070 (fixed)	Measurements conducted in 0.1 M UO_2^{2+} solutions prepared from solid uranyl nitrate. E_0 = 17185 eV. Amplitude reduction factor (S_0^2) = 0.9. K-Space data range 1–13 Å^{-1}. Atypically large ΔE_0 values in their fits (−9.6 to 12.3).
Wahlgren et al. [164]	EXAFS	4.5 ± 0.4	AxO – 1.78 ± 0.005 σ^2 = 0.0015 EqO – 2.41 ± 0.01 σ^2 = 0.0062	0.05 M UO_2^{2+} in 0.1 M $HClO_4$. E_0 = 17185 eV. (S_0^2) = 1.0. K-Space data range 3–13.5 Å^{-1}. Additionally report theoretical quantum chemistry results.
Sémon et al. [137]	EXAFS	$HClO_4$ solutions 4.2 – 4.9 ± 10% - not systematic CF_3SO_3H solutions 4.7–4.5 ± 0.5 – weakly systematic	AxO – 1.75–1.76 ± 0.01 σ^2 = 0.0013 – 0.0021 EqO – 2.41–2.42 ± 0.02 σ^2 = 0.0013 – 0.0021	0.01 M UO_2^{2+} in 0.1–11.5 M $HClO_4$ √ 0.01 M UO_2^{2+} in 5–10 M CF_3SO_3H. E_0 = 17186 eV. (S_0^2) = 1.0. K-Space data range 2–13.0 Å^{-1}. Solid uranyl perchlorate samples were fit with 2 EqO distances of 2.36 and 2.47. σ^2 values for these paths were 0.003 and 0.004 respectively. Report results from quantum mechanical calculations of uranyl perchlorate, triflic and nitrate complexes in gas phase.
Neuefeind et al. [121]	X-Ray Scattering	5 with a small percentage of 4	AxO – 1.766 ± 0.001 EqO – 2.420 ± 0.001	0.5 mol/kg water UO_2^{2+} in 1 molal $HClO_4$.
Hennig et al. [70]	EXAFS	5.2 ± 0.78	AxO – 1.76 ± 0.02 σ^2 = 0.0014 EqO – 2.41 ± 0.02 σ^2 = 0.0075 (fixed)	0.01 M UO_2^{2+} in 0.1 M $HClO_4$.E_0 = 17185 eV. (S_0^2) = 0.9. K-Space data range 3.2–12.7 Å^{-1}.
Soderholm et al. [146]	HEXS	4.86 ± 0.07	AxO – 1.766 ± 0.001 EqO – 2.420 ± 0.001	0.5 molal UO_2^{2+} in dilute [sic] $HClO_4$. Hypothesise an equilibrium between 4 and 5 coordinated uranyl ions with 5 oxygens being favoured by 1.19 ± 0.42 kcal/mol (ratio of 5–4 coordinated between 3.8 and 16).
Hennig et al. [69]	EXAFS	5.2 ± 0.78	AxO – 1.76 ± 0.02 σ^2 = 0.0016 EqO – 2.41 ± 0.0071	0.01 M UO_2^{2+} in 0.1 M $HClO_4$. E_0 = 17185 eV. (S_0^2) = 1.0. K-Space data range 3.2–16.7 Å^{-1}. Results from quantum chemical calculations are also reported.
Ikeda-Ohno et al. [74]	EXAFS	5.0 ± 0.5	AxO – 1.77 ± 0.01 σ^2 = Not specified EqO = 2.40 ± 0.01 σ^2 = Not specified	0.04 M UO_2^{2+} in 1.0 M $HClO_4$. E_0 = 17185 eV. (S_0^2) = 0.9. K-Space data range 2.0–20.0 Å^{-1}. Results from DFT calculations are also reported.
Duvail et al. [43]	EXAFS, SWAXS	5.3 ± 0.5	AxO – 1.77 ± 0.01 σ^2 = 0.0018 EqO - 2.42 ± 0.01 σ^2 = 0.0080	0.01 M UO_2^{2+} in 0.2 M $HTcO_4$. E_0 = 17185 eV. (S_0^2) = 1.0. K-Space data range 1.7–16.9 Å^{-1}. Results from molecular dynamics simulations are also reported.

Uranyl and its complexes all share the same general structure. At their core the uranium atom bonds covalently with two oxygen atoms that reside at opposite poles along an axis, forming the linear uranyl moiety. These axial oxygen atoms almost invariably maintain a distance from the core uranium of about 1.77 Å in all uranyl complexes. The main exception to this may be found in monomeric uranyl hydroxyl complexes (discussed in the relevant section below). Coordinating water molecules or ligands bond around the equator of this uranyl molecule typically forming a pentagonal or hexagonal bipyramid structure. Bonding ligands typically substitute either one or two equatorial water molecules. Presently available above-ambient-temperature data suggest that as temperature increases the number of equatorial water molecules tends to decrease [135,153]. In complexes that contain no equatorially bound water (e.g. uranyl di-/tri-acetate or the uranyl citrate dimer),

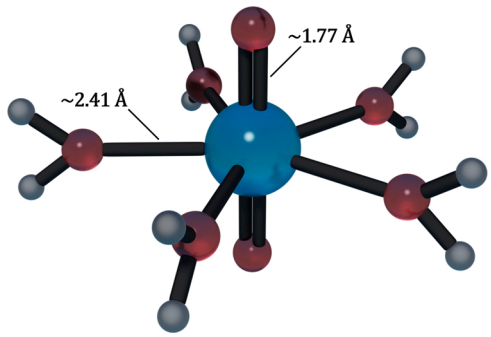

Fig. 1. A to-scale idealised depiction of the uranyl aqua ion. Uranium is blue, oxygen red and hydrogen grey.

their structure appears to undergo almost no change from room temperature to 250 °C [119,7,8].

The aim of this work was to conduct high temperature in situ XAS measurements to a) characterise uranyl and its chloride, sulfate, carbonate and hydroxyl complexes over a wide range of temperatures and identify trends in their coordination behaviour b) attempt to verify recently published thermodynamic data [112,2,34,82] by comparing measured and calculated solution speciation. XAS observations and data interpretations were supplemented with MD calculations which focussed on chloride and sulfate complexes up to temperatures of 400 °C and pressures up to 20 kbar. This work is additionally supported by an exhaustive review of prior studies on the structures of these complexes, and a summary of what little high temperature structural data are presently available for uranyl complexes in general. Focus has been placed on EXAFS studies, but mention is made of studies using other techniques when deemed particularly relevant. Brief summaries of prior computational studies are also reported.

1.1. The Uranyl aqua ion

A summary of investigations into the structure of the uranyl ion is presented in Table 1. All investigations reviewed were conducted at ambient conditions. Thanks to this significant body of work the structure of the uranyl ion has been well defined. Uranyl is typically studied in acidic solutions containing perchloric or trifluoromethanesulfonic (triflic) acid, both of which are incapable of forming complexes with uranyl even at extremely high (~10 M) concentrations [137]. Thus, these acids provide a means to create solutions that can dissolve concentrations of uranium measurable by XAS (concentrations above 5 mM are measurable but those around and above 100 mM are preferable) without risking the introduction of ligands such as chloride, sulfate or carbonate.

Invariably, the uranyl aqua ion comprises two axial oxo bonds at around 1.77 ± 0.01 Å and ~5 equatorially coordinated water molecules with average U-O distances of ~2.41 ± 0.01 Å. The generally accepted structure for the uranyl ion is shown in Fig. 1. To explain derived coordination values below 5 it has been suggested that there may exist a rapid equilibrium between 4 and 5 equatorial water molecules [146], however the overall contribution of tetragonal uranyl is likely minimal under ambient conditions.

The uranyl aqua ion has been the subject to a number of computational studies (e.g., [104,118,123,164,63]. Fivefold coordination has invariably been determined to be the most stable arrangement for the uranyl ion relative to four or six-fold structures, consistent with experimental studies. Calculated bond distances vary somewhat based on the specific technique used, but generally match experimental values within ± 0.05 Å. There has been at least one molecular dynamics study conducted for temperatures above 25 °C [102]. Simulations were carried out up to 200 °C and suggested that fivefold coordination is maintained up to those temperatures with no significant change in bond distances. More detailed reviews of theoretical work on the uranyl ion may be found in Bühl et al. [20] and Lynes et al. [104].

Table 2
Summary of experimental investigations into the structure of uranyl chloride complexes. All experiments were conducted at room temperature. NEqO refers to the number of equatorial oxygen atoms, NCl the number of the equatorial chloride atoms. Axial oxygen distances are not described here as they were practically identical across all fits and works, 1.78 ± 0.01 Å. The confidence of reported uncertainties is typically not discussed at all but can generally be assumed to be 1σ unless otherwise stated (C.I. – confidence interval).

Publication	Technique (s) used	Chloride concentration-NEqO - NCl // Respective distances (Å)	Other notes
Allen et al. [4]	EXAFS	1 M HCl – 5.0 – 0.3 // 2.41 – 2.71 2 M HCl – 4.8 – 0.4 // 2.41 – 2.72 4 M HCl – 3.9 – 1.0 // 2.41 – 2.71 6 M HCl – 3.1 – 1.5 // 2.44 – 2.73 8 M HCl – 2.7 – 1.8 // 2.48 – 2.73 10 M HCl – 2.50 – 2.0 // 2.50 – 2.73 12 M LiCl – 2.2 – 2.2 // 2.51 – 2.73 14 M LiCl – 1.9 – 2.6 // 2.52 – 2.73	Measurements conducted on solutions containing 0.1 M O_2^{2+}. E_0 = 17185 eV. Amplitude reduction factor (S_0^2) = 0.9. K-Space data range 1–13 Å^{-1}. Atypically large ΔE_0 values in their fits (−9.6 to −12.3). Uncertainties in NEqO and NCl are ± 0.3. (95% C.I.) Uncertainties in distances for both are ± 0.012. Debye Waller factors σ^2 were fixed to 0.0070 for EqO and 0.0050 for EqCl.
Hennig et al. [70]	EXAFS	3 M Cl^- – 3.9 – 1.0 // 2.41 – 2.73 6 M Cl^- - 1.7 – 2.3 // 2.42 – 2.73 9 M Cl^- - 1.4 – 2.7 // 2.51 – 2.74	0.01 M UO_2^{2+} in 0.1 M *HCl* with chloride added as *LiCl*. E_0 = 17185 eV. (S_0^2) = 0.9. K-Space data range 3.2–12.7 Å^{-1}. Uncertainties in NEqO and NCl are ± 15% (0.6–0.2). Uncertainties in distances for both are ± 0.02. The Debye Waller factors σ^2 for EqO and EqCl were fixed to 0.0075 and 0.0050 Å^2 respectively.
Soderholm et al.[147]	HEXS	2.5 m Cl^- - 4.2 – 1.0 // 2.40 – 2.72 3.0 m Cl^- - 3.7 – 1.4 // 2.40 – 2.72 3.5 m Cl^- - 3.5 – 1.5 // 2.40 – 2.72 4.0 m Cl^- - 2.9 – 1.8 // 2.41 – 2.72 4.5 m Cl^- - 2.5 – 2.0 // 2.41 – 2.72 5.0 m Cl^- - 2.2 – 2.1 // 2.41 – 2.72 5.5 m Cl^- - 2.0 – 2.3 // 2.42 – 2.72 6.0 m Cl^- - 1.7 – 2.6 // 2.41 – 2.72 6.5 m Cl^- - 1.8 – 2.6 // 2.41 – 2.72	Measurements conducted on solutions containing 0.5 m UO_2^{2+} with chloride added as HCl. Uncertainties for both EqO and EqCl are ± 0.02 for their distances and ± 0.1 for their coordination. The confidence interval for these uncertainties is 3-sigma in both cases.

1.2. Uranyl chloride complexes

The results from previous experimental studies on the structure of uranyl chloride complexes are summarised in Table 2. All investigations reviewed were conducted at ambient conditions. In uranyl chloride

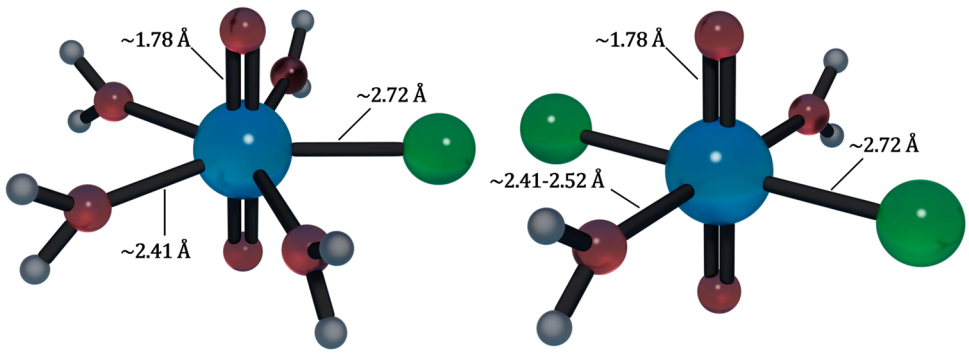

Fig. 2. To-scale idealised depictions of uranyl chloride complexes. Structures are based on the DFT calculations of Bühl et al. [20]. Note that the dichloride complex may contain either two or three equatorial water molecules, and both cis- and trans-configurations are expected to co-exist as they have very similar free energies. Here we show an example of the tetragonally coordinated trans form. Uranium is blue, oxygen red, chlorine green and hydrogen grey.

complexes chloride ions substitute for equatorial water molecules and remain on the equatorial plane. Axial oxygen distances remain at around 1.78 ± 0.01 Å regardless of the concentration of chloride in solution. According to EXAFS studies equatorial oxygen distances appear to be sensitive to solution chloride concentration with variation from 2.41 Å to 2.52 Å as chloride concentrations increase and the average number of bonded chloride ions changes from ≤1 to ≥2; however such variation was not observed with HEXS (2.41 ± 0.01 Å; [147]) despite similar chloride concentration ranges being explored with both techniques. Both techniques however agree that regardless of chloride concentration the uranyl-chloride bond distance remains at a constant 2.72 ± 0.01 Å distance. Idealised structures for the monochloride (UO_2Cl^+) and dichloride ($UO_2Cl_2^0$) complexes are shown in Fig. 2.

All experimental work suggests that the monochloride complex UO_2Cl^+ maintains fivefold coordination with the equator hosting four water molecules and a single chloride ion. This fivefold configuration is further supported by the computational work of Soderholm et al. [147]. It was noted in experimental work that as the average number of equatorial chloride ions approached 2 the number of equatorially coordinated waters approached 2–2.5 suggesting a mix of fivefold (pentagonal bipyramid) and fourfold (tetragonal bipyramid) arrangements are possible for the dichloride $UO_2Cl_2^0$ complex. Based on trends observed in these prior works it seems likely that the trichloride complex $UO_2Cl_3^-$ is fourfold coordinated though no study has managed to produce a solution solely predominant in this complex. The computational work of Bühl et al. [20] suggests a tetragonal arrangement for both the dichloride and trichloride complexes; it also suggests that the cis- and trans-isomers of these two complexes have very similar free energies; hence Fig. 2 shows the trans-form selected by Bühl et al. [20].

There is a discrepancy between the average chloride and oxygen coordinations reported by Allen et al. [4] and those reported by Hennig et al. [70] and Soderholm et al. [147]. This discrepancy is most obvious at 6.0 M total chloride. The latter two studies both match each other within uncertainty and suggest a predominance of $UO_2Cl_2^0$ with a minor contribution from $UO_2Cl_3^-$, whereas the older study suggests a 50/50 contribution of UO_2Cl^+ and $UO_2Cl_2^0$. We suggest that this discrepancy may simply be due to inappropriate threshold energy choice (E_0) used during fitting by Allen et al. [4]. This choice is suggested by the reporting of anomalously large ΔE_0 values ranging from − 9.6 to − 12.3. Such large values can lead to fits producing erroneous but still reasonable appearing coordination values – this effect is discussed in detail by Kelly and Ravel [85]. Regardless, the coordination reported for the pure species by Allen et al. [4] align well with all subsequent experimental and computational studies i.e. pentagonal for UO_2Cl^+ and tetragonal for $UO_2Cl_2^0$.

1.3. Uranyl sulfate complexes

Key experimental studies on the structure of uranyl sulfate complexes are summarised in Table 3. All investigations reviewed were conducted at ambient conditions. The monosulfate $UO_2SO_4^0$ and disulfate $UO_2(SO_4)_2^{2-}$ complexes have been the main focus of structural studies though, based on our speciation calculations, Hennig et al. [68] may have partly characterised the trisulfate $UO_2(SO_4)_3^{4-}$ complex in their HEXS study. Sulfate ligands bond on the uranyl equatorial plane and may substitute either one (as a monodentate bond) or two (bidentate) water molecules with computational work suggesting the bidentate arrangement to be slightly (<20 kJ/mol) more energetically favourable [161,30,69]. Computational and experimental work suggest that all three major sulfate complexes maintain fivefold equatorial coordination.

Axial oxygen distances remain similar to the pure uranyl ion regardless of species at around 1.78 ± 0.01 Å. Equatorial oxygen distances vary depending on whether a single or two shell approach is used during fitting. In single shell approaches U-EqO distances have been found to be ~2.41 Å – identical to pure uranyl. In two shell models U-EqO distances may be split into two populations one at ~2.35 Å and another at ~2.48 Å corresponding to water oxygens. These two distinct oxygen distances are also observed in DFT models [161], however works utilising HEXS were apparently unable to distinguish the two and only report a single oxygen distance of ~2.41 Å.

U-S distances vary between monodentate and bidentate bonding arrangements. EXAFS work suggests that in monodentate arrangements U-S distances are around 3.56 ± 0.01 Å with similar distances (~3.58 ± 0.01) being measured in synthetic potassium zippeite ($K(UO_2)_2SO_4(OH)_3H_2O$) using both EXAFS and XRD [69,163]. HEXS work however seems to suggest a greater distance of ~3.67–3.69 Å. The reason for this discrepancy between EXAFS and HEXS of aqueous monodentate sulfate is not clear but interference from other atomic paths (namely the three main multiple scattering U-$O_{(ax)}$ paths which have a mean path distance of ~3.55 Å) and the fact that pure monosulfate solutions were not measured by the works that identified monodentate sulfate may together have led to the fitting of shorter bond distances in the EXAFS-based studies.

For the bidentate sulfate complex, good agreement exists across all works regardless of technique for the U-S distance, which has been determined to be 3.11 ± 0.01 Å.

While there exists general agreement that the uranyl disulfate complex $UO_2(SO_4)_2^{2-}$ contains two bidentate sulfate ions, the bonding behaviour of sulfate in $UO_2SO_4^0$ is somewhat less clear. Moll et al. [115] provides the only investigation of a solution in which the monosulfate complex is predominant (~82%), and was able to adequately describe its EXAFS spectra using a model implying solely bidentate sulfate.

Table 3
Summary of experimental investigations into the structure of uranyl sulfate complexes. All experiments were conducted at room temperature. NEqO refers to the number of equatorial oxygen atoms, NS the number of the equatorial sulfur atoms (and by extension the number of bonding sulfate molecules). For ease of presentation DW factors have been multiplied by 10^3. (f) denotes a value was fixed. Axial oxygen distances are not listed here as they were practically identical across all fits and works, 1.78 ± 0.01 Å. The confidence of reported uncertainties is typically not discussed at all but can generally be assumed to be 1σ unless otherwise stated (C.I. – confidence interval).

Publication	Technique (s) used	Solution ID-NEqO - NS // Respective distances (Å) // respective Debye-Waller factors (Å^2)	Other notes

Moll et al. [115]	EXAFS
	^{17}O NMR
		A – 5.0 – 1(f) // 2.41 – 3.11(f) // 8.4 – 10.5
		B – 5.0 – 1(f) // 2.40 – 3.14 // 8.2 – 8.6
		C – 5.0 – 2.2 // 2.43 – 3.11 // 10.7 – 7.5
		D – 5.0 – 2.1 // 2.43 – 3.10 // 11.9 – 7.2
			Measurements conducted on solutions containing 0.05 M UO_2^{2+}. In samples A and B sulfate was introduced solely as H_2SO_4. In sample C and D it was introduced solely as Na_2SO_4. pH was adjusted using $NaClO_4$, though $NaOH$ was added to sample D. E_0 = 17185 eV. Amplitude reduction factor (S_0^2) = 0.9. K-Space data range 2.5–17.8 Å^{-1}. △E_0 was fixed to − 7.0 eV, fixing this value is somewhat atypical. Its magnitude is also somewhat high though not entirely unacceptable. Uncertainties in NEqO and NS are ± 0.4 and ± 0.5 when not fixed. Uncertainties in distances for both are ± 0.012. Solution speciation was provided by the paper: A - 0.5 M H_2SO_4 // 12% UO_2^{2+} **82% $UO_2SO_4^0$**; B – 10 M H_2SO_4 //**50% $UO_2SO_4^0$ 50% $UO_2(SO_4)_2^{2-}$**; C - 0.5 M Na_2SO_4 pH 2.00 // **88% $UO_2(SO_4)_2^{2-}$**; D – 1 M Na_2SO_4 pH 5.25 – mix of hydroxyl sulfate ternary species.

Neuefeind et al. [120]	HEXS	2.42 Å response identified as EqO. 3.67 Å response identified as monodentate sulfate.	Measurements conducted on a solution containing 0.5 molal UO_2^{2+} with 0.5 m H_2SO_4 – our calculations suggest a uranyl speciation distribution of 28% UO_2^{2+}, **46% $UO_2SO_4^0$**, 18% $UO_2(SO_4)_2^{2-}$.
Hennig et al. [69]	EXAFS	B – 2.5/2.1 – 0.6 // 2.35/2.47 – 3.09 C – 2.4/2.2 – 1.6 // 2.35/2.48 – 3.11 D – 2.4/2.5 – 1.9 // 2.35/2.49 – 3.12 E – 2.5/2.4 – 2.0 // 2.35/2.49 – 3.12 F – 4.4/1.4 – 0.3/0.6 // 2.39/2.51 – 3.11/3.57 // 7.3/7.3 – 6.0(f)/9.0 (f) G – 4.2/0.8 – 0.3/0.5 // 2.39/2.50 – 3.07/3.56 // 7.6/7.6 – 6.0(f)/9.0 (f)	Solutions comprised 0.05 M (B,C,D,E,G) or 0.5 M (F) U and varying concentrations of H_2SO_4 and $(NH_4)_2SO_4$. E_0 = 17185 eV. Amplitude reduction factor (S_0^2) = 1.0. K-Space data range 3.2–16.7 Å^{-1}. Uncertainties in N are ± 15%, Distance uncertainties are ± 0.02 Å. DW factors for EqO and S were fixed for compositions B-E to 0.0055 and 0.0060 respectively. Two equatorial oxygen distances were used in all fits. For compositions F and G two sulfate distances were described. Speciation was provided by the paper: B – 16% UO_2^{2+} 27% $UO_2SO_4^0$ **54% $UO_2(SO_4)_2^{2-}$** 3% $UO_2(SO_4)_3^{4-}$; C - 3% UO_2^{2+} 19% $UO_2SO_4^0$ **75% $UO_2(SO_4)_2^{2-}$** 2% $UO_2(SO_4)_3^{4-}$; D - 2% UO_2^{2+} 21% $UO_2SO_4^0$ **76% $UO_2(SO_4)_2^{2-}$**; E - 21% $UO_2SO_4^0$ **76% $UO_2(SO_4)_2^{2-}$**; F - **38% UO_2^{2+}** 31% $UO_2SO_4^0$ 30% $UO_2(SO_4)_2^{2-}$; G - **43% UO_2^{2+}** 40% $UO_2SO_4^0$ 16% $UO_2(SO_4)_2^{2-}$.
Hennig et al. [68]	HEXS	EqO – 2.41 Å S(Bidentate) – 3.12 Å S(monodentate) – 3.69 Å These values were identical for both solutions	Two solution compositions were investigated; however, the form of sulfate is unclear, H_2SO_4 and $(NH_4)_2SO_4$ were both mentioned as mean of introducing it into solution but the exact quantities used are unclear: D - 0.46 M U, 0.49 M SO_4^{2-}; E - 0.46 M U, 3.45 M SO_4^{2-}. Solution speciation was calculated by us as it was not provided by the original reference. It was surmised that uranyl was introduced as UO_3 and sulfate solely via H_2SO_4 for D and a mix of 0.46 M H_2SO_4 and 3 M $(NH_4)_2SO_4$ for E. D - 26% UO_2^{2+} **50% $UO_2SO_4^0$** 17% $UO_2(SO_4)_2^{2-}$;

(continued on next page)

Table 3 (*continued*)

Publication	Technique (s) used	Solution ID-NEqO - NS // Respective distances (Å) // respective Debye-Waller factors (Å^2)	Other notes
			E - 20% UO_2^{2+} 17% $UO_2SO_4^0$ 17% $UO_2(SO_4)_2^{2-}$ **44%** $\boldsymbol{UO_2(SO_4)_3^{4-}}$.

Subsequent works however have only investigated solutions with a maximum of ~50% $UO_2SO_4^0$, making it difficult to determine whether apparent bidentate responses are solely from co-present $UO_2(SO_4)_2^{2-}$ or if the solution contains a mix of monodentate and bidentate $UO_2SO_4^0$. The HEXS studies of Neuefeind et al. [120] and Hennig et al. [68] both investigated solutions with practically identical speciation containing ~ 50% $UO_2SO_4^0$. Yet, Neuefeind et al. [120] only identified a 3.67 Å monodentate response, while Hennig et al. [68] were able to identify 3.11 Å and 3.67 Å responses corresponding to both bidentate and

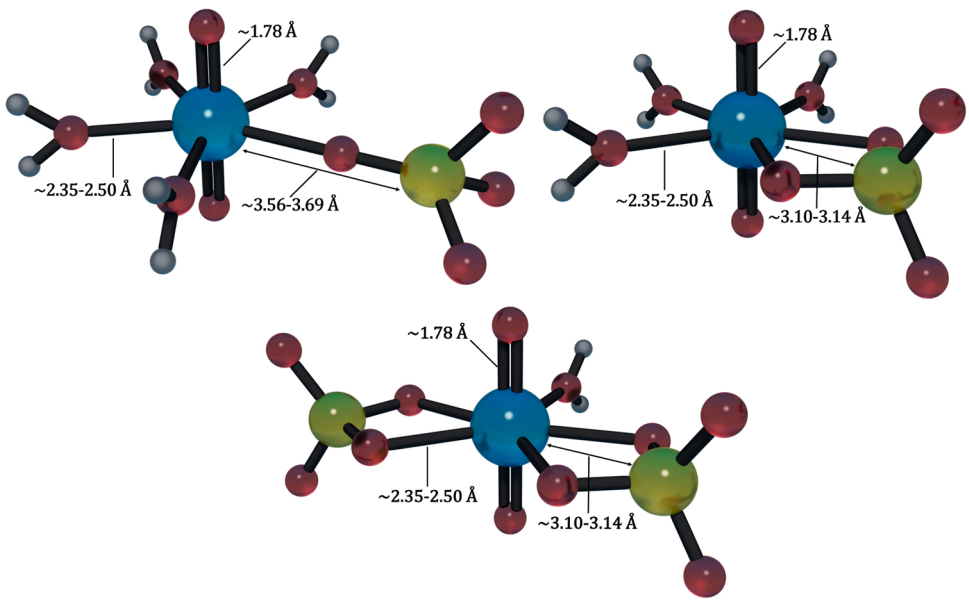

Fig. 3. To-scale idealised depictions of uranyl sulfate complexes. Structures are based on the DFT calculations of Hennig et al. [69]. Note how the monosulfate complex may contain either a monodentate or bidentate sulfate ion and how the U-S distance significantly differs between the two arrangements. Uranium is blue, oxygen red, sulfur yellow and hydrogen grey.

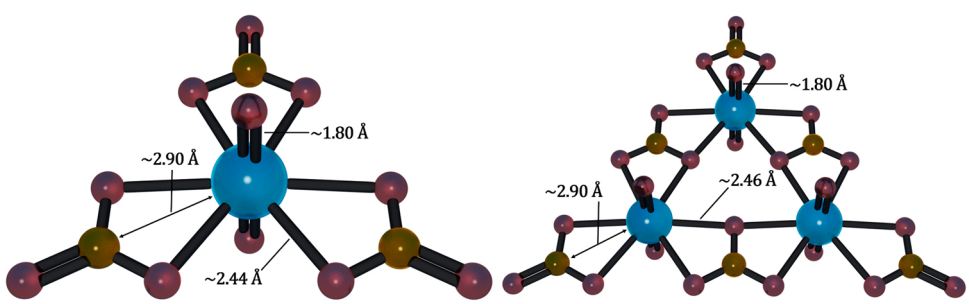

Fig. 4. To-scale idealised depictions of uranyl carbonate complexes, $UO_2(CO_3)_3^{4-}$ on the left and $(UO_2)_3(CO_3)_6^{6-}$ on the right. Structures are based on those calculated by [106]. Uranium is blue, oxygen red and carbon orange.

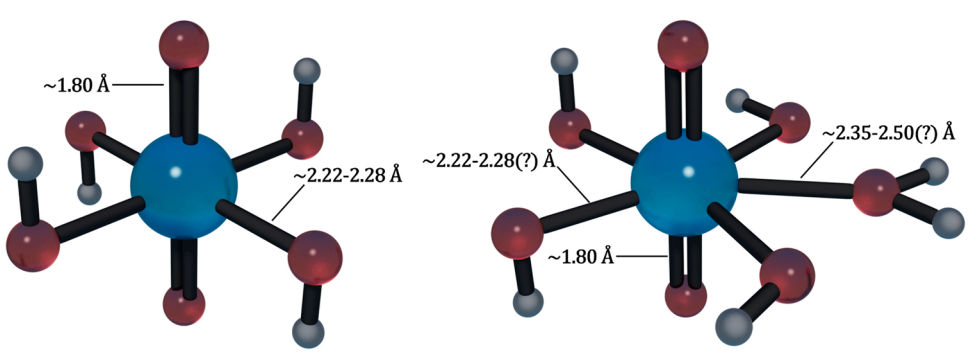

Fig. 5. Two likely structures of the 1,4 uranyl hydroxyl complex. Structure for the pure 1,4 is based on the calculated geometry of Ingram et al. [76]. Structure for the fivefold coordinated 1,4-H_2O complex is based upon gas phase calculations reported by Vallet et al. [162]. Note that bonded hydroxyls may occupy a number of different orientations and permutations of such – the orientations shown here are merely one example of many possibilities. Uranium is blue, oxygen red and hydrogen grey.

Table 4
Summary of experimental XAS structural studies on aqueous uranyl carbonate complexes and some of their solid analogues. Axial oxygen distances are consistently around 1.80 ± 0.02 in all studies. Parameters are reported for 3 main bonds/scatter paths, U-O(carbonate), U-C(carbonate) and U-O(distal carbonate) in that order. Values are reported for coordination (N), distance/path length (r(Å)) and Debye-Waller (DW) factors (σ^2(Å^2 ×10^3)). DW factors are multiplied by 10^3 for ease of presentation. The confidence of reported uncertainties is typically not discussed at all but can generally be assumed to be 1σ unless otherwise stated.

Publication	Technique (s) used	Path parameters. Coordination (N), Bond length (r, Å) and Debye-Waller factors (×10^3 Å^2). Uncertainties in brackets where reported.	Other notes
Allen et al. [3]	EXAFS NMR XRD Raman	$K_4[UO_2(CO_3)_3]$(s) N-6–3–3 (All fixed) r-2.42–2.89–4.12 σ^2-5.9–3.0–5.6 $(UO_2)_3(CO_3)_6^{6-}$ (aq) N-6–3–3 (All fixed) r-2.46–2.90–4.17 σ^2-7.5–3.9–5.6	Measurements conducted on a solid analogue equivalent of $UO_2(CO)_3^{4-}$ namely $K_4[UO_2(CO_3)_3]$, a solution containing 0.2 M U at pH 5.7 comprising at least 99% $(UO_2)_3(CO_3)_6^{6-}$ and solid $[C(NH_2)_3]_6[(UO_2)_3(CO_3)_6]$. Derived distance parameters were identical for the latter two. E_0 value used during fits was not provided. Amplitude reduction factor (S_0^2) was also not reported. K-Space data range 2.5–12.5 Å^{-1}. Coordination numbers were fixed for all fits. Uncertainties for distances do not seem to have been reported.
Docrat et al.[37]	EXAFS	$UO_2(CO_3)_3^{4-}$ N-6–3–3 (All fixed) r-2.43(2)– 2.89 (4)– 4.13(4) σ^2-14–7–13	Measurements conducted on a solution containing 10 mM U and 1 M Na_2CO_3 at a pH of 11.95. Solution comprised of 99% $UO_2(CO_3)_3^{4-}$. E_0 value used during fits was not provided. Amplitude reduction factor (S_0^2) was also not reported. K-Space data range 3–16 Å^{-1}. Coordination numbers were fixed for all paths.
Ikeda et al. [73]	EXAFS	$UO_2(CO_3)_3^{4-}$ N-6–3–3 (All fixed) r-2.44–2.92–4.17 σ^2-5.9–3.0–3.0	Measurements conducted on a solution containing 50 mM U with 1.4 M Na_2CO_3 at pH 11.9. E_0 = 17185 eV. Amplitude reduction factor (S_0^2) = 0.9. K-Space data range 2–20 Å^{-1}. Uncertainties in all distances are ± 0.01 Å. Coordination numbers were fixed for all paths.

monodentate sulfate bonding patterns. Similarly confusing interpretations are found in the EXAFS results of Hennig et al. [69]; two of their solutions contained ~30% $UO_2SO_4^0$ (though with differing proportions of other species due to differing solution compositions), yet the fit for one (Solution B) suggested the sole presence of bidentate sulfate whereas the fit for the other (Solution F) suggested the presence of both monodentate and bidentate sulfate. Little clarification may be found in works utilising vibrational spectroscopy. The Raman spectroscopy study of Nguyen-Trung et al. [122] solely suggests bidentate coordination for the monosulfate complex, whereas the infrared spectroscopy study of Gál et al. [51] solely identifies monodentate coordination.

We suggest that the reason for this apparent lack of consistency is the very small (<20 kJ/mol) difference in Free energy between the bidentate and monodentate coordination modes. A similarly small (~6 kJ/mol) energy difference between mondentate and bidentate coordination modes was calculated for the yttrium monosulfate ($Y(SO_4)^+$) complex by Guan et al. [57]. Such a small energy difference likely makes equilibria between the two configurations highly sensitive to solvent effects and perhaps even the analytical technique used – the high intensity X-Rays used in XAS for instance are known to induce water radiolysis and redox changes [108]. Given the variety of solution compositions investigated and experimental techniques utilised, a sensitivity to such factors could explain the corresponding variety in coordination mode interpretations.(Fig. 3, Fig. 4 and Fig. 5).

1.4. Uranyl carbonate complexes

Uranyl may form a variety of ternary carbonate complexes particularly with divalent alkaline earths (e.g. Mg, Ca, Sr) and hydroxyl anions [15,160,38,39,55,59,60,77,78,84,86,95–97]. For the sake of brevity and relevance to hydrothermal conditions (where ternary complexes are regarded as generally less stable than simple binary complexes; [77,78], we will solely focus upon binary uranyl carbonate complexes.

Major works on the structure of binary uranyl carbonate complexes are reported in Table 4. All investigations reviewed were conducted at ambient conditions. It is difficult to produce solutions solely predominant in the monocarbonate $UO_2CO_3^0$ or dicarbonate $UO_2(CO_3)_2^{2-}$ complexes, so all EXAFS studies to date have focussed on the tricarbonate $UO_2(CO_3)_3^{4-}$ and/or the trinuclear hexacarbonate $(UO_2)_3(CO_3)_6^{6-}$ complexes, sometimes referred to as the triscarbonato or hexakiscarbonato complexes respectively. We will refer to the two as the tricarbonate and trimeric carbonate complexes respectively.

Experimental works suggest that carbonate bonds invariably in a bidentate fashion around the uranyl equator. Hence the tricarbonate and trimeric complexes have been suggested to manifest six-fold equatorial coordination. However, it is worth noting that all prior EXAFS fits reviewed here have explicitly fixed the number of equatorial oxygen atoms to six, hence forcing three bidentate carbonate bonds. These fixed models were supported by comparison with the structures of a number of solid analogues; for example Allen et al. [3] used $[C(NH_2)_3]_6[(UO_2)_3(CO_3)_6]$. Similar sixfold coordination is also found in cejkaite ($(Na_4(UO_2)(CO_3)_3)$ [127], agricolite ($K_4(UO_2)(CO_3)_3$) [144] and rutherfordine (UO_2CO_3) [47].

The presence of six-fold coordination for the tricarbonate and trimeric carbonate complexes is supported by an abundance of computational work [105,106,118,134,158,160,36,49,56,6,73,91]. Most of these studies are based on static geometry optimisation in vacuum or in dielectric media though the works of Tirler and Hofer [158], Marchenko et al. [106] and Moreno Martinez et al. [118] employed molecular dynamics simulations and explicitly accounted for water molecules in the solvent. The earlier two works suggested that fivefold coordination may in fact be favoured with one carbonate ion bonding monodentately in the tricarbonate complex however, the latter work supports the six-fold coordination model.

The static geometry optimisation works of [36,105] suggest that carbonate is solely bonded bidentately in both the monocarbonate $UO_2CO_3^0$ and dicarbonate $UO_2(CO_3)_2^{2-}$ complexes. To our knowledge no EXAFS or similar structural verification of these models has been conducted.

Bonding distances in uranyl tricarbonate and the trimeric carbonate complexes are well established experimentally. Equatorial U-O(carbonate) bond lengths are agreed to be ~2.43 ± 0.02 Å, only slightly longer than the bonds lengths of equatorial waters in the uranyl aqua ion

Table 5
Summary of key structural investigations of uranyl hydroxyl complexes. Structural parameters are listed for both axial and equatorial oxygen bonds and appear in that order. In the cases of [116] and [159], who studied solutions containing polynuclear hydroxyl complexes, parameters for the U-U scattering path are also listed. Parameters that were fixed during fitting are denoted with (f). The confidence of reported uncertainties is typically not discussed at all but can generally be assumed to be 1σ unless otherwise stated.

Publication	Technique (s) used	Parameters - Coordination (N), Bond length (r, Å) and Debye-Waller factors ($\times 10^3$ Å^2)	Other notes
Clark et al.[27]	EXAFS	3.5 M TMA-OH solution N-2(f)– 5.3(5) r-1.79(1)– 2.22(1) σ^2-1.7–3.7 Solid $[Co(NH_3)_6]_2[UO_2(OH)_4]_3$N-2(f)– 3.9(5) r-1.81(1)– 2.21(1) σ^2-2.0–4.3	Measurements conducted on a 3.5 M tetramethylammonium hydroxide (TMA-OH). solution containing ~0.1 M U and a solid analogue of $UO_2(OH)_4^{2-}$; $[Co(NH_3)_6]_2[UO_2(OH)_4]_3$. E_0 value used during fits was not provided. Amplitude reduction factor (S_0^2) was set to 0.8. K-Space data range 3.00–11.70 Å^{-1}. Fourier transform of reported data shows only a single wide peak instead of the usual 2 distinct peaks visible in FT of non-complexed uranyl spectra. Solution was interpreted to be predominant in $UO_2(OH)_5^{3-}$.
Wahlgren et al. [164]	EXAFS	1 M TMA-OH N-2(f)– 5.0(5) r-1.82(1)– 2.24(1) σ^2-1.5–5.6 3 M TMA-OH N-2(f)– 5.3(5) r-1.82(1)– 2.24(1) σ^2-1.4–5.5	Measurements conducted on two solutions of 1 and 3 M TMA-OH. Both contained 0.055 M U. E_0 = 17,185 eV. Amplitude reduction factor (S_0^2) was set to 1.0. K-Space data range 3.8–15.1 Å^{-1}. Authors suggest despite observed fivefold coordination the predominant species is $UO_2(OH)_4^{2-}$.
Moll et al. [116]	EXAFS ^{17}O NMR	A - 0.05 M TMA-OH (pH 4.1) N-2.2(3)– 5.5(6)– 1.4(4) r-1.79(1)– 2.41(1)– 3.80(1) σ^2-1.2–11.4–5.7 C - 0.5 M TMA-OH (pH 13.7) N-1.8(3)– 4.2(6) r-1.83(1)– 2.26(1) σ^2-1.0–4.6 D - 3.0 M TMA-OH (Re-evaluation of data from Wahlgren et al.[164]. N-1.8(3)– 4.6(6) r-1.83(1)– 2.24(1) σ^2-1.0–4.3	Measurements conducted on solutions containing 0.05 M U and varying concentrations of TMA-OH E_0 = 17,185 eV. Amplitude reduction factor (S_0^2) was set to 0.8. K-Space data range 2.5–15/17 Å^{-1}. Solution speciation for solutions A and C were reported in the work. D was presumed to be predominated by $UO_2(OH)_4^{2-}$ with a possible minor contribution of $UO_2(OH)_5^{3-}$. A – 10% UO_2^{2+}, 30% $(UO_2)_2(OH)_2^{2+}$, 60% $(\boldsymbol{UO_2})_3(\boldsymbol{OH})_5^{+}$. C – 100% $\boldsymbol{UO_2(OH)_4^{2-}}$.
Tsushima et al. [159]	EXAFS FTIR UV-Vis	P1– pH 2.98 N-2(f)– 5.0(6)– 0.5(2) r-1.770(2)– 2.412(7)– 3.88(2) σ^2-1.2–10–6(f) P2 - pH 4.04 N-2(f)– 5.3(5)– 0.7(1) r-1.771(1)– 2.408(6)– 3.82(1) σ^2-1.51–13–6(f) P3 - pH 3.96 N-2(f)– 5.3(4)– 0.7(2) r-1.766(1)– 2.407(5)– 3.83(1) σ^2-1.46–10.7–6(f) P4 - pH 4.22 N-2(f)– 4.6(4)– 0.5(2) r-1.769(2)– 2.410(5)– 3.83(2) σ^2-1.4–10–6(f)	Measurements were conducted on solutions containing variable concentrations of U and TMA-OH. U was introduced as $O_2(NO_3)_2$. E_0 = 17,185 eV. Amplitude reduction factor was not provided. K-Space data range 3.1–14.7 Å^{-1} for P1-P3, 3,1–12.5 Å^{-1} for P4. 4 Solutions were studied: P1 – 534 mM U, 0.39 M TMA-OH – pH 2.98; P2 – 47 mM U, 50 mM TMA-OH – pH 4.04; P3 – 17 mM U, 5 mM TMA-OH – pH 3.96; P4 – 4 mM U, 5 mM TMA-OH – pH 4.22. Exact speciation was not provided but predominant species were given as: P1 - $(UO_2)_2(OH)_2^{2+}$; P2 - $(UO_2)_2(OH)_2^{2+}$ + $(UO_2)_3(OH)_5^{+}$ + minor UO_2^{2+}; P3 - $(UO_2)_2(OH)_2^{2+}$ + $(UO_2)_3(OH)_5^{+}$ + UO_2^{2+}; P4 - $(UO_2)_3(OH)_5^{+}$ + minor UO_2^{2+}.
Moll et al. [117]	EXAFS	N-2(f)– 4(f) r-1.82(1)– 2.28(1) σ^2-1.4–4.2	Measurements were conducted on solutions containing 50–100 mM U and 1.0–3.5 M TMA-OH. Some solutions used methanol as a medium. E_0 not provided. Amplitude reduction factor (S_0^2) not provided. K-Space data range ~2.5–17 Å^{-1}. Solution compositions were reported as below: S1 – 50 mM U – 1.0 M TMA-OH – Water; S2 – 50 mM U – 3.0 M TMA-OH – Methanol; S3 – 50 mM U – 3.5 M TMA-OH – Methanol; S4 – 100 mM U – 3.0 M TMA-OH – Water; S5 – 50 mM U – 3.0 M TMA-OH –Methanol. Despite the variety of solution compositions all derived bond properties were practically identical. S1 was likely predominant in $UO_2(OH)_4^{2-}$. The authors suggest that the other solutions were predominant in $UO_3(OH)_3^{3-}$ and/or binary uranyl-methanol-hydroxyl complexes.

(2.41 Å). U-C(carbonate) bond lengths lie around 2.89–2.92 Å. Another distance often measured is that between the core uranium and distal carbonate oxygens – this is agreed to be around 4.13–4.17 Å.

1.5. Uranyl hydroxyl complexes

Uranyl may form a wide variety of binary, ternary, polymeric, polynuclear and polymetallic complexes with the hydroxyl ion. A detailed review of this great variety is provided by Knope and Soderholm [89]. For expedience, uranyl hydroxyl complexes may be referred

Table 6
A summary of prior XAS studies on the structure of the uranyl ion in nitrate solutions conducted above 25 ºC. Focus is placed on the change in equatorial oxygen coordination with increasing temperature. (f) denotes a value was fixed during fitting. Values from [16] are not reported here as they were originally sourced from [153]. The confidence of reported uncertainties is typically not discussed at all but can generally be assumed to be 1σ unless otherwise stated.

Publication	Temperatures investigated (ºC) and determined equatorial oxygen coordinations.	Other notes
Schofield et al.[135]	25 – 4.5/4.2 70 – 4.5/4.8 115 – 4.9/4.4 160 – 4.7/4.4 205 – 3.7/3.0 250 – 3.1/5(f) + 1(f) Nitrogen	Measurements conducted on 2 solutions both containing 0.1 M $UO_2(NO_3)_2{\cdot}6H_2O$. One contained 0.2 M NO_3^- the other 1.0 M NO_3^- with 0.8 M introduced as KNO_3. E_0 value used during fits was not provided. Amplitude reduction factor (S_0^2) was not provided. K-Space data range 3–15 Å^{-1}. Coordination numbers are reported for both solutions, left numbers for the 0.2 M nitrate solutions, right numbers for the 1.0 M nitrate solution. The spectrum measured for the 1.0 M nitrate solution at 250 ºC was attributed to a pure solution of the uranyl mononitrate complex. Uncertainties were assumed to be ± 10%.
Testemale [153]	30 – 5.6(0.8) / 3.2(0.9)+ 2.2 (0.4) 100 – 5.2(0.7) / 3.3(1.0)+ 1.9(0.5) 200 – 4.7(1.0) / 2.1(0.3)+ 1.9(0.3) 300 – 3.6(0.6) / 1.5(0.4)+ 2.7(0.8) 350 – 2.7(0.5) / 1.2(0.3)+ 2.3(0.6) 375 – 1.5(1.2) / 1.3(0.7)+ 3.4(1.1)	Measurements conducted on a solution made using 0.1 M $UO_2(NO_3)_2{\cdot}6H_2O$. E_0 value used during fits was not provided. Amplitude reduction factor (S_0^2) = 1.0. K-Space data range 3–15 Å^{-1}. Coordination numbers are reported for the single and two shell equatorial oxygen models reported.

to simply by the numbers of uranyl and hydroxyl ions they are composed of, so (1,3) refers to $UO_2(OH)_3^-$, (3,4) to $(UO_2)_3(OH)_4^{2+}$ and so on. Here we review work conducted on a subset of uranyl hydroxyl species, specifically those likely to be relevant at hydrothermal conditions. This includes the mononuclear 1,1, 1,2, 1,3, 1,4 complexes and the polynuclear 2,2 and 3,5 complexes. All investigations reviewed were conducted at ambient conditions. Due to limitations in the sensitivity of XAS, all prior experimental work discussed here has been limited to acidic (≤4) or highly basic (≥13) pH conditions, where sufficient concentrations of uranyl can be dissolved in solution. This has restricted the range of hydroxyl complexes that have been characterised using XAS: of all the binary uranyl hydroxyl complexes only three complexes that are recognised by the NEA [55] have been characterised, namely the mononuclear 1,4 ($UO_2(OH)_4^{2-}$) complex that predominates in highly alkaline solutions, and the polynuclear 2,2 ($(UO_2)_2(OH)_2^{2+}$) and 3,5 ($(UO_2)_3(OH)_5^+$) complexes that predominate under moderately acidic solutions. Some works have suggested the significant presence of the 1,5 ($UO_2(OH)_5^{3-}$) [27] or trioxo ($UO_3(OH)_3^{3-}$) [117] complexes based on derived equatorial oxygen coordinations and edge-shifts. However, overall experimental support for the existence of the 1,5 complex is mixed [116,164] and computational works universally suggest that the 1,5 complex is unstable [104,136,148,162,164,25,76]. While the trioxo complex is possibly present as a transient form during 1,4 "-yl" oxygen transfer [18,139], its predominance in highly alkaline solutions has yet to be definitively proven. These two points of uncertainty are discussed in detail below.

Table 7
Summary of solution compositions. Solution speciation was calculated using the thermodynamic model described in the supplementary material.

Solution ID	Solution Composition	Notes
A	0.056 m UO_3 3.86 m $HClO_4$	Predominated by UO_2^{2+} at all temperatures. Temperature range: 25 – 222 ºC.
B	0.081 m UO_3 2.77 m HCl	Predominant species changed from UO_2^{2+} to UO_2Cl^+ to $UO_2Cl_2^0$ as temperature increased – see supplementary materials for exact species distributions. Temperature range: 25 – 312 ºC.
C	0.22 m UO_3 0.22 m H_2SO_4	Predominated by $UO_2SO_4^0$ at all temperatures. 66% at 25 ºC and > 80% above 80 ºC – see supplementary materials for exact species distributions. Temperature range 25–247 ºC.
D	0.09 m UO_3 0.12 m HCl 1.01 m Na_2SO_4	Predominated by $UO_2(SO_4)_2^{2-}$ (>80%) at all temperatures. Temperature range 25–266 ºC.
E	0.005 m UO_3 0.32 m HCl 0.50 m Na_2SO_4	Contained a roughly equal mix of $UO_2SO_4^0$ and $UO_2(SO_4)_2^{2-}$ up to 150 ºC above which $UO_2(SO_4)_2^{2-}$ become increasingly prevalent – see supplementary materials for exact species distributions. Temperature range 25–222 ºC.
F	0.018 m UO_3 0.93 m $NaHCO_3$	Predominated by $UO_2(CO_3)_3^{4-}$ at room temperature and probably at all higher temperatures, however a lack of high temperature, experimentally derived thermodynamic data make this difficult to verify. Temperature range 25–247 ºC.
G	Solid UO_3 3.51 m $NaOH$	Predominated by $UO_2(OH)_4^{2-}$ at all temperatures Temperature range 88–326 ºC.

In both mononuclear and polynuclear complexes hydroxyl ions bond along the uranyl equator and may bridge constituent uranyl groups in polynuclear complexes. Average U-O(eq) distances are very similar for both the 2,2 and 3,5 complexes at around 2.41 ± 0.01 Å. This value likely represents an average of the U-OH and U-H_2O distances as the two molecules tend to bond at significantly different distances from each other. U-O(ax) distances for the 2,2 and 3,5 species also remain similar to the pure uranyl ion at ~1.77 ± 0.01 Å. The 1,4 complex however, has far shorter U-O(eq) distances that vary around 2.22 – 2.28 Å. This is coupled with a slight lengthening of the U-O(ax) distances to ~1.80–1.82 Å. Very similar distances were observed in a solid analogue ($[Co(NH_3)_6]_2[UO_2(OH)_4]_3$) of the 1,4 complex by Clark et al. [27].

There has been some debate regarding the nature of uranyl speciation under highly alkaline conditions. Clark et al. [27] investigated uranyl in a 3.5 M tetramethylammonium (TMA-OH) solution and concluded that, under such conditions, uranyl speciation was dominated by a fivefold-coordinated pentahydroxy species, $UO_2(OH)_5^{3-}$. This assertion was based on the derivation of fivefold equatorial oxygen coordination at a distance consistent with hydroxyl bonding as suggested by their measurements of solid $[Co(NH_3)_6]_2[UO_2(OH)_4]_3$. However, the EXAFS work of Moll et al. [116] on a solution containing 0.5 M TMA-OH clearly derived fourfold equatorial oxygen coordination for the 1,4 complex. Such a difference in apparent speciation might be ascribed to the differences in alkalinity of the solutions studied by the two works. Indeed, Wahlgren et al. [164] studied two highly alkaline solutions containing 1.0 and 3.0 M TMA-OH and produced fits implying fivefold equatorial oxygen coordination in both solutions.

However, Wahlgren et al. [164] rejected the presence of the 1,5 complex and asserted that the fourfold-coordinated 1,4 complex is predominant under highly alkaline conditions using the following

Table 8
Summary of fitting ranges used and path parameter data sources as well as relevant notes on the fitting models used.

Solution ID	*k*-Range used for FTs and fitting	Solid analogue used for feff path calculations	Notes
A	2–13	$UO_2(ClO_4)_2{\cdot}5H_2O$Fischer [48]	All three axial oxygen MS paths were included in fits with parameters fixed to 2 × that of the fitted single scatter axial oxygen path.
B	2–13 2–12.5 for 312 °C spectrum	$Li(H_2O)_2[(UO_2)_2Cl_3(O)(H_2O)]$Bean et al.[13]	
C	2–13	$Na_{10}[(UO_2)(SO_4)_4](SO_4)_2{\cdot}3H_2O$Burns and Hayden[22]	
D	2–13	$Na_{10}[(UO_2)(SO_4)_4](SO_4)_2{\cdot}3H_2O$Burns and Hayden[22]	
E	2–13	$Na_{10}[(UO_2)(SO_4)_4](SO_4)_2{\cdot}3H_2O$Burns and Hayden[22]	Fluorescence rather than transmission data were used for fitting.
F	2–13	$Na_4(UO_2)(CO_3)_3$Plášil et al.[127]	Fits were done in k-space. All three axial oxygen MS paths were included in the same manner as Sol A. Fitting model was based on that reported by[84].
G	2–12	$UO_2(OH)_2$Taylor and Hurst [152]	E_0 value of 17177 eV was used rather than 17,182 eV.

arguments. **(i)** The solubility study of Yamamura et al. [165] only found evidence for the 1,4 complex in similarly alkaline solutions (up to pH 13.75). **(ii)** Despite the equatorial coordination numbers of ~5, the bond distances derived from the EXAFS analysis for equatorial oxygens were almost identical to the unequivocally fourfold coordinated 1,4 solid analogue ($[Co(NH_3)_6]_2[UO_2(OH)_4]_3$) studied by Clark et al. [27]. One would expect the addition of another OH^- group to increase the distance of all equatorial oxygens – indeed, computational work universally agrees that U-OH distances may differ by ≥ 0.1 Å between the 1,4 and 1,5 complexes [148,162,164,19,76] – such a large difference should be easily resolvable in EXAFS. **(iii)** Coordination numbers derived from EXAFS are prone to wide uncertainty margins and are sensitive to empirical parameters – particularly the amplitude reduction factor S_0^2 and threshold energy (E_0) [83,85] which are typically fixed during fitting. Given the high precision of bond distances measured by EXAFS this makes them a potentially better metric for deducing coordination than actually derived coordination numbers. (**iv**) Wahlgren et al. [164] also noted that fixing equatorial coordination to four had little effect on the quality of their fits. A re-evaluation of their data by Moll et al. [116] suggested equatorial coordination in the 3.0 M TMA-OH solution to be closer to four (4.6) rather than the originally derived 5.3.

DFT studies have suggested that the 1,4 complex has a fourfold coordinated/tetragonal bipyramid structure [104,136,148,162,164,25,76] and that it is significantly more stable than the 1,5 complex. The general instability of the 1,5 complex was further supported by the Car-Parrinello molecular dynamics (CPMD) study of Bühl et al. [19]. In addition, this work also noted that when surrounded by counterions (ammonium (NH_4^+) ions were used in their simulations) the 1,4 complex coordinates with an additional water molecule alongside its 4 hydroxyl ligands thus forming a pentagonal bipyramid. The DFT work of [162] suggests that the U-OH bond lengths for such a fivefold complex may only be slightly (~0.04 Å) longer than those of its fourfold counterpart, making this coordinated water potentially challenging to distinguish from the 4 hydroxyl groups with EXAFS, especially if solutions contained a mix of $UO_2(OH)_4^{2-}$ and $UO_2(OH)_4^{2-}(H_2O)$ as possible suggested by the Moll et al. [116] reinterpretation of the Wahlgren et al. [164] 3.0 M TMA-OH solution data.

Moll et al., ($year$) [117] suggest that in highly alkaline 3.0 M TMA-OH solutions the uranyl trioxo ($UO_3(OH)_3^{3-}$) complex may be favoured over the 1,4 or the 1,5 complexes. This assertion was based on their own DFT calculations (in turn based on the prior computational works of Shamov and Schreckenbach [139] and Bühl and Schreckenbach (2010)) that suggested the greater stability of the trioxo over the 1,5 complex and the observation of an edge shift (~ −0.5 eV) in the measured spectrum of a methanol based 3.0 M TMA-OH solution relative to a water based 1.0 M TMA-OH solution. This edge shift was compared to that observed for spectra of protactinium(V), in which a ~1 eV edge shift was attributed to the formation of an oxo bond [93]. It is worth noting that Wahlgren et al. [164] investigated water-based solutions with identical TMA-OH concentrations (1.0 and 3.0 M) yet did not note any edge shifts. The formation of deprotonated uranyl-methanol-hydroxyl complexes may serve as an explanation for the observed edge shift meaning the presented evidence is not definitive proof of the trioxo complex's existence. Furthermore, calculated structures of the trioxo complex indicate it to manifest fourfold equatorial coordination (1 oxo bond and 3 hydroxyl groups) meaning that its presence cannot adequately explain prior EXAFS measurements under similar pH conditions, whose fits suggest fivefold coordination. Thus, at present, while the trioxo complex may appear as an ephemeral transitionary compound during 1,4 "yl"-oxo transfer, present evidence does not adequately support its *predominance* in highly alkaline solutions.

As it stands neither the 1,5 nor the $UO_3(OH)_3^{3-}$ complexes are recognised in the latest NEA review [55] and as far as we know, no thermodynamic data exist for either making quantitative descriptions of their stabilities relative to the 1,4 complex difficult.

Considering the arguments of Wahlgren et al. [164], the solubility study of Yamamura et al. [165], the fitting results of Moll et al. [116] and the abundance of computational work discussed above we suggest the following behavioural pattern for uranyl hydroxyl complexes under highly alkaline conditions. At lower ionic strengths (I = ~1 M) the 1,4 complex predominates and manifests fourfold coordination [116]. As ionic strength rises 1,4 coordinates with a water molecule becoming fivefold coordinated; this structure is supported by the molecular dynamics work of [19] and explains the results of Clark et al. [27] and Wahlgren et al. [164] without having to invoke the presence of a 1,5 complex. The addition of a water molecule may also explain the intensification of a 765 cm^{-1} Raman band over a pH range of 13.34–14.38 observed in the work of Quiles et al. [129] that was attributed to the 1,5 complex. (Table. 5)

1.6. Uranyl aqua ion and uranyl complex structures under hydrothermal conditions

All the experimental works described above were conducted at or below 25 °C. XAS studies on uranyl complexation at elevated temperatures are comparatively sparse. To our knowledge only the uranyl aqua ion [135,153,16] along with its nitrate [135], carbonate [81], acetate

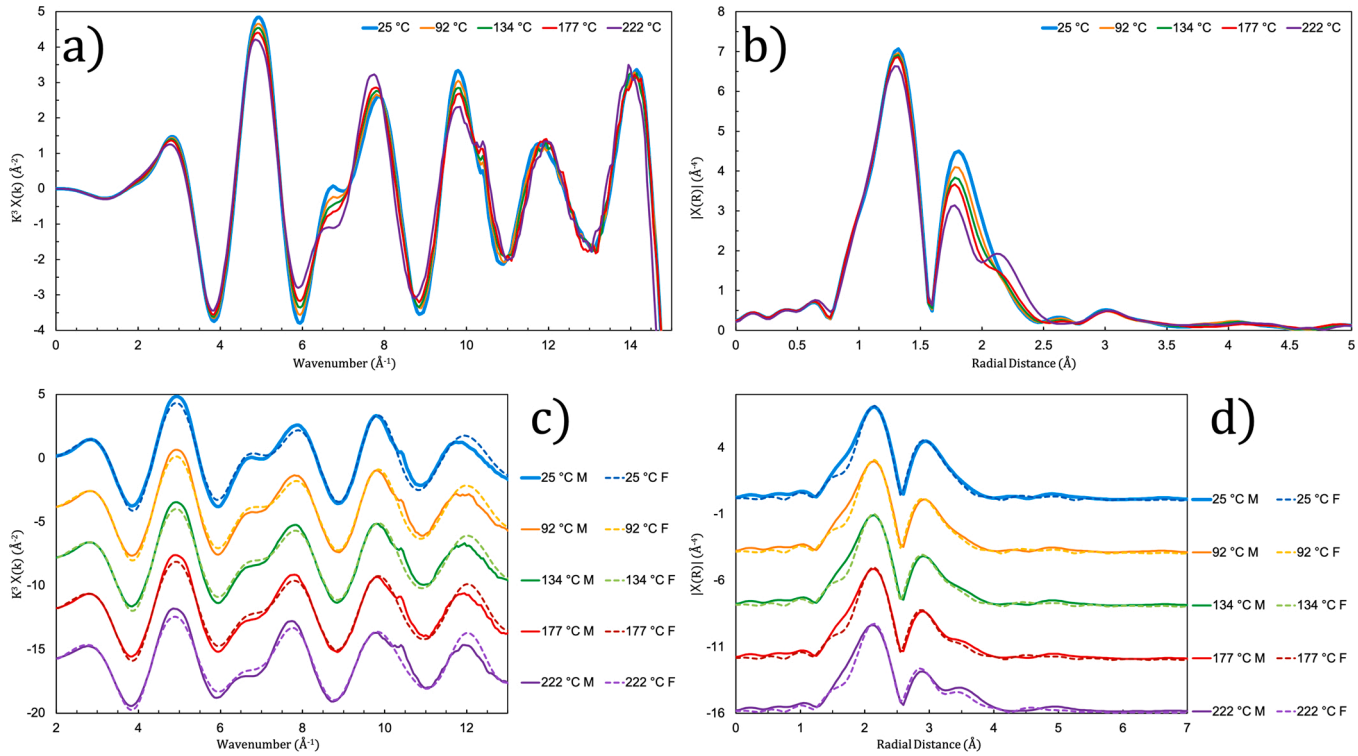

Fig. 6. Plots of EXAFS data and fits for the UO_2^{2+}-predominated Solution A. **a)** k^3-weighted EXAFS spectra. **b)** Magnitude of Fourier transforms of k^3-weighted EXAFS spectra. **c)** Measured EXAFS spectra (solid lines) plotted alongside modelled spectra (dashed lines). **d)** Magnitude of Fourier transforms of measured (solid lines) and modelled (dashed lines) EXAFS spectra. Fourier transforms have not been phase corrected.

[7,119], and citrate [8] complexes have been characterised at elevated temperatures. Of the uranyl nitrate complexes, only the mononitrate was observed and only in a single solution at a single temperature (250 °C) [135]. Characterisation of uranyl carbonate complexes has also been very limited, with [81] only reporting qualitative results up to 125 °C without any fitting results.

The pure uranyl ion has been investigated in nitrate solutions up to 375 °C and appears to undergo progressive dehydration with increasing temperature. The exact temperature relation of this dehydration process is somewhat poorly constrained at temperatures ≥ 200 °C, with Testemale [153] suggesting equatorial coordination to be between 4 and 4.7 depending on the fitting model used (two or single shell of equatorial waters), whereas Schofield et al. [135] suggest values around 3.0–3.7 with an apparent dependence upon the concentration of nitrate in solution. These coordination changes are summarised in Table 6. Reported U-O(ax) and U-O(eq) distances are similar to those determined at room temperature (Table 1), and remain constant with temperature.

When using a two-shell model for equatorial O(water), increasing temperature is associated with an increase in the number of equatorial oxygens in the outer ~2.50 Å shell and a decrease of those in the inner ~2.37 Å shell. It is unclear if this is a real effect as the single shell models of both Schofield et al. [135] and Testemale [153] do not seem to indicate a systematic temperature-linked increase in the average equatorial oxygen bond length. However, this may be explained by Debye-Waller (DW) factor obfuscation - the DW factors for single shell oxygens are significantly higher than those for two shell oxygens indicating greater bond length variance. Given the correlation between DW factors and bond distances this could lead to fits accounting average bond length changes as changes in the DW factor.

There has been at least one molecular dynamics study on the uranyl ion conducted for elevated temperatures [102]. This work suggests that uranyl retains fivefold coordination up to 200 °C which is roughly consistent with available experimental results.

The effect of temperature on the coordination geometry of uranyl acetate complexes up to 250 °C is dependent upon the Ac/U ratio in solution [7,119]. At higher Ac/U ratios, where the diacetate and triacetate complexes predominate, temperature appears to have little effect on equatorial oxygen coordination. Conversely, in solutions with lower Ac/U ratios where the monoacetate complex is more prevalent, equatorial oxygen coordination systematically decreases. This decrease in coordination is likely a result of the loss of equatorial waters as observed in the pure hydrated uranyl ion.

In citrate-bearing solutions, [8] found the $(UO_2)_2(cit)_2^{2-}$ dimer to be predominant over the full investigate temperature range (25–200 °C) with no significant change in coordination; this is consistent with the fact that the dimer contains no coordinating water molecules. Bond distances in both citrate and acetate complexes remain relatively constant with temperature, with any changes observed likely being a result of shifts between monodentate and bidentate bonding modes.

Overall, what little work is available suggests that uranyl complexes generally retain their structure as temperature increases; however the number of coordinating water molecules is mutable and systematically decreases with rising temperature.

2. Methodology

Experiments were conducted on homogeneous aqueous solutions prepared at room temperature and loaded into glassy carbon cells for in situ XAS measurement at elevated temperature and pressure using the mAESTRO autoclave system. Maximum temperatures were dictated by solution composition (e.g. decomposition of $HClO_4$ at temperatures beyond 250 °C) or by solution behaviour at high temperature where beam-induced redox effects typically led to photo-reduction and precipitation of uranium at which point measurements were terminated. Precipitation was monitored using the absorbance step height in transmission, which is proportional to uranium concentration. Solution compositions were chosen to permit characterisation of UO_2^{2+}, UO_2Cl^+,

Table 9
Derived fitting parameters for Solution A. ΔE was permitted to change at each temperature but was constant across scattering paths. (f) indicates that the parameter was fixed during fitting. R – bond length, N – Coordination, DW – Debye-Waller factor, WAD - Weighted Average distance, weighted for coordination, TC – Total Coordination. All reported uncertainties correspond to a 1σ confidence interval.

Path	T (°C)	R (Å)	N	DW (σ^2, $Å^2$)	ΔE (eV)
Solution A					
U – O (axial)	25	1.77 (1)	2(f)	0.0023	-0.06
	92	1.77 (1)	2(f)	0.0024	-0.32
	134	1.77 (1)	2(f)	0.0024	-0.31
	177	1.77 (1)	2(f)	0.0024	-0.33
	222	1.77 (1)	2(f)	0.0026	0.18
U – O (equatorial)	25	2.36 (3)	2.84 ± 0.95	0.0026	WAD: 2.41(3)
		2.47 (2)	2.32 ± 0.61	0.0026	TC: 5.16 ± 1.56
	92	2.36 (3)	2.77 ± 0.92	0.0032	WAD: 2.41(3)
		2.48 (3)	2.32 ± 0.60	0.0032	TC: 5.09 ± 1.52
	134	2.36 (2)	2.71 ± 0.81	0.0034	WAD: 2.42(2)
		2.49 (2)	2.39 ± 0.54	0.0034	TC: 5.1 ± 1.35
	177	2.36 (2)	2.52 ± 0.60	0.0030	WAD: 2.43(2)
		2.50 (2)	2.37 ± 0.44	0.0030	TC: 4.89 ± 1.04
	222	2.36 (2)	2.10 ± 0.50	0.0023	WAD: 2.44(2)
		2.51 (2)	2.45 ± 0.55	0.0023	TC: 4.55 ± 1.05

$UO_2Cl_2^0$, $UO_2SO_4^0$, $UO_2(SO_4)_2^{2-}$, $UO_2(CO_3)_3^{4-}$ and $UO_2(OH)_4^{2-}$. Methodological details are given below.

2.1. X-Ray Absorption Spectroscopy Experiments

2.1.1. Solution Chemistries

Uranium was introduced into every solution as solid UO_3, which was synthesised via thermal denitration of uranyl nitrate [126]. Briefly, uranyl nitrate was heated to and maintained at 450 °C for 48 h then measured with powder XRD to verify its total conversion to UO_3. Precisely weighted amounts of UO_3 were then dissolved in either perchloric acid ($HClO_4$), hydrochloric acid (HCl), sulfuric acid (H_2SO_4) or in a sodium bicarbonate $NaHCO_3$ solution. In the case of solution G (Table 7), a solid ~1 mg pellet of UO_3 was simply loaded into the mAESTRO cell along with a 3.5 m NaOH solution, since UO_3 in poorly soluble in this solution at room temperature. Perchloric acid was chosen as the background acid for Solution A to permit a high concentration of solubilised U without complexation – most prior room temperature studies dedicated to uranyl have also used perchloric acid (see the relevant section in the introduction). Detailed solution compositions and speciation are reported in Table 7, further speciation details are reported in the supplementary materials.

2.1.2. Apparatus design: The mAESTRO autoclave system

XAS experiments were performed using the mAESTRO hydrothermal cell [100,155,156,45] at 25 – 313 °C and a pressure of 600 bar at the XAS beamline at the Australian Synchrotron in Melbourne, Australia. The mAESTRO cell consists of an external water-cooled high-pressure vessel equipped with beryllium windows enabling the collection of transmission and fluorescence X-ray signals concurrently. The sample is contained inside a glassy carbon tube with an internal diameter of 4 mm. Pressure is applied to the sample by two glassy carbon pistons, using helium as a pressure medium. The glassy carbon tube is placed inside a small cylindrical resistive heater; the heater and tube are then installed inside the high-pressure vessel.

2.1.3. Synchrotron data collection specifics

Extended X-ray Absorption Fine Structure (EXAFS) data were collected at the uranium LIII-edge (17,166 eV). The beam energy was calibrated with a Zr foil, such that the maximum of the first derivative was at 17,998 eV. The Australian Synchrotron is a 3 GeV ring and was operated in top-up mode with a current of 200 mA. The XAS beam line uses a Si(111) double-crystal monochromator (DCM), providing an energy resolution ΔE/E of ~1.5×10^{-4} eV. The FWHM (full width at half maximum) beam size at the sample was 750×140 μm^2. The incident and transmitted beam intensities were measured with ion chambers, with fluorescence XANES and EXAFS data collected concurrently with a 30 element Ge fluorescence detector (Canberra). Solutions were typically measured ~3 times at each temperature up to a k value of 15 – data from these measurements were then averaged to improve the signal/noise ratio. Over the course of multiple measurements each solution was exposed to each temperature for ~2 h.

2.1.4. EXAFS data analysis procedure

EXAFS data were processed and fit using the Athena and Artemis codes from the HORAE package [131]. Transmission data were used for all solutions except solution E for which fluorescence data were used. The edge energy value (E_0) used for background removal and normalisation was set to 17,182 eV for the spectra of all solutions except solution G for which a value of 17177 eV was used. These values were chosen in order to keep ΔE values relatively low (<5 eV) during fitting following the recommendations of Kelly and Ravel [85]. Scattering path phases and parameters were calculated using the feff6 code [166] from a range of solid uranyl compounds. These compounds are listed in Table 8. The amplitude reduction factor (S_0^2) was fixed to 1.0 for all fits for all solutions. ΔE was set to be common for each path at a given temperature but was permitted to be different at each temperature. Data for all solutions except solution F (which was fit in *k*-space) were fit in *R*-space using three k weights of 1,2 and 3 which were fit simultaneously for each spectrum. Axial oxygen multiple scattering paths (MS) were generally omitted unless otherwise stated as their inclusion generally made no discernible improvement to fit quality. For all temperatures and solutions the coordination of axial oxygens was fixed to 2. Reported uncertainties were calculated by the Artemis code. More detailed discussions of how these uncertainties are calculated may be found in [149,83,84].

2.1.5. Thermodynamic calculations of solution speciation at ambient and elevated temperatures

To aid in fitting efforts and to verify recently derived high temperature formation constants for uranyl chloride and sulfate complexes thermodynamic calculations were conducted to model the expected speciation of the studied solutions. Calculations were performed using the GEMS Selektor program [92] utilising the Extended Debye-Hückel equation of state modified for solutions dominated in 1:1 electrolytes [124,125,67] (e.g. NaCl, HCl, NaOH) (Eq. 4.1). Where A and B are the Debye-Hückel parameters, γ_i, Z_i, Γ and $\dot{a}$ are the individual molal activity coefficients, the ionic charge, a molarity to molality conversion factor and ionic size of ion 'i'. The effective ionic strength calculated using the molal scale is I and b_γ is the extended-term parameter for the chosen 1:1 background electrolyte.

$$\log\gamma_i = -\frac{A \bullet [Z_i]^2 \bullet \sqrt{I}}{1 + B \bullet \mathring{a} \cdot \sqrt{I}} + \Gamma + b_\gamma I \quad (4.1)$$

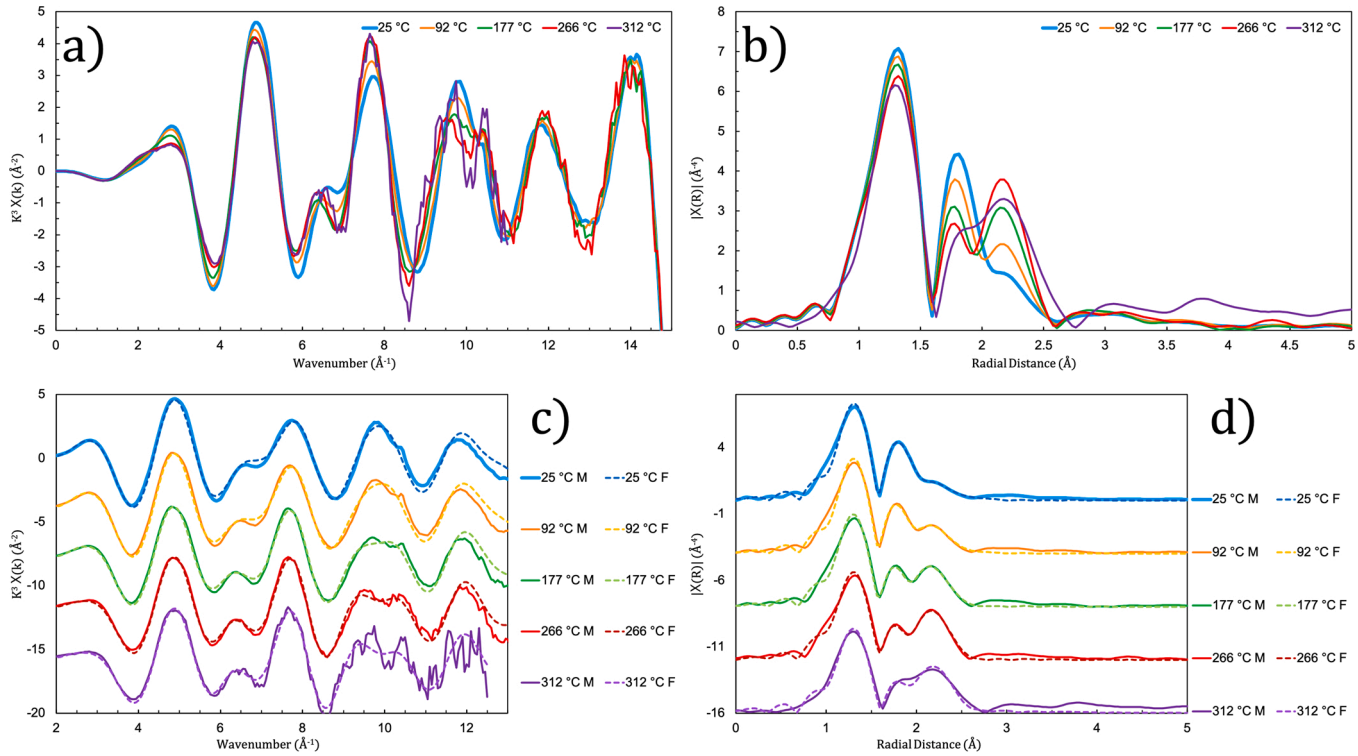

Fig. 7. Plots of EXAFS data and fits for Solution B, predominated by uranyl chloride species. **a)** k^3-weighted EXAFS spectra. **b)** Magnitude of Fourier transforms of k^3-weighted EXAFS spectra. **c)** Measured EXAFS spectra (solid lines) plotted alongside modelled spectra (dashed lines). **d)** Magnitude of Fourier transforms of measured (solid lines) and modelled (dashed lines) EXAFS spectra. Fourier transforms have not been phase corrected.

Table 10
Derived fitting parameters for Solution B. ΔE was permitted to change at each temperature but was constant across scattering paths. (f) indicates the parameter was fixed during fitting. R – bond length, N – Coordination, DW – Debye-Waller factor. Expected chloride coordination based on thermodynamic calculations are presented alongside coordination numbers derived from our fits. We report values calculated using both interpretations of the data of [34] – stepwise/absolute (see [111]). All reported uncertainties correspond to a 1σ confidence interval.

Path	T (°C)	R (Å)	N	DW (σ^2, Å^2)	ΔE (eV)	
Solution B						
U – O (axial)	25	1.77(1)	2(f)	0.0022	-3.05	
	92	1.77(1)	2(f)	0.0024	-3.26	
	177	1.77(1)	2(f)	0.0026	-3.28	
	266	1.77(1)	2(f)	0.0029	-3.14	
	312	1.78(1)	2(f)	0.0030	-1.07	
U – O (equatorial)	25	2.41(1)	4.33 ± 0.63	0.0067		
	92	2.43(2)	4.09 ± 0.75	0.0088		
	177	2.45(3)	3.57 ± 1.10	0.0126		
	266	2.47(4)	2.75 ± 0.33	0.0159(f)		
	312	2.49(5)	2.69 ± 0.46	0.0177(f)		
					Expected Coordination Migdisov et al. [112]	Expected Coordination Dargent et al. [34]
U – Cl	25	2.72(2)	0.46 ± 0.38	0.0014	*0.61*	*2.45/1.24*
	92	2.72(2)	0.83 ± 0.47	0.0042	*0.71*	*2.33/1.08*
	177	2.71(2)	1.51 ± 0.63	0.0059	*1.19*	*2.71/0.96*
	266	2.70(1)	2.27 ± 0.46	0.0067	*1.79*	*2.97/0.96*
	312	2.70(1)	2.42 ± 0.66	0.0071	*1.92*	*2.99/0.97*

In all thermodynamic calculations, we defined the experimental system with the following aqueous species: H^+, OH^-, Cl^-,HCl^0, Na^+, $NaCl^0$, $NaOH^0$, SO_4^{2-}, $NaSO_4^-$, HSO_4^-, ClO_4^-, $NaCO_3^-$, $NaHCO_3^0$, HCO_3^-, CO_3^{2-}, CO_2^0, UO_2^{2+}, UO_2Cl^+, $UO_2Cl_2^0$, $UO_2SO_4^0$, $UO_2(SO_4)_2^{2-}$, UO_2OH^+, $UO_2(OH)_2^0$, $UO_2(OH)_3^-$, $UO_2(OH)_4^{2-}$, $UO_2CO_3^0$, $UO_2(CO_3)_2^{2-}$, $UO_2(CO_3)_3^{4-}$, $\gamma UO_{3(cr)}$, $Na_2U_2O_{7(cr)}$. Data were sourced from; [112,114,141,142,150,151,2,34,55,79,82].

2.2. Molecular dynamics calculations

Ab initio MD simulations were conducted with Car-Parrinello Molecular Dynamics (CPMD, version 3.1.17) [26]. Density functional theory in CPMD is employed by the means of a plane-wave basis set of atomic orbitals and pseudopotentials. BLYP pseudopotentials [14,94] were used to depict interactions of valence electrons in combination with local density approximation functional (LDA) [90]. The BLYP functional has been proved to produce a good description of water [98]. However, previous studies [53] also show that the liquid simulated with BLYP is somewhat overstructured at room temperature. The calculated

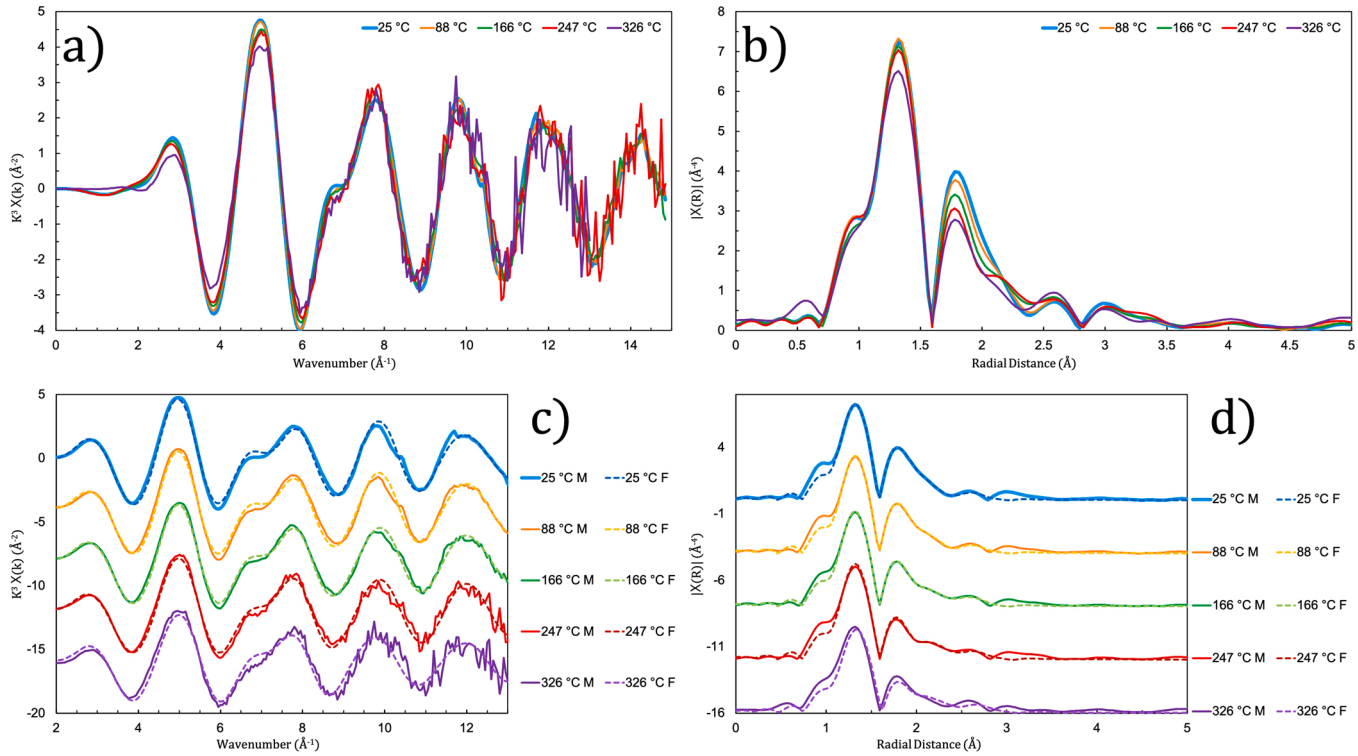

Fig. 8. Plots of EXAFS data and fits for Solution C, containing predominantly $UO_2SO_4^0$. **a)** k^3-weighted EXAFS spectra. **b)** Magnitude of Fourier transforms of k^3-weighted EXAFS spectra. **c)** Measured EXAFS spectra (solid lines) plotted alongside modelled spectra (dashed lines). **d)** Magnitude of Fourier transforms of measured (solid lines) and modelled (dashed lines) EXAFS spectra. Fourier transforms have not been phase corrected.

melting temperature with BLYP is 323 K [42] and some studies had successfully reproduced water at ambient condition by employing a slightly higher temperature to system to avoid glassy behaviours (e.g. Bankura et al. [11]); therefore, in this study, we conducted simulations at 77 ℃ to represent those solutions at room temperature. For uranium, the same pseudopotential was employed as Bühl et al. [17]. A timestep of 3 a.u. (0.073 fs) and fictitious electron mass of 400 a.u. were employed in the simulation. Periodic boundary conditions were applied in order to minimize surface effects. The simulations were performed in an NVT ensemble. Nosè thermostat was used to control the temperatures of ions and electrons. The pressure of the system is reflected by the choice of the density of the system. The densities of the investigated systems were chosen according to the equation of state of NaCl-bearing solutions [40,41].

Simulations were performed with solutions containing 1 UO_2^{2+} and a total of 111 H_2O molecules, with 2 SO_4^{2-} + 2 Na^+ (box 1) and 4 Cl^- + 2 H^+ (box 2). Simulations were conducted at 77 C (to approximate room temperature), 150 ℃, 300 ℃ and 400 ℃ with pressure varying from 600 bar to 20 kbar. Details of the simulation boxes are presented in the Supplementary material (Table S1). To achieve good statistics, all calculations were conducted for over 15 picoseconds (ps) with an equilibration of 1–2 ps. *Ab initio* MD requires large computational resources and as such simulation times are limited to ranges on the order of tens of picoseconds. Although classical MD enables much longer simulation times and a larger box than ab initio MD [21], the accuracy of results from classical MD relies on empirical force fields, which are fitted to match experimental data, i.e., hydration, free energy [61]. The reliability of the force fields depends on the experimental data and therefore is case sensitive [35]. The nature of the complicated electron configurations of the transition metals makes it hard for classical MD to present reliable properties [140]. In ab initio MD, these atoms are described as (pseudo-)potentials quantumly and we need not worry about interatomic forces. Previous studies suggest that despite the short time frames typical of ab initio MD simulations the structures derived are still reliably accurate [101,109,58]. The ion exchange of the first shell of uranyl may not be observed due to the short simulation time of ab initio MD. Several different initial configurations were chosen to test the structure and the stability of different complexes (Table 17). Time-averaged stoichiometric and geometric information was obtained with VMD [72]. Bond distances and coordination number (CN) were retrieved from radial distribution functions (RDF) and their integrals. Debye-Waller factors were calculated following equations in section 2.3 in Campbell et al. [24].

3. Results and discussions

For each solution below, we report normalised and background-corrected k^3 weighted EXAFS data, the magnitude of the Fourier transforms (FTs) of these k^3 weighted EXAFS data, and modelled spectra + FTs produced by the shell-by-shell fitting. Chosen scattering paths and the fitting parameters used to model them have also been tabulated (Tables 4.9–4.15). It must be noted that the FT plots presented below have *not* been phase corrected – as such while bond lengths/scattering path distances will be referred to by their true values, features present in FTs will be referred to by their non-phase corrected *apparent* plotted distances, e.g. the typical true axial oxygen distance was around 1.78 Å in most solutions, however, in our plotted FTs the corresponding peak may be found at ~1.3 Å.

3.1. The Uranyl aqua ion – Solution A

At all temperatures (25 – 222 ºC) the most likely predominant species in solution A (0.056 m U and 3.86 m $HClO_4$; Table 7) is the hydrated uranyl aqua ion, $UO_2^{2+}{\cdot}nH_2O$ with *n* varying depending on temperature. EXAFS spectra and the magnitude of their FTs along with modelled spectra/FTs are shown in Fig. 6, and fitting parameters are listed in Table 9. The FTs display typical features for uranyl with a large peak at ~1.3 Å, which corresponds to the axial oxygen single-scattering path, a

Table 11
Derived fitting parameters for Solution C. ΔE was permitted to change at each temperature but was constant across scattering paths. (f) indicates the parameter was fixed during fitting. R – bond length, N – Coordination, DW – Debye-Waller factor, WAD - Weighted Average distance, weighted for coordination, TC – Total Coordination. All reported uncertainties correspond to a 1σ confidence interval.

Path	T (°C)	R (Å)	N	DW (σ^2, $Å^2$)	ΔE (eV)
Solution C					
U – O (axial)	25	1.77 (1)	2(f)	0.0022	-0.93
	88	1.77 (1)	2(f)	0.0021	-0.99
	166	1.77 (1)	2(f)	0.0023	-1.23
	247	1.77 (1)	2(f)	0.0022	-0.85
	326	1.78 (1)	2(f)	0.0032	0.93
U – O (equatorial)	25	2.35 (1)	2.32 ± 0.69	0.0031	WAD: 2.41(2)
		2.47 (3)	2.40 ± 0.72	0.0031	TC: 4.72 ± 1.41
	88	2.35 (2)	1.99 ± 0.49	0.0035	WAD: 2.41(3)
		2.47 (3)	2.27 ± 0.61	0.0035	TC: 4.26 ± 1.10
	166	2.35 (3)	2.07 ± 0.51	0.0034	WAD: 2.41(3)
		2.47 (3)	2.34 ± 0.66	0.0034	TC: 4.41 ± 1.17
	247	2.34 (3)	1.75 ± 0.46	0.0022	WAD: 2.42(3)
		2.48 (3)	2.05 ± 0.62	0.0022	TC: 3.80 ± 1.08
	326	2.34 (f)	1.40 ± 0.58	0.0038	WAD: 2.42(f)
		2.48 (f)	2.16 ± 0.64	0.0038	TC: 3.56 ± 1.22
U – S	25	3.19 (2)	1(f)	0.0083	$C^3 = 0.00148$
	88	3.19 (7)	1(f)	0.0071	$C^3 = 0.00153$
	166	3.18 (5)	1(f)	0.0061	$C^3 = 0.00139$
	247	3.17 (6)	1(f)	0.0066	$C^3 = 0.00124$
	326	3.13 (8)	1(f)	0.0078	$C^3 = 0.00059$

second major peak at ~1.8 Å corresponding to water-linked equatorial oxygens, and a peak/shoulder at ~2.25 Å which we have interpreted to correspond to a second equatorial water-linked oxygen shell. While the axial oxygen peak changes little with temperature, the two equatorial oxygen peaks both show notable changes with temperature. As temperature increases the ~1.8 Å peak decreases in magnitude while the ~2.25 Å peak intensifies. These observations suggested temperature-linked changes in equatorial coordination, which was confirmed by our fits.

A two equatorial-water-oxygen shell model was used as it produced higher quality fits particularly at higher temperatures where the shoulder/peak at ~2.25 Å in *R*-space became increasingly more intense. To minimise the number of free-floating parameters it was assumed that the two equatorial oxygen scattering paths had the same Debye-Waller (DW) factor.

Our results suggest that the coordination of equatorial oxygens changes little from 25 to 134 °C; however, as temperature increases further more drastic changes occur with a drop to a minimum of 4.55 oxygens at 222 °C. This relatively small dehydration is consistent with the theoretical predictions of [102], whose calculations suggest that fivefold coordination is maintained up to 200 °C. Relative to prior high temperature results, we obtained slightly higher coordination numbers compared to [135] and to the two-shell model of [153], though our values are very similar to the latter's one-shell model (Table 6).

In addition, our two-shell fit suggests that as temperature increases the diameter of the outer oxygen shell increases slightly from 2.47 to 2.51 Å, and that coupled with this diameter increase the number of oxygen atoms in the outer shell increases and eventually exceeds the number of oxygen atoms in the inner shell.

3.2. Uranyl chloride complexes – Solution B

Thermodynamic calculations based off data reported by Migdisov et al. [112] (see supplementary material for details) suggest that the predominant species shifted from UO_2^{2+} to UO_2Cl^+ to $UO_2Cl_2^0$ as temperature increased from 25 to 312 °C in Solution B (0.081 m U and 2.77 m HCl; Table 8). EXAFS spectra and the magnitude of their FTs along with modelled spectra/FTs are shown in Fig. 7, and fitting parameters are reported in Table 10. Typical axial and equatorial oxygen features are visible in the un-phase-corrected FTs at ~1.3 Å and ~1.8 Å, while the shoulder/peak at ~2.25 Å has been attributed to the equatorial chlorine. The main change observed with temperature was a decrease in the magnitude of the equatorial oxygen peak and an intensification of the chloride peak. These changes in the FTs were attributed to a change in solution speciation with temperature as suggested by thermodynamic calculations.

Our model assumed one equatorial oxygen shell and one equatorial chloride shell. A two equatorial oxygen shell model resulted in unacceptably large uncertainty ranges for all parameters. DW factors for equatorial oxygens at 266 and 312 °C had to be fixed; otherwise their path length and coordination numbers had unreasonably large uncertainty ranges. The chosen DW factors were based on linear extrapolation of the values determined at 25, 92 and 177 °C.

Our fitting results suggest a strong decrease in the number of equatorial oxygen atoms with increasing temperature, from 4.33 at 25 °C to 2.69 at 312 °C, concurrently with an increase in the number of equatorial chloride ions from 0.46 to 2.42 over the same temperature range. Our derived coordination values suggest fivefold coordination for both UO_2Cl^+ and $UO_2Cl_2^0$ which is consistent with prior room temperature studies though a total coordination of 4.5 is generally suggested for $UO_2Cl_2^0$. Alongside our fitting parameters in Table 10 we have also reported values for *expected* average chloride coordination calculated using weighted averages based on thermodynamically calculated speciation. These values have been calculated using formation constants for the UO_2Cl^+ and $UO_2Cl_2^0$ complexes derived by Migdisov et al. [112], and values for the same complexes along with $UO_2Cl_3^-$ reported by Dargent et al. [34]. There has been some discussion [33,111] on values reported by Dargent et al. [34] regarding whether their values were reported as absolute or stepwise formation constants. For the sake of completeness, we have taken the values reported in Table 2 in [34] and interpreted them in two ways, either as absolute (according the format of Eq. 4.2) or stepwise (according to the format of 4.3).

$$UO_2^{2+} + \mathrm{n}Cl^+ \leftrightharpoons UO_2Cl_n^{2-\mathrm{n}} \tag{4.2}$$

$$UO_2Cl_n^{2-\mathrm{n}} + \mathrm{Cl} \leftrightharpoons UO_2Cl_{(\mathrm{n}+1)}^{2-(\mathrm{n}+1)} \tag{4.3}$$

The average numbers of coordinated chlorides calculated using the data of Migdisov et al. [112] are within uncertainty of our experimental values. Discrepancies can be attributed to a few effects. Primarily, Migdisov et al. [112] did not report formation constants for the $UO_2Cl_3^-$ complex – as such we could not model contributions from this complex which readily explains discrepancies for higher temperatures where our data suggest this species becomes more prevalent. It is also possible that uranyl chloride complexes have 2 equatorial oxygen shells. In solution A, the outer oxygen shell corresponds to a peak in the FTs that manifests at a similar distance to the chloride peak in Solution B. As such it is

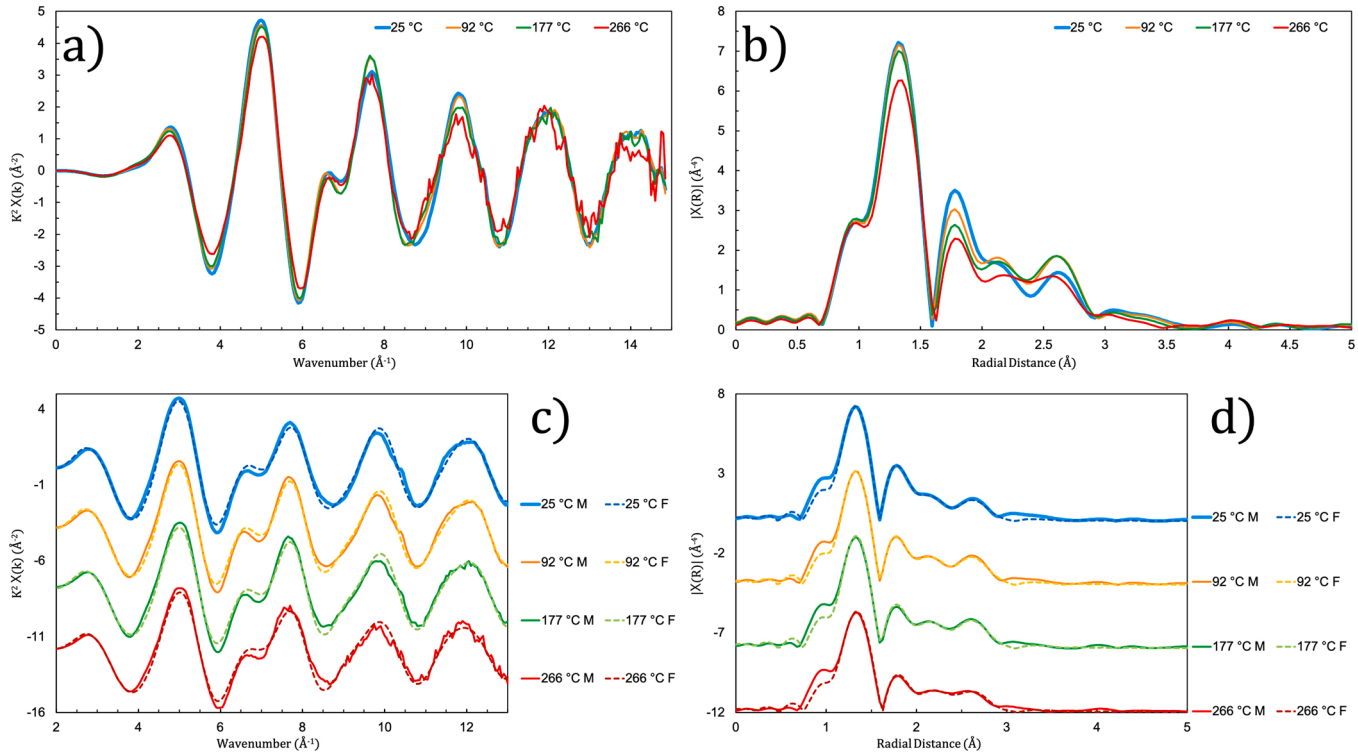

Fig. 9. Plots of EXAFS data and fits for Solution D, containing predominated the $UO_2(SO_4)_2^{2-}$ uranyl complex. **a)** k^3-weighted EXAFS spectra. **b)** Magnitude of Fourier transforms of k^3-weighted EXAFS spectra. **c)** Measured EXAFS spectra (solid lines) plotted alongside modelled spectra (dashed lines). **d)** Magnitude of Fourier transforms of measured (solid lines) and modelled (dashed lines) EXAFS spectra. Fourier transforms have not been phase corrected.

possible that some of the 2.25 Å peak amplitude, which in this fitting model was attributed to chloride, may in fact contain some contribution from second-shell equatorial oxygen, leading to chloride coordination values that are slightly too high.

In contrast, average chloride coordination values calculated using the data of Dargent et al. [34] do not describe our modelled coordination values satisfactorily regardless of which interpretation of their formation constants is used. Hence, we recommend the use of thermodynamic data reported by Migdisov et al. [112] rather than those reported by Dargent et al. [34] when modelling uranyl chloride complexation.

3.3. Uranyl sulfate complexes – Solutions C, D and E

3.3.1. Solution C

Spectra and fit results for Solution C containing 0.22 m UO_3 and 0.22 m H_2SO_4 collected over a temperature range of 25 – 326 ºC are reported below. Thermodynamic calculations using data reported by either Kalintsev et al. [82] or Alcorn et al. [2] suggest that $UO_2SO_4^0$ is the predominant uranyl complex in this solution, with only minor contributions (<30% altogether) from UO_2^{2+} and $UO_2(SO_4)_2^{2-}$ at temperatures < 100 ºC. Detailed solution speciation are provided in the supplementary material. EXAFS spectra and the magnitude of their FTs along with modelled spectra/FTs are shown in Fig. 8., and fitting parameters are reported in Table 11. Typical axial and equatorial oxygen features are visible in the FTs at ~1.3 Å and ~1.8 Å. As observed in Solution A the equatorial oxygen region displays a main peak and a secondary shoulder which intensifies as temperature increases. The small peak at ~2.6 Å was attributed to equatorial sulfur atoms. The apparent peak at ~3.0 Å was deemed to be a truncation feature on account of a similar feature occurring in the FTs of Solution A. This is contrary to the interpretation of [69] who attributed this feature to the sulfur atoms of monodentately bound sulfate.

A two equatorial oxygen shell model was used with both shells being assigned the same DW factor. In view of the predicted predominance of $UO_2SO_4^0$, the coordination of equatorial sulfur was fixed to 1 at all temperatures. In addition, fit quality was notably enhanced when a third cumulant factor was added to the U-S single scattering path.

Our fitting results suggest a decrease in equatorial oxygen coordination with rising temperature with values that are ~0.5 atoms lower than for the uranyl aqua ion at similar temperatures.

At all temperatures it appears that sulfate in $UO_2SO_4^0$ favours a bidentate bonding mode, though we report slightly longer U-S distances (~3.18 Å) compared to the prior room-temperature studies of [115] and [69] (~3.11 Å). Unlike [69], we were unable to produce fits that suggested significant monodentate sulfate bonding. Our longer U-S distances may be explained by a minor contribution of monodentate sulfate or due to the inclusion of a 3rd cumulant parameter – the positive effect this parameter had on fit quality suggests an asymmetric distribution of sulfate bond lengths compared to other bond types.

3.3.2. Solution D

Thermodynamic calculations using data reported either by Kalintsev et al. [82] or Alcorn et al. [2] suggest that uranyl speciation in Solution D (0.09 m UO_3, 1.01 m Na_2SO_4 and 0.12 m HCl) was predominated almost entirely (≥80%) by the $UO_2(SO_4)_2^{2-}$ complex with at all temperatures investigated. EXAFS spectra and the magnitude of their FTs along with modelled spectra/FTs are shown in Fig. 9, and fitting parameters are reported in Table 12, over the temperature range of 25 – 266 ºC. The typical axial peak is visible in the FTs at ~1.3 Å and three peaks are visible between 1.5 Å and 3.0 Å. The first two peaks at ~1.8 Å and 2.1 Å have been attributed to equatorial oxygens contributed by sulfate and water. No distinction between distances and oxygen source was made. The peak at ~2.6 Å has been attributed to sulfur bound to equatorial sulfate. This peak is noticeably more intense than in the FTs of Solution C, qualitatively suggesting more bound sulfate molecules. The absence of any peaks at greater distances suggests that most if not all sulfate molecules are bound in a bidentate fashion.

Table 12
Derived fitting parameters for Solution D. ΔE was permitted to change at each temperature but was constant across scattering paths. (f) indicates the parameter was fixed during fitting. R – bond length, N – Coordination, DW – Debye-Waller factor, WAD - Weighted Average distance, weighted for coordination, TC – Total Coordination. All reported uncertainties correspond to a 1σ confidence interval.

Path	T (°C)	R (Å)	N	DW (σ^2, $Å^2$)	ΔE (eV)
Solution D					
U – O (axial)	25	1.78 (1)	2(f)	0.0023	-0.84
	92	1.78 (1)	2(f)	0.0023	-0.62
	177	1.78 (1)	2(f)	0.0023	-0.09
	266	1.79 (1)	2(f)	0.0031	1.10
U – O (equatorial)	25	2.35 (2)	2.24 ± 0.54	0.0028	WAD: 2.43(2)
		2.49 (2)	2.59 ± 0.57	0.0028	TC: 4.83 ± 1.11
	92	2.36 (2)	1.97 ± 0.46	0.0030	WAD: 2.44(2)
		2.50 (2)	2.64 ± 0.66	0.0030	TC: 4.61 ± 1.12
	177	2.35 (3)	1.60 ± 0.48	0.0020	WAD: 2.44(2)
		2.50 (2)	2.25 ± 0.74	0.0020	TC: 3.85 ± 1.22
	266	2.35 (3)	1.37 ± 0.38	0.0016	WAD: 2.44(2)
		2.50 (2)	1.82 ± 0.51	0.0016	TC: 3.19 ± 0.89
U – S	25	3.18 (4)	1.92 ± 0.93	0.0083	$C^3 = 0.00076$
	92	3.18 (3)	2.30 ± 0.83	0.0066	$C^3 = 0.00079$
	177	3.19 (3)	1.96 ± 0.86	0.0053	$C^3 = 0.00096$
	266	3.20 (3)	1.78 ± 0.68	0.0062	$C^3 = 0.00116$

The fitting model was identical to that used for Solution C, except that the coordination of sulfur was permitted to change rather than fixed to one. As seen in Solutions A, B and C the total coordination of equatorial oxygens decreases with rising temperature, with the outer shell being increasingly favoured with temperature. At temperatures above 100 °C, the total equatorial oxygen coordination appears to be slightly lower (~0.5 atom difference) relative to the monosulfate predominated Solution C. This suggests a trend where the addition of a sulfate molecule reduces average equatorial oxygen coordination by 0.5 at elevated temperatures. At 25 °C the uranyl ion and both sulfate complexes exhibit similar equatorial oxygen coordination numbers. Little change is seen in U-O(eq) distances with rising temperature.

The coordination of sulfur changes relatively little with temperature generally remaining around 2 with minor deviations above and below suggesting possible minor contributions from $UO_2SO_4^0$ and $UO_2(SO_4)_3^{4-}$. Overall, these results broadly verify the experimentally derived thermodynamic data of [82] and [2]. Sulfur distances are again slightly higher than that usually reported in the literature for bidentately bound sulfate but this is likely due to the introduction of a 3rd cumulant factor in our fitting model which permitted a more accurate replication of our measured spectra and their FTs.

3.3.3. Solution E

Thermodynamic calculations suggest that $UO_2(SO_4)_2^{2-}$ is the predominant form of uranyl in solution E (0.005 m UO_3, 0.50 m Na_2SO_4 and 0.32 m HCl) at all temperatures (25–222 °C), coexisting with some $UO_2SO_4^0$. Using the thermodynamic data from Kalintsev et al. [82], the relative contributions of $UO_2SO_4^0$ and $UO_2(SO_4)_2^{2-}$ vary from 30/70 to close to 50/50. Calculations using the data of Alcorn et al. [2] suggest that the contribution of $UO_2SO_4^0$ never exceeds 30% and that at all temperatures above ~75 °C the contribution of $UO_2(SO_4)_2^{2-}$ exceeded 80%. Speciation diagrams using both data sources are provided in the supplementary materials.

EXAFS spectra and the magnitude of their FTs along with modelled spectra/FTs are shown in Fig. 10, and fitting parameters in Table 13. Data reported for Solution E are fluorescence data rather than transmission data, hence the greater noise visible in the EXAFS spectra. The same spectral features as observed in Solutions C and D are visible at the same locations in *R*-space (compare Figs. 4.8 and 4.9).

The fitting model used was identical to that used for Solutions C and D except that the coordination of sulfur was fixed at 25 °C to 1.5, since otherwise the fitting model returned non-physical results. Again, the subtle peak visible at 3.0 Å was interpreted to be a truncation feature rather than a scatter-related feature. The usual decrease in total equatorial oxygen coordination is visible with rising temperature. The total coordination of equatorial oxygen (4.07) is somewhat lower at 25 °C than determined for Solutions C (4.72) and D (4.83), though there is significant overlap between the uncertainty ranges (~ ± 1) of all these values. Regardless, total equatorial oxygen coordination numbers converge for all three solutions at temperatures around and above 177 °C. This suggests that the structure of uranyl sulfate complexes may in part be controlled by such factors as absolute uranium concentrations and U/SO_4^{2-} ratios – ratios studied here were 1:1, 1:10 and 1:100 for solutions C, D and E respectively.

In a similar fashion to Solution B we have compared the average coordination of sulfur determined by our fitting model to average coordination from distribution of species calculations based on the thermodynamic properties of uranyl sulfate complexes reported by Kalintsev et al. [82] and Alcorn et al. [2]. The calculated coordination values for both sets of properties are reported in Table 13 alongside the results from our fitting model. Coordination values calculated using either data source generally overlap within error with the experimental values, though those based on the data of Kalintsev et al. [82] are slightly more accurate.

3.4. Uranyl carbonate complexes – Solution F

Spectra and fit results for Solution F containing 0.018 m UO_3 and 0.93 m $NaHCO_3$ collected over a temperature range of 25 – 247 °C are reported below. Presently, no experimentally derived thermodynamic data for uranyl carbonate complexes exist for temperatures above 25 °C, but the recent experimental work of Kalintsev et al. [81] suggests that at 200 and 250 °C and carbonate concentrations below 0.3 m uranyl carbonate complexes are unlikely to predominate, instead being superseded by hydroxyl complexes. With this in mind, we used extrapolations of room temperature data [62] made using the three-term approximation technique and coefficients described by [71] as implemented by the GEMS Selektor program [92] to identify possible stable species in solution F. These calculations, suggested that $UO_2(CO_3)_3^{4-}$ was the predominant species (>95% of total solubilised uranium) at all temperatures with the most prevalent non-carbonate species being $UO_2(OH)_4^{2-}$.

EXAFS spectra and the magnitude of their FTs along with modelled spectra/FTs are shown in Fig. 11, and fitting parameters in Table 14. Overall, the FTs were similar to those previously reported for $UO_2(CO_3)_3^{4-}$ at room temperature, with the only temperature-related change being a systematic decrease in the intensity of the equatorial oxygen peak at ~1.9 Å. The peak/shoulder at ~2.5 Å was attributed to the U-C single scattering path, that at ~3.0 was partly explained by U-O (ax) multiple scattering paths, and the peak at ~3.5 Å was attributed to the single scattering U-O(distal-carbonate) path along with the U-C-O (distal-carbonate) multiple scattering paths.

The fitting model used was nearly identical to that used by Kelly et al.

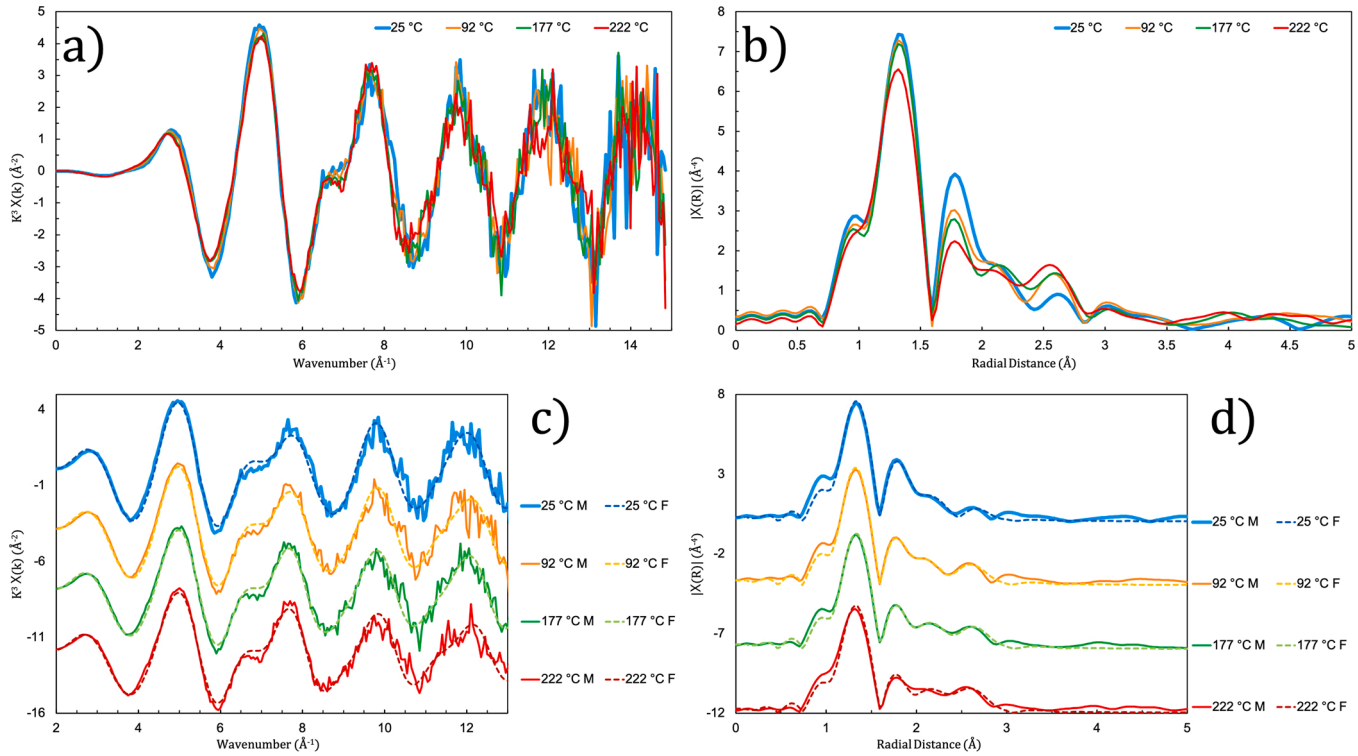

Fig. 10. Plots of EXAFS data and fits for Solution E containing a mix of $UO_2SO_4^0$ and $UO_2(SO_4)_2^{2-}$. **a)** k^3-weighted EXAFS spectra. **b)** Magnitude of Fourier transforms of k^3-weighted EXAFS spectra. **c)** Measured EXAFS spectra (solid lines) plotted alongside modelled spectra (dashed lines). **d)** Magnitude of Fourier transforms of measured (solid lines) and modelled (dashed lines) EXAFS spectra. Fourier transforms have not been phase corrected.

Table 13
Derived fitting parameters for Solution E. ΔE was permitted to change at each temperature but was constant across scattering paths. (f) indicates the parameter was fixed during fitting. R – bond length, N – Coordination, DW – Debye-Waller factor, WAD - Weighted Average distance, weighted for coordination, TC – Total Coordination. Expected coordination values are reported using thermodynamic properties from [2,82]. All reported uncertainties correspond to a 1σ confidence interval.

Path	T (°C)	R (Å)	N	DW (σ^2, Å^2)	ΔE (eV)	
Solution E						
U – O (axial)	25	1.78(1)	2(f)	0.0019	-0.44	
	92	1.78(1)	2(f)	0.0021	-1.40	
	177	1.79(1)	2(f)	0.0021	-0.81	
	222	1.78(1)	2(f)	0.0026	-1.39	
U – O (equatorial)	25	2.35(3)	1.85 ± 0.51	0.0007	WAD: 2.42(3)	
		2.48(3)	2.22 ± 0.65	0.0007	TC: 4.07 ± 1.15	
	92	2.33(6)	1.62 ± 0.59	0.0024	WAD: 2.42(5)	
		2.47(5)	2.51 ± 1.21	0.0024	TC: 4.13 ± 1.80	
	177	2.34(4)	1.49 ± 0.50	0.0019	WAD: 2.43(3)	
		2.49(3)	2.20 ± 0.87	0.0019	TC: 3.69 ± 1.37	
	222	2.34(f)	1.56 ± 0.51	0.0028	WAD: 2.43(f)	
		2.49(f)	2.25 ± 0.58	0.0028	TC: 3.81 ± 1.09	
					Expected Coordination	
U – S	25	3.18(7)	1.5(f)	0.0095	*1.53/1.61*	$C^3 = 0.00091$
	92	3.18(6)	1.15 ± 0.86	0.0039	*1.47/1.86*	$C^3 = 0.00106$
	177	3.15(3)	1.80 ± 0.98	0.0060	*1.61/1.95*	$C^3 = 0.00091$
	222	3.15(2)	1.61 ± 0.78	0.0046	*1.73/1.96*	$C^3 = 0.00102$

[84], sans the inclusion of Ca or Na scattering paths. Coordination numbers for all scattering paths were fixed at all temperatures. Despite the strict constraints used, our data were well explained by this model, suggesting that if solution carbonate concentrations are high enough the $UO_2(CO_3)_3^{4-}$ complex may be stable in solution at least for several hours. The peak at 3.0 Å was not fully replicated but as with other solutions reported in this work, we attribute it to truncation - it is probably not a physically linked feature but rather a FT artifact.

Overall, our data and fits suggest that uranyl carbonate complexes may be stable at elevated temperatures in concentrated carbonate solutions. Note that this does not necessarily invalidate the conclusions of Kalintsev et al. [81], whose solubility study concluded that such complexes were unstable at temperatures above 100 °C. There are two points that must be considered. Firstly, the solubility study only reports results for solutions containing carbonate concentrations up to 0.3 m; this EXAFS study measured a solution containing 0.93 m carbonate. It is possible that we have simply identified a high-enough carbonate concentration to stabilise uranyl carbonate complexes at high temperature – though from an environmental perspective this is an extreme value – even 0.3 m may be considered extreme. Secondly, the destabilisation of uranyl-carbonate complexes is associated with slow precipitation kinetics even at temperatures in excess of 100 °C – with equilibrium

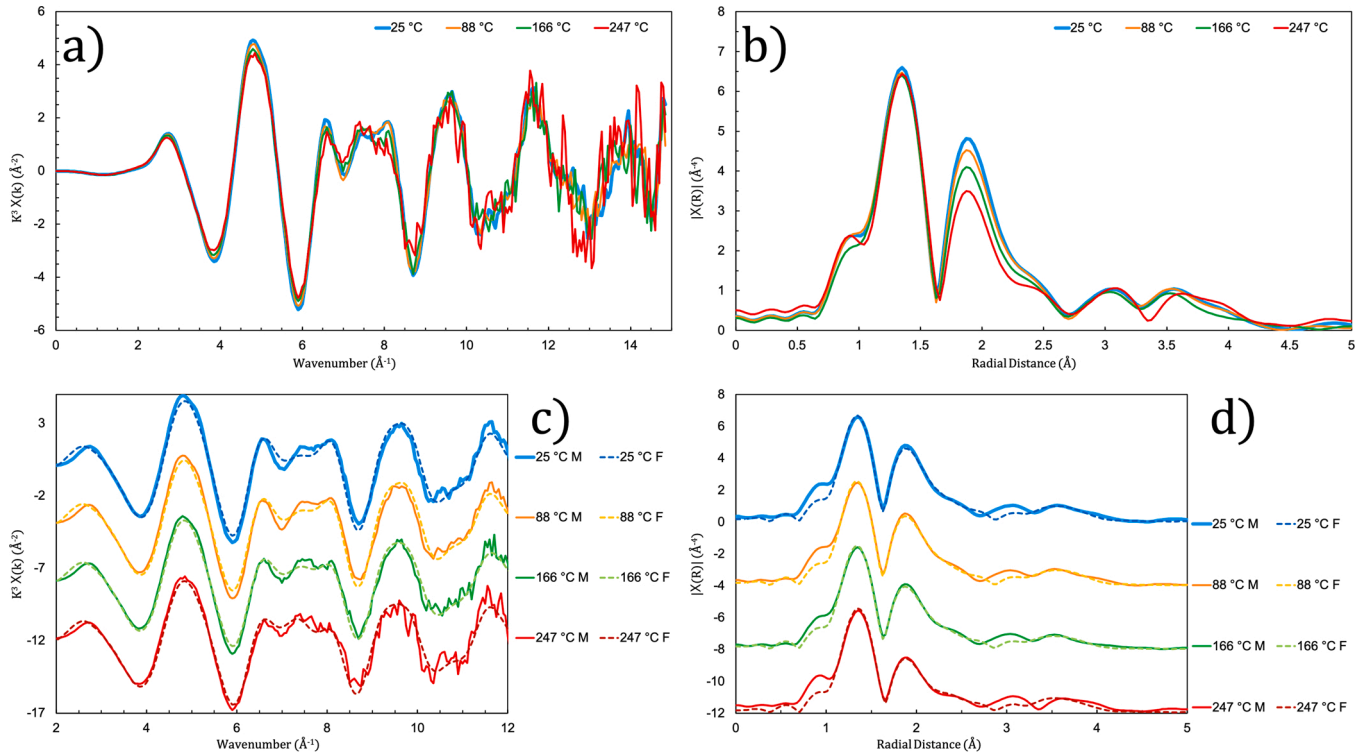

Fig. 11. Plots of EXAFS data and fits for Solution F, containing uranyl probably predominated as $UO_2(CO_3)_3^{4-}$. **a)** k^3-weighted EXAFS spectra. **b)** Magnitude of Fourier transforms of k^3-weighted EXAFS spectra. **c)** Measured EXAFS spectra (solid lines) plotted alongside modelled spectra (dashed lines) derived from our fitting procedure. **d)** Magnitude of Fourier transforms of measured (solid lines) and modelled (dashed lines) EXAFS spectra. Fourier transforms have not been phase corrected.

between solid and solution taking more than 24 h to be achieved (Alcorn and Kalintsev pers. comm.). Thus, it is possible that we may simply be observing metastable uranyl carbonate complexes as the solution measured was only exposed to temperatures exceeding 100 ºC for ~9 h altogether.

3.5. Uranyl hydroxyl complexes – Solution G

EXAFS spectra and fit results for Solution G which comprised a solid pellet of UO_3 submerged in 3.51 m NaOH collected over a temperature range of 88 – 326 ºC are plotted in Fig. 12, and fitting parameters are reported in Table 15. No spectra were collected at 25 ºC due to slow dissolution kinetics. Using the thermodynamic calculation model described earlier it was determined that this solution was likely to be predominated by $UO_2(OH)_4^{2-}$ at all temperatures. Spectra and FTs displayed little change with temperature suggesting the same species was predominant over the entire investigated temperature range.

Spectra FTs at all temperatures manifest a single broad peak at ~1.6 Å (Fig. 12b,d). A similar single peak was observed by Clark et al. [27] for a 3.5 M TMA-OH solution measured up to a wavenumber of 12 Å^{-1}. Where data over a wider K-range was available (e.g., Wahlgren et al. [164], 15 Å^{-1}; and Moll et al. [116], 17 Å^{-1}), this broad peak is resolvable as two peaks, one corresponding to axial oxygens and the other to equatorial hydroxyl-linked oxygens. As our data are limited in resolution due to the low concentration of dissolved uranium, we are unable to explicitly resolve two peaks but this did not preclude fitting.

The fitting model incorporated two equatorial oxygen shells. One shell was assigned to oxygen molecules associated with bound hydroxyl molecules; the coordination number of this shell was optimised during fitting. The second shell was assigned to a fixed number (1) of water molecules at a fixed distance of 2.42 Å with a fixed DW factor; these fixed values were based on averages determined from fitting results for Solution A as these provided the clearest possible parameters for equatorial water oxygens. These values needed to be fixed due to restrictions on the number of free-floating parameters permitted by the limited resolution of our data.

Our fits suggest that four equatorial hydroxyl-linked oxygen atoms are present at all temperatures except at 326 ºC, where this number appears to drop to ~3.5, potentially indicating the increasing prevalence of $UO_2(OH)_3^-$ or fourfold coordinated $UO_2(OH)_4^{2-}$. Thus, this model suggests that it is possible for $UO_2(OH)_4^{2-}$ to manifest overall fivefold coordination with four hydroxyl molecules and one water molecule. In turn this potentially reconciles prior computational work discussed in the introduction which argued for the instability of the $UO_2(OH)_5^{3-}$ and prior EXAFS work which for highly alkaline solutions repeatedly suggested equatorial oxygen coordination numbers of ~4.5–5. This model suggests that it is possible for $UO_2(OH)_4^{2-}$ to manifest fivefold coordination and that the presence of $UO_2(OH)_5^{3-}$ need not be invoked. This provides the first experimental validation of the molecular dynamics results reported by Bühl et al. [19], who's results suggested such a 4-OH^- 1-H_2O structure.

3.6. Ab initio molecular dynamics results

Results of simulations of uranyl speciation in Cl^- and SO_4^{2-}-bearing solutions are listed in Table 16 (box 1) and Table 17 (box 2). Fig. 13 shows calculated structures of different UO_2^{2+}-Cl^-/ SO_4^{2-} complexes. Radial distribution functions (RDF) and the integral of RDF of simulations under 600 bar are presented in Fig. 14. Fig. 15 shows U-S/Cl distances over simulation time of some individual simulations.

From room temperature to 400 C, all simulations suggest U-O(ax) distances of 1.82–1.85 Å in both boxes, which is consistent with the previous simulations (1.77 – 1.85 Å, [102,123,20,5]). U-O(eq) distances showed significant variance with temperature with minimum values of ~2.44–2.46 Å being calculated at 25–150 ºC and maximum values of

Table 14
Derived EXAFS fitting parameters for Solution F. Parameters for U – O(ax) multiple scattering paths are presented together and are identical in all cases at each temperature except the Debye-Waller factor for MS1, which was defined as 4 × rather than 2 × the Debye Waller factor of U – O (axial). The path lengths for these scattering paths were defined as 2 × the U – O(ax) single scatter path distance. Besides coordination (MS4 = 6, MS5 = 3), the parameters for both U – C – O(dist) multiple scattering paths were identical to each other with the path lengths and Debye Waller factor being defined as identical to the U – O(dist) single scattering path. R – bond length, N – Coordination, DW – Debye-Waller factor, (f) indicates the parameter was fixed during fitting. All reported uncertainties correspond to a 1σ confidence interval.

Path	T (°C)	R (Å)	N	DW (σ^2, $Å^2$)	ΔE (eV)
Solution F					
U – O (axial)	25	1.81 (1)	2(f)	0.0023	-0.70
	88	1.81 (1)	2(f)	0.0023	-0.84
	166	1.81 (1)	2(f)	0.0024	-0.80
	247	1.81 (1)	2(f)	0.0023	0.03
U – O (equatorial)	25	2.44 (1)	6(f)	0.0069	
	88	2.45 (1)	6(f)	0.0074	
	166	2.45 (1)	6(f)	0.0085	
	247	2.45 (2)	6(f)	0.0104	
U – C	25	2.90 (2)	3(f)	0.0030	
	88	2.90 (2)	3(f)	0.0038	
	166	2.90 (2)	3(f)	0.0044	
	247	2.90 (3)	3(f)	0.0044	
U – O (carb-dist)	25	4.19 (3)	3(f)	0.0063	
	88	4.18 (3)	3(f)	0.0063	
	166	4.18 (3)	3(f)	0.0075	
	247	4.20 (4)	3(f)	0.0065	
MS1 – U – O(ax) – U - O (ax)	25	3.61 (2)	2(f)	0.0045/ 0.0090	
MS2 – U – O(ax1) – O (ax2)	88	3.61 (2)	2(f)	0.0047/ 0.0094	
MS3 – U – O(ax1) – U – O (ax2)	166	3.61 (2)	2(f)	0.0048/ 0.0096	
	247	3.63 (2)	2(f)	0.0046/ 0.0091	
MS4 – U – C – O(dist)	25	4.19 (3)	6(f)/3 (f)	0.0063	
MS5 – U – C – O(dist) – C	88	4.18 (3)	6(f)/3 (f)	0.0063	
	166	4.18 (3)	6(f)/3 (f)	0.0075	
	247	4.20 (4)	6(f)/3 (f)	0.0065	

~2.48–2.55 Å being calculated at 300 – 400 °C. Lower end values were consistent with prior theoretical studies [20,4,70] but are little higher than the typical experimentally derived single-shell distance of ~2.41 Å determined at room temperature. Higher pressures lead to a systematic shortening of U-O(eq) distances with minimum values of 2.40 – 2.42 Å being calculated at 400 °C 20 kb. It is worth noting that pressure had little effect on the U-O(ax) distance.

3.6.1. Uranyl sulfate complexes

In the UO_2- SO_4^{2-} (box 1) calculations, the $[UO_2(H_2O)_5]^{2+}$ complex remained stable for 15 ps at 150 °C. At 300 °C, the simulation was started with a configuration of $[UO_2(H_2O)_6(SO_4)]$. An additional SO_4^{2-} bonded with UO_2^{2+} and one water rapidly deprotonated leading to the configuration of $[UO_2(H_2O)(SO_4)(HSO_4)(OH)]^{2-}$ until 12.7 ps after which the structure stabilized as $[UO_2(H_2O)_2(OH)(SO_4)_2]^{3-}$. As shown in Fig. 15 (a), both SO_4^{2-} molecules bonded with UO_2^{2+} in monodentate configurations in the first 9.2 ps, then in 1 bi- and 1 mono- dentate configurations with a very short period (~1 ps) in a doubly bidentate arrangement. U-S distances were 3.13 Å when monodentate and 3.74 when bidentate, coinciding with values from previous DFT calculations - 3.11 – 3.12 Å and 3.65 – 3.74 Å [2,161]. At 400 C, one SO_4^{2-} bonded with UO_2^{2+} at initiation and remained bonded during the whole simulation. This SO_4^{2-} was bound monodentately for 44% and bidentately for 56% of the 15 ps simulation time with it evidently stabilising in the bidentate configuration after ~8.5 ps (Fig. 15(b)). Deprotonation also occurred at the start of the simulation creating a configuration of $[UO_2(H_2O)_{1.9}(SO_4)(OH)]^-$. The liberated hydrogen bonded with the free SO_4^{2-} becoming HSO_4^- at a far distance from UO_2^{2+} in the box. The bond distance of U-OH is 2.19 Å, slightly shorter than that of U-OH_2. As shown in Fig. 14(a), the U-O RDF peaks of 300 °C and 400 °C split into one at 2.19/2.23 Å and one at 2.51/2.55 Å, respectively. At high pressure (3 kbar, 5 kbar and 20 kbar) and 400 °C, the UO_2^{2+}-SO_4^{2-} complexes remained stable with a hydration number of 3 (includes 1 OH), 2.3 and 3.1 at 3 kbar, 5 kbar and 20 kbar, respectively. Evidently, higher pressures encourage higher numbers of equatorially coordinated water molecules.

3.6.2. Uranyl chloride complexes

A number of different starting configurations were used in box 2 calculations – this was done to permit the observation of stable arrangements for the hydrated uranyl ion along with its mono- and dichloride complexes. Results at 25 and 300 °C from jobs 2a and 2d1 suggest that equatorial water coordination of the hydrated uranyl aqua ion drops slightly (5–4.9) over this temperature interval – such a subtle change is consistent with the prior 25–200 °C MD calculations of [102] but somewhat at odds with the experimental fits reported here (Section 4.1) and in prior literature [135,153] which suggest more drastic decreases in equatorial water coordination (around 3–4 expected at 250 °C).

Calculated structures for uranyl chloride complexes suggest a decrease in coordinating water molecules as temperature increases with the monochloride complex changing from 4 (at 150 and 300 °C jobs 2c, 2d2, and 2e) to 3.3 (at 400 °C job 2i1) and the dichloride complex changing from 2.8 (300 °C job 2 f) to 2.2 (400 °C job 2 h). However, it should be noted that calculated hydration for the dichloride complex at 400 °C appears to be dependent on the job's initial configuration – jobs 2 h and 2i were both conducted at 400 °C but the former initiated with a structure of $[UO_2(H_2O)_5Cl]^+$ and the latter with $[UO_2(H_2O)_5Cl_2]^0$ – thus while job 2 h suggests dichloride complex hydration to be 2.2 job 2i suggests a hydration of 2.9. Evidently, longer simulation times may be appropriate in future investigations. Regardless, the suggestion that the number of equatorially coordinated waters decreases in uranyl chloride complexes as temperature increases is consistent with our experimental XAS observations (Section 4.2).

As in the box 1 sulfate calculations increasing pressure seems to stabilise higher numbers of equatorially coordinated water molecules though at no point was total coordination (waters and chlorides) calculated to rise above 5. These MD results also suggest that for a given concentration of chloride the dichloride complex supersedes the monochloride complex which again is completely in line with our experimental observations.

4. Discussion

The results reported here serve to consolidate present understanding or uranyl speciation at elevated temperatures by in situ characterisation

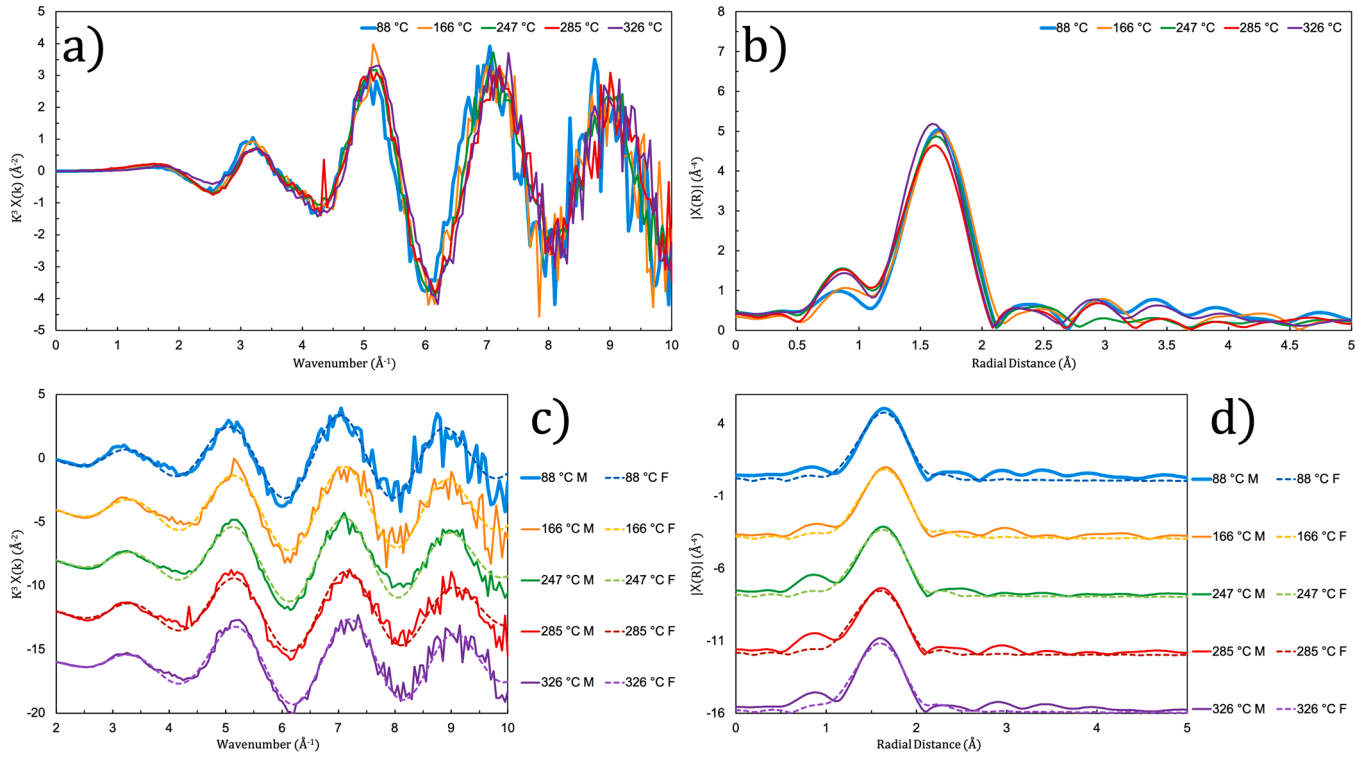

Fig. 12. Plots of EXAFS data and fits for Solution G, probably predominated by $UO_2(OH)_4^{2-}$. **a)** k^3-weighted EXAFS spectra. **b)** Magnitude of Fourier transforms of k^3-weighted EXAFS spectra. **c)** Measured EXAFS spectra (solid lines) plotted alongside modelled spectra (dashed lines) derived from our fitting procedure. **d)** Magnitude of Fourier transforms of measured (solid lines) and modelled (dashed lines) EXAFS spectra. Fourier transforms have not been phase corrected.

Table 15
Derived fitting parameters for Solution G. ΔE was permitted to change at each temperature but was constant across scattering paths. U – O(water) parameters were set to be identical at all temperatures. (f) indicates the parameter was fixed during fitting. R – bond length, N – Coordination, DW – Debye-Waller factor. All reported uncertainties correspond to a 1σ confidence interval.

Path	T (°C)	R (Å)	N	DW (σ^2, Å^2)	ΔE (eV)
Solution F					
U – O (axial)	88	1.89 (1)	2(f)	0.0070	-0.46
	166	1.88 (1)	2(f)	0.0088	0.68
	247	1.87 (1)	2(f)	0.0071	1.14
	285	1.86 (1)	2(f)	0.0069	1.07
	326	1.84 (1)	2(f)	0.0080	0.56
U – O (hydroxyl)	88	2.27 (1)	4.19 ± 0.84	0.0043	
	166	2.27 (1)	3.97 ± 0.78	0.0033	
	247	2.27 (1)	3.91 ± 0.70	0.0042	
	285	2.26 (1)	4.08 ± 0.79	0.0053	
	326	2.25 (1)	3.48 ± 0.75	0.0026	
U – O (water)	All Temps	2.42(f)	1(f)	0.0032(f)	

of complexes present in solution and may help inform further computational efforts not only for uranyl but for other actinides as well. Regarding the uranyl chloride and sulfate systems, the lack of any drastic temperature-linked coordination changes coupled with good general agreement between inferred speciation and calculated speciation determined using the data derived by Migdisov et al. [112], Alcorn et al. [2] and Kalintsev et al. [82] validates the speciation models used by these works as well as the thermodynamic properties that they report. The large swathe of data reported here should also prove valuable in informing any further computational work focussed on the speciation behaviour of aqueous actinides particularly those that are difficult to conduct experiments with like neptunium and plutonium.

It should be noted that in many of the fitting models reported here the Debye-Waller (DW) factor for the equatorial water-bound oxygen and sulfur atoms seems to drop with temperature. Similar patterns were observed by Schofield et al. [135] and Testemale [153]. This may seem unusual given that the DW factor is generally understood as a measure of thermal disorder and should steadily increase in temperature. Indeed, for all the other bonding atoms (axial oxygens, equatorial ligands, equatorial oxygens associated with carbonate atoms etc.) this is case. However, the DW factor also accounts for general structural disorder as well and thus will be affected by the structural arrangement of a given atom type around a target [83]. As temperature increases the coordination of equatorial water oxygen decreases – this is likely to be accompanied by a transition from a pentagonal bi-pyramid structure to a tetragonal bi-pyramid leading to different electrostatic/structural/vibrational dynamics in turn leading to unusual DW-temperature trends. Where the structure or arrangement of a bond type does not really change as in the axial oxygen atoms then the DW-temperature trend behaves as expected.

4.1. *The effect of temperature on the structure of uranyl complexes*

The effect of temperature on the structure of uranyl complexes appears to be common over most of the complexes characterised in this study and those characterised in prior works [119,135,153,7,8]. Equatorial oxygen coordination decreased in nearly all cases with the most significant changes occurring at temperatures above 200 °C. This is consistent with the computational study of [102] who suggested that

Table 16
Simulation details and results for box 1 calculations. Note that the number of water molecules in each 'stable species' is a weighted average using the time that a given integer number of coordinating waters was present as the weighting factor.

Job ID	T (C), P (bar)	Time (ps)	Initial configuration	Stable species	U=O_2		U-OH_2/U-OH (*)			U-S			U-O (SO_4)		
					R (Å)	σ^2 (Å^2)	R (Å)	CN	σ^2 (Å^2)	R (Å)	CN	σ^2 (Å^2)	R (Å)	CN	σ^2 (Å^2)
1a	150, 600	15.8	$[UO_2(H_2O)_7]^{2+}$	$[UO_2(H_2O)_5]^{2+}$	1.82	0.001	2.46	5	0.0110						
1b	300, 600	0.7–12.7	$[UO_2(H_2O)_6(SO_4)]^0$	$[UO_2(H_2O)(OH)(HSO_4)]^{2-}$	1.84	0.0021	2.23 * 2.51	1 1	0.0305	3.13/ 3.74	2		2.41	2	
	300, 600	12.7–27.7		$[UO_2(H_2O)_2(OH)(SO_4)_2]^{3-}$			2.54	2	0.0200				2.42	2.7	
1c	400, 600	15.3	$[UO_2(H_2O)_4(SO_4)]^0$	$[UO_2(H_2O)_{1.9}(OH)(SO_4)]^-$	1.85	0.0022	2.19 * 2.55	1 1.9		3.10/ 3.67	1		2.39	1.6	
1d	400, 3k	15.8	$[UO_2(H_2O)_4(SO_4)]^0$	$[UO_2(H_2O)_2(OH)(SO_4)]^-$	1.84	0.0020	2.19 * 2.50	1 2	0.0072	3.10/ 3.66	1		2.30/ 2.41	1.3	
1e	400, 5k	16.89	$[UO_2(H_2O)_6(SO_4)]^0$	$[UO_2(H_2O)_{2.3}(SO_4)]^0$	1.85	0.0020	2.50	2.3		3.16/ 3.73	1	0.0117/ 0.0289	2.38/ 2.52	1.5	0.0207/ 0.0258
1 g	400, 20k	18.97	$[UO_2(H_2O)_6]^{2+}$	$[UO_2(H_2O)_{3.1}(SO_4)]^0$	1.83	0.0022	2.4	3.1		3.15/ 3.67	1		2.4	1.6	

equatorial coordination was near-constant up to 200 ºC for the pure uranyl ion.

The exception to this trend was the uranyl carbonate complex $UO_2(CO_3)_3^{4-}$ present in Solution F, which, similar to the citrate dimer complex characterised by Bailey et al. [8] up to 200 ºC, was accurately modelled presuming no coordination changes at all with temperature – this is consistent with both complexes containing no equatorially bound water. All equatorial oxygens in both complexes are instead contributed by bidentately bound equatorial complexes – carbonate or citrate.

The validity of a fixed coordination model for Solution F whose dataset displays a systematic decrease in FT peak magnitude highlights a particular issue of EXAFS fitting. In other solutions the assertion that equatorial oxygen coordination systematically decreased with temperature was linked to observations of the decrease in the magnitude of relevant equatorial oxygen linked peaks (typically found at ~1.7–2.0 Å) in the FTs of solution spectra. However, despite a similar decrease in peak magnitude observed for solution F a model with fixed equatorial oxygen coordination was readily able to explain our measured data. This was due to the correlation between peak magnitude, coordination and DW factors during the fitting process – in the case of solution F, peak magnitude decrease was accounted for in the model by an increasing DW factor. This raises the question of whether the observed drops in peak magnitudes of other solutions were truly due to changes in coordination. To test this, we altered the fitting model of Solution A by fixing equatorial oxygen coordination to 5 at all temperatures while still permitting the DW factor to float. We found that such a model was unable to adequately replicate our measured data with fits becoming increasingly poor for higher temperature data. This in turn suggests that despite the correlations between peak magnitude, coordination and DW factors the fitting procedure used is probably robust enough to distinguish the effects of the DW factor and coordination on peak magnitude – at least to some extent. Further, the linkage between peak magnitude and coordination decrease is strengthened by ab initio molecular dynamics results reported in this work. Our simulations noted temperature-linked drops in equatorial coordination consistent with our EXAFS fitting results. It is through this multi-faceted approach that we can, with some measure of confidence, state that the coordination values generated by our EXAFS fits are reflective of the truth even if their precision leaves something to be desired.

4.2. *A proxy for the structures of neptunyl and plutonyl complexes at high temperatures?*

An additional benefit of the work described here is its potential applicability to the complexation behaviour of plutonium and neptunium aqueous complexes. These two radionuclides while generally irrelevant in natural ore-forming systems are of concern when considering geological nuclear waste repositories as they are a component of some high-level waste forms [46,110]. When mobile in groundwater systems, neptunium is generally present in its pentavalent oxidation state while plutonium may be present either in its pentavalent or hexavalent states [132]. In both pentavalent and hexavalent states the two elements typically manifest as linear actinyl ($Ac(V)O_2^+$/$Ac(VI)O_2^{2+}$) ions with structures very similar to the uranyl ion. At ambient conditions these ions can form a wide variety of inorganic complexes with stoichiometries and structures nearly identical to their uranyl counterparts. Allen et al., ($year$) [10,28,29,4,50,52,55,75,9]. Table 18 lists presently known neptunyl(V) and plutonyl(V/VI) chloride, sulfate, carbonate and hydroxyl complexes with clear uranyl(VI) analogues [55].

A number of limitations and concerns render it difficult to apply the same high temperature experimental techniques used in this work on the plutonyl and neptunyl systems. But, given the commonality in the structures of uranyl, neptunyl and plutonyl complexes at room temperature, we can tentatively assert that as temperature increases up to 250–300 ºC complexes of the latter two elements likely do not

Table 17
Simulation details and results for box 2 calculations.

Job ID	T (C), P (bar)	Time (ps)	Initial configuration	Stable species	U=O_2		U-OH_2/U-OH (*)			U-Cl		
					R (Å)	σ^2 (Å^2)	R (Å)	CN	σ^2 (Å^2)	R (Å)	CN	σ^2 (Å^2)
2a	25, 1	22.6	$[UO_2]^{2+}$	$[UO_2(H_2O)_5]^{2+}$	1.82	0.0009	2.44	5	0.0082			
2b	150, 600	21.2	$[UO_2(H_2O)_5]^{2+}$	$[UO_2(H_2O)_5]^{2+}$	1.82	0.0009	2.46	5	0.0107			
2c	150, 600	18.8	$[UO_2(H_2O)Cl]^{+}$	$[UO_2(H_2O)_4Cl]^{+}$	1.81	0.0011	2.45	4	0.0125	2.76	1	0.0114
2d1	300, 600	0–20.8	$[UO_2]^{2+}$	$[UO_2(H_2O)_{4.9}]^{2+}$	1.82	0.0016	2.49	4.9	0.0171			
2d2		20.8–27.9		$[UO_2(H_2O)_4Cl]^{+}$	1.82	0.0016	2.53	4	0.0244	2.75	1	0.0156
2e	300, 600	17.2	$[UO_2(H_2O)Cl]^{+}$	$[UO_2(H_2O)_4Cl]^{+}$	1.82	0.0130	2.53	4	0.0258	2.74	1	0.0152
2 f	300, 600	17.2	$[UO_2(H_2O)_4Cl_2]^{0}$	$[UO_2(H_2O)_{2.8}Cl_2]^{0}$	1.82	0.0016	2.51	2.8		2.77	2	0.0209
2 g	400, 600	22.6	$[UO_2(H_2O)_4]^{2+}$	$[UO_2(H_2O)_{3.1}(OH)]^{+}$	1.83	0.0017	2.15*	1	0.0053			
							2.48	3.1				
2 h	400, 600	17.5	$[UO_2(H_2O)_5Cl]^{+}$	$[UO_2(H_2O)_{2.2}Cl_2]^{0}$	1.82	0.0017	2.46	2.2		2.69	2	0.0120
2i1	400, 600	0–12.4	$[UO_2(H_2O)_5Cl_2]^{0}$	$[UO_2(H_2O)_{3.3}Cl]^{+}$	1.81	0.0024	2.44	3.3		2.72	1	0.0151
2i2		12.4–17.5		$[UO_2(H_2O)_{2.9}Cl_2]^{0}$	1.82	0.0016	2.5	2.9		2.69	2	0.0196
2j	400, 20k	24.2	$[UO_2(H_2O)]^{2+}$	$[UO_2(H_2O)_5]^{2+}$	1.83	0.0021	2.45	5				
2k	400, 20k	26.1	$[UO_2(H_2O)Cl]^{+}$	$[UO_2(H_2O)_{2.9}Cl_2]^{0}$	1.82	0.0018	2.42	2.9		2.77	2	0.0218
2 l	400, 20k	27.0	$[UO_2Cl_2]^{0}$	$[UO_2(H_2O)_{2.9}Cl_2]^{0}$	1.82	0.0021	2.42	2.9		2.76	2	0.0192

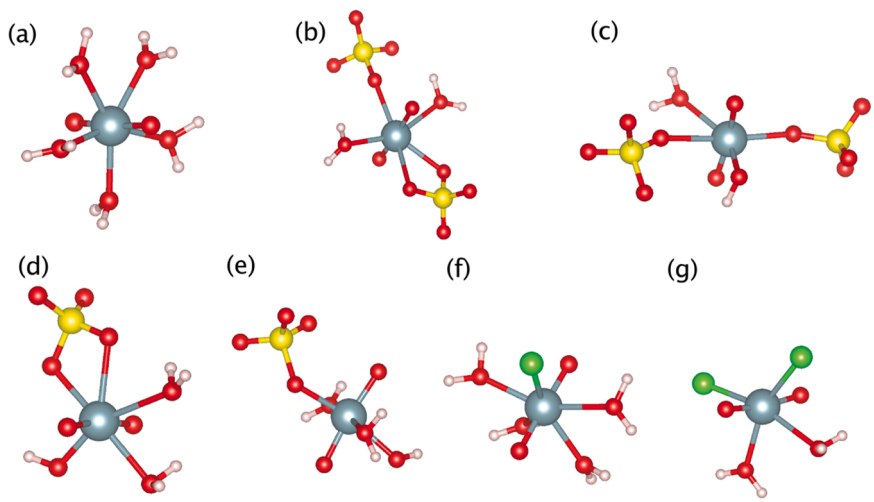

Fig. 13. structure of hydrated uranyl and UO_2^{2+}-Cl^-/SO_4^{2-} complexes. (a). $UO_2(H_2O)_5^{2+}$; (b). $UO_2(H_2O)_2(SO_4)_2^{2-}$, with 1 SO_4^{2-} bonding as bidentate and 1 SO_4^{2-} as monodentate; (c). $UO_2(H_2O)(SO_4)_2(OH)^{3-}$, with 2 SO_4^{2-} bonding as monodentate; (d) and (e). $UO_2(H_2O)_2(SO_4)(OH)^-$, with SO_4^{2-} bonding as bidentate and monodentate, respectively; (f). $UO_2(H_2O)_4Cl^+$; (g). $UO_2(H_2O)_2Cl_2$.

experience any major structural or stoichiometric changes. Their complexes likely follow a simple, intuitive progression to higher-ligand-number species and trend towards reduced hydration. Exact shifts in hydration will likely differ between uranyl, neptunyl and plutonyl and the computational work of [102] suggests that U(V) hydration drops more drastically with temperature relative to U(VI) – this is probably also true of Np(V) and Pu(V).

4.3. Possibilities for future work

With all this in mind it would undoubtedly be instructive to conduct similar hydrothermal experiments discussed here utilising different structural characterisation techniques such as HEXS or NMR. To our knowledge no experiments utilising these techniques have yet been conducted for uranyl or its complexes at temperatures above ambient.

While we have reported high temperature structural data for a wide variety of uranyl complexes in this work there still remain a number of fruitful possibilities for future investigation. Our data suggest that the $UO_2Cl_3^-$ complex may become more prevalent at elevated temperatures – however no reliable data (thermodynamic or structural) yet exist for this complex at above-ambient temperatures. We were unable to confidently experimentally identify the presence of monodentate uranyl sulfate complexes. A closer investigation into the possible effect of solution ionic strength on the bonding behaviour of sulfate may elucidate why. Additionally/alternatively, some other technique beyond EXAFS might be utilised to this end as the single scatter peak of sulfur in monodentately-bound sulfate is somewhat difficult to resolve with EXAFS. Carbonate complexes bear closer scrutiny with particular care being taken to ensure that true solid-aqueous equilibrium has been achieved prior to measurements. It is likely this will necessitate prior heat treatment of target solutions to avoid cutting into valuable beam-time. If possible, the mono- and dicarbonate complexes along with their relationship with the tricarbonate should also be investigated. The investigation of hydroxyl complexes has been very limited in this work only targeting their behaviour at very high pH. While more neutral pH conditions may be difficult to study with XAS on account of uranium's low solubility at such conditions, sufficient uranium is soluble at moderately acidic (~pH 4) conditions [159] that should permit study of polynuclear hydroxyl complexes and their stability at elevated temperatures. Of particular interest would be direct observation of the transition from polynuclear to mononuclear hydroxyl complexes as temperature rises, a phenomenon that has been inferred in prior time-resolved laser fluorescence spectroscopy works [167,44,87,88].

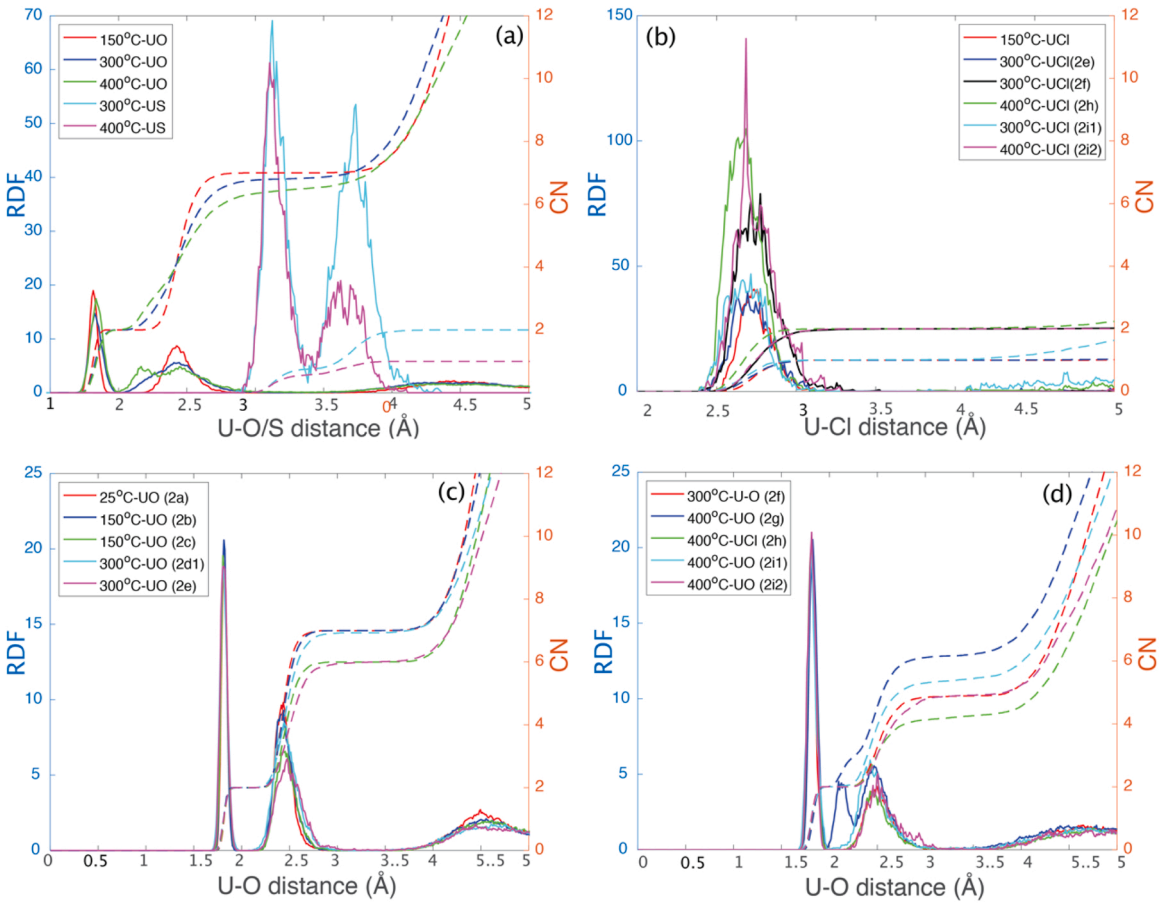

Fig. 14. Radial distribution functions (RDF, left axis, solid lines) and the integral of RDF (coordination number, CN, right axis, dashed line) of the simulations. (a). U-O and U-S of box1; (b) U-Cl of box 2; (c) and (d). U-O of box 2.

5. Conclusions

In summary, the structures of uranyl and its chloride, sulfate, carbonate and hydroxyl complexes generally change relatively little between 25 °C and ~200 °C. At higher temperatures up to 326 °C the number of equatorial water molecules around these complexes appears to drastically decrease. Our results for the pure uranyl ion at high temperature generally agree with prior high temperature works though we suggest a more subtle trend of equatorial water loss with temperature in line with prior computational work. Given their structural similarities we also expect that similar temperature-dependent behaviour should be observed for the environmentally relevant complexes of $Np(V)O_2^+$, $Pu(V)O_2^+$ and $Pu(VI)O_2^{2+}$which is important to note given the practical difficulties of studying them with EXAFS at high temperature. We have observed temperature-linked speciation changes in the uranyl-chloride system with $UO_2Cl_2^0$ and possibly $UO_2Cl_3^-$ becoming increasingly more prevalent as temperature rises. In addition, we have made comparisons between implied chloride speciation derived from our EXAFS data and calculated speciation using data reported by Dargent et al. [34] and Migdisov et al. [112]. We have found that data from the latter publication far better describe our data and recommend using it over the former publication's data. Regarding sulfate, both $UO_2SO_4^0$ and $UO_2(SO_4)_2^{2-}$ have been well characterised however we were unable to find convincing evidence for the presence of monodentate sulfate and suggest that the monodentate-bidentate relationship may be sensitive to solution ionic strength. We have also tested the predictive capacity of the thermodynamic data reported by Alcorn et al. [2] and Kalintsev et al. [82] for the uranyl sulfate complexes and found that they both adequately described speciation in the studied solutions. Uranyl tricarbonate ($UO_2(CO_3)_3^{4-}$) was identified over a range of temperatures and its structure was found to be practically identical over all temperatures likely due to the lack of any equatorially bound water molecules. We have also characterised uranyl in a highly alkaline NaOH solution and suggest that at such conditions it may manifest as the $UO_2(OH)_4^{2-}$ complex coupled with a single equatorial water molecule thus potentially reconciling the results of previously contradictory experimental and computational works. Results from MD supports the trends determined experimentally with XAS and have additionally noted that as pressure rises equatorial coordination of water rises and U-O(ax) bonding distances contract with U-O(ax) distances remain relatively unchanged. Absolute values for coordination and bond distances calculated by MD were however a little higher than those determined experimentally. Altogether this work has served to consolidate and enhance our present understanding of the high temperature aqueous behaviour of uranium, neptunium and plutonium with applications to both natural and artificial hydrothermal systems.

Declaration of Competing Interest

The authors declare the following financial interests/personal relationships which may be considered as potential competing interests: Joel Brugger reports financial support was provided by the Australian Research Council.

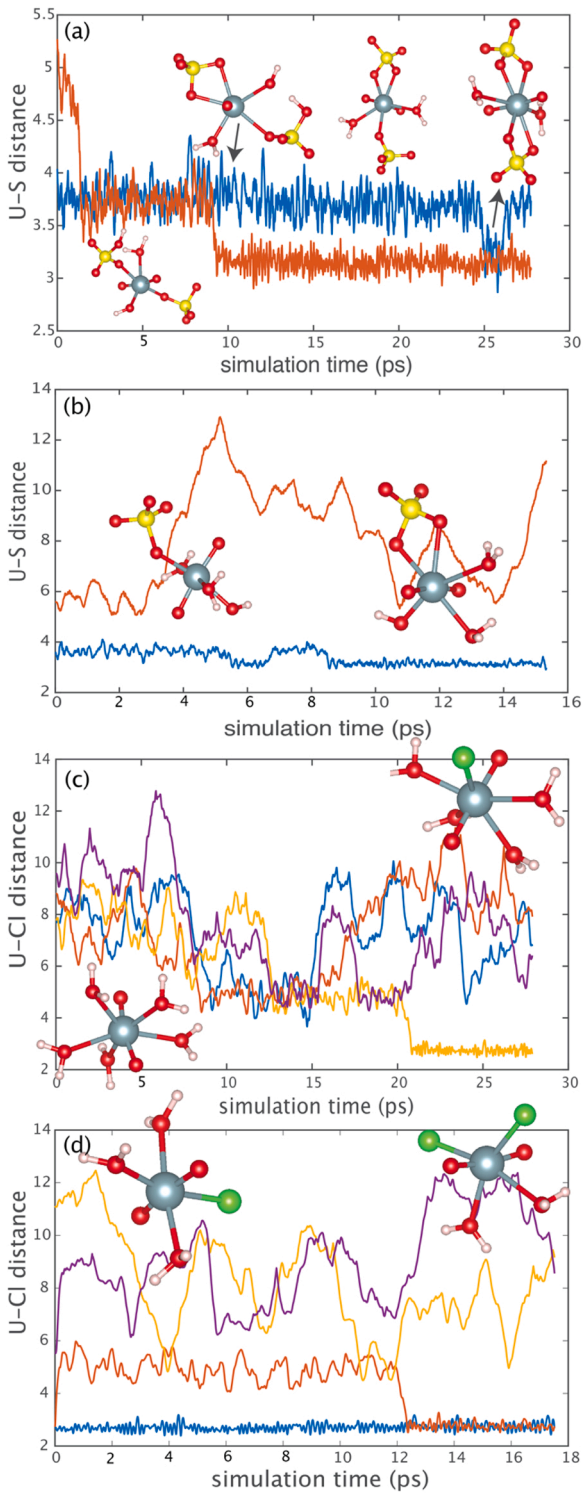

Fig. 15. The distance of U-S/Cl over time of simulation jobs: (a), 1b; (b), 1c; (c), 2d; (d), 2i. Each coloured line corresponds to an individual SO_4^{2-} or Cl^- ion in the simulation box. Hence, the two coloured lines in (a) and (b) each correspond to one of the SO_4^{2-} molecules present in box 1. Note the differences in distance variance between stably bonded and unbound ligands – particularly evident in b-d.

Table 18
Binary hydroxyl, chloride, sulfate and carbonate Np(V), Pu(V) and Pu(VI) complexes with analogues in the U(VI) system.

Np (V)	Pu (V)	Pu (VI)	
NpO_2OH^0	PuO_2^+	PuO_2^{2+}	$PuO_2SO_4^0$
$NpO_2(OH)_2^-$	PuO_2OH^0	PuO_2OH^+	$PuO_2(SO_4)_2^{2-}$
$NpO_2SO_4^-$	$PuO_2SO_4^-$	$PuO_2(OH)_2^0$	$PuO_2CO_3^0$
$NpO_2CO_3^-$	$PuO_2CO_3^-$	$PuO_2(OH)_3^-$	$PuO_2(CO_3)_2^{2-}$
$NpO_2(CO_3)_2^{3-}$	$PuO_2(CO_3)_2^{3-}$	$(PuO_2)_2(OH)_2^{2+}$	$PuO_2(CO_3)_3^{4-}$
$NpO_2(CO_3)_3^{5-}$	$PuO_2(CO_3)_3^{5-}$	PuO_2Cl^+	$(PuO_2)_3(CO_3)_6^{6-}$
$(NpO_2)_3(CO_3)_6^{6-}$		$PuO_2Cl_2^0$	

Data Availability

Data will be made available on request.

Acknowledgements

This research was supported by the Laboratory Directed Research and Development program of Los Alamos National Laboratory under project number 20180007DR; the Department of Energy's Spent Fuel and Waste Disposition campaign (SF-23LA01030902); by the Australian Research Council Grant DP190100216; and by an Australian Government Research Training Program Scholarship to A. Kalintsev. The MD simulation of this work was supported by resources provided by the Pawsey Supercomputing Centre with funding from the Australian Government and the Government of Western Australia, the National Computational Infrastructure (NCI) supported by the Australian Government, and the high-performance computers in CSIRO. We thank Prof. Michael Bühl for sharing the pseudopotential of uranium for ab initio MD simulations.

Environmental Implication

When high level nuclear waste is buried there is a risk that the engineered barriers put in place to isolate it from the environment could fail and thus permit it to interact with groundwater. While most waste repository designs do not expect to realise local-rock temperatures above 100 °C some designs may experience temperatures in excess of 200 °C with waste-surface temperatures reaching 300–400 °C. By understanding uranium's complexation behaviour under such conditions, we can accurately model the uranium solubility in heated groundwaters and thus assess the degree of uranium migration away from buried waste sites and into the environment.

Appendix A. Supporting information

Supplementary data associated with this article can be found in the online version at doi:10.1016/j.jhazmat.2023.131309.

References

[1] Aberg, M., Ferri, D., Glaser, J., Grenthe, I., 1983. Structure of the Hydrated Dioxouranium(VI) ion in aqueous solution. An X-ray-diffraction and H1 NMR study. Inorg Chem 22, 3986–3989.
[2] Alcorn, C.D., Cox, J.S., Applegarth, L., Tremaine, P.R., 2019. Investigation of uranyl sulfate complexation under hydrothermal conditions by quantitative raman spectroscopy and density functional theory. J Phys Chem B 123, 7385–7409.
[3] Allen, P.G., Bucher, J.J., Clark, D.L., Edelstein, N.M., Ekberg, S.A., Gohdes, J.W., Hudson, E.A., Kaltsoyannis, N., Lukens, W.W., Neu, M.P., Palmer, P.D., Reich, T., Shuh, D.K., Tait, C.D., Zwick, B.D., 1995. Multinuclear NMR, Raman, EXAFS, and X-ray diffraction studies of uranyl carbonate complexes in near-neutral aqueous

solution. X-ray structure of [C(NH2)3]6[(UO2)3(CO3)6].cntdot.6.5H2O. Inorg Chem 34, 4797–4807.
[4] Allen, P.G., Bucher, J.J., Shuh, D.K., Edelstein, N.M., Reich, T., 1997. Investigation of aquo and chloro complexes of UO22+, NpO2+, Np4+, and Pu3+ by X-ray absorption fine structure spectroscopy. Inorg Chem 36, 4676–4683.
[5] Atta-Fynn, R., Johnson, D.F., Bylaska, E.J., Ilton, E.S., Schenter, G.K., de Jong, W. A., 2012. Structure and Hydrolysis of the U(IV), U(V), and U(VI) Aqua Ions from Ab Initio Molecular Simulations. Inorg Chem 51, 3016–3024.
[6] Austin, J.P., Sundararajan, M., Vincent, M.A., Hillier, I.H., 2009. The geometric structures, vibrational frequencies and redox properties of the actinyl coordination complexes AnO2(L)nm; An = U, Pu, Np; L = H2O, Cl–, CO32-, CH3CO2–, OH–) in aqueous solution, studied by density functional theory methods. Dalton Trans 5902.
[7] Bailey, E., Mosselmans, J., Schofield, P., 2004. Uranyl acetate speciation in aqueous solutions—an XAS study between 25° C and 250° C. Geochim Cosmochim Acta 68, 1711–1722.
[8] Bailey, E., Mosselmans, J., Schofield, P., 2005. Uranyl-citrate speciation in acidic aqueous solutions—an XAS study between 25 and 200C. Chem Geol 216, 1–16.
[9] Balasubramanian, K., Cao, Z., 2007. Theoretical studies on structures of neptunyl carbonates: NPO2(CO_3)(m)(H2O)(n)(q-) (m=1-3, n=0-3) in aqueous solution. Inorg Chem 46, 10510–10519.
[10] Balasubramanian, K., Chaudhuri, D., 2008. Computational modeling of environmental plutonyl mono-, di- and tricarbonate complexes with Ca counterions: Structures and spectra: Puo(2)(CO_3)(2)(2-), PuO2(CO_3)(2)Ca, and PuO2(CO_3)(3)Ca-3. Chem Phys Lett 450, 196–202.
[11] Bankura, A., Karmakar, A., Carnevale, V., Chandra, A., Klein, M.L., 2014. Structure, dynamics, and spectral diffusion of water from first-principles molecular dynamics. J Phys Chem C 118, 29401–29411.
[12] Bastrakov, E., Jaireth, S., Mernagh, T., 2010. Solubility of uranium in hydrothermal fluids at 25C to 300C. In: Australia, G. (Ed.), Implications for the Formation of Uranium Deposits. Canberra, p. 91.
[13] Bean, A.C., Xu, Y., Danis, J.A., Albrecht-Schmitt, T.E., Scott, B.L., Runde, W., 2002. Aqueous reactions of U (VI) at high chloride concentrations: syntheses and structures of new uranyl chloride polymers. Inorg Chem 41, 6775–6779.
[14] Becke, A.D., 1988. Density-functional exchange-energy approximation with correct asymptotic behavior. Phys Rev A 38, 3098.
[15] Bernhard, G., Geipel, G., Reich, T., Brendler, V., Amayri, S., Nitsche, H., 2001. Uranyl(VI) carbonate complex formation: validation of the Ca2UO2(CO_3)(3)(aq.) species. Radiochim Acta 89, 511–518.
[16] Brugger, J., Liu, W., Etschmann, B., Mei, Y., Sherman, D.M., Testemale, D., 2016. A review of the coordination chemistry of hydrothermal systems, or do coordination changes make ore deposits? Chem Geol 447, 219–253.
[17] Bühl, M., Diss, R., Wipff, G., 2005. Coordination environment of aqueous uranyl (VI) ion. J Am Chem Soc 127, 13506–13507.
[18] Bühl, M., Schreckenbach, G., 2010. Oxygen exchange in uranyl hydroxide via two "nonclassical" ions. Inorg Chem 49, 3821–3827.
[19] Bühl, M., Schreckenbach, G., Sieffert, N., Wipff, G., 2009. Effect of counterions on the structure and stability of aqueous uranyl (VI) complexes. a first-principles molecular dynamics study. Inorg Chem 48, 9977–9979.
[20] Bühl, M., Sieffert, N., Golubnychiy, V., Wipff, G., 2008. Density functional theory study of uranium (VI) aquo chloro complexes in aqueous solution. J Phys Chem A 112, 2428–2436.
[21] Bühl, M., Wipff, G., 2011. Insights into uranyl chemistry from molecular dynamics simulations. ChemPhysChem 12, 3095–3105.
[22] Burns, P.C., Hayden, L.A., 2002. A uranyl sulfate cluster in Na10 [(UO2)(SO4) 4] (SO4) 2·3H2O. Acta Crystallogr Sect C: Cryst Struct Commun 58, i121–i123.
[23] Buscheck, T.A., Glascoe, L.G., Lee, K.H., Gansemer, J., Sun, Y., Mansoor, K., 2003. Validation of the multiscale thermohydrologic model used for analysis of a proposed repository at yucca mountain. J Contam Hydrol 62–63, 421–440.
[24] Campbell, L., Rehr, J., Schenter, G., McCarthy, M., Dixon, D., 1999. XAFS Debye–Waller factors in aqueous Cr+ 3 from molecular dynamics. J Synchrotron Radiat 6, 310–312.
[25] Cao, Z., Balasubramanian, K., 2009. Theoretical studies of UO2(OH)(H2O)n+, UO2(OH)2(H2O)n, NpO2(OH)(H2O)n, and PuO2(OH)(H2O)n+ (n≤21) complexes in aqueous solution. J Chem Phys 131, 164504.
[26] Car, R., Parrinello, M., 1985. Unified approach for molecular dynamics and density-functional theory. Phys Rev Lett 55, 2471.
[27] Clark, D.L., Conradson, S.D., Donohoe, R.J., Keogh, D.W., Morris, D.E., Palmer, P. D., Rogers, R.D., Tait, C.D., 1999. Chemical speciation of the uranyl ion under highly alkaline conditions. Synthesis, structures, and oxo ligand exchange dynamics. Inorg Chem 38, 1456–1466.
[28] Clark, D.L., Conradson, S.D., Ekberg, S.A., Hess, N.J., Neu, M.P., Palmer, P.D., Runde, W., Tait, C.D., 1996. EXAFS studies of pentavalent neptunium carbonate complexes. Structural elucidation of the principal constituents of neptunium in groundwater environments. J Am Chem Soc 118, 2089–2090.
[29] Clark, D.L., Hobart, D.E., Neu, M.P., 1995. Actinide carbonate complexes and their importance in actinide environmental chemistry. Chem Rev 95, 25–48.
[30] Craw, J.S., Vincent, M.A., Hillier, I.H., Wallwork, A.L., 1995. Ab initio quantum chemical calculations on Uranyl UO22+,Plutonyl PuO22+, and their nitrates and sulfates. J Phys Chem 99, 10181–10185.
[31] Cross, J., Moreton, A., Tweed, C., 1995. Thermodynamic modelling of radioactive waste disposal. Assessment of near-field solubility. UK Nirex Ltd.
[32] Cuney, M., 2009. The extreme diversity of uranium deposits. Miner Depos 44, 3–9.
[33] Dargent, M., Dubessy, J., Bazarkina, E., Truche, L., 2018. Uranyl-chloride speciation and uranium transport in hydrothermal brines: comment on Migdisov et al.(2018)" A spectroscopic study of uranyl speciation in chloride-bearing solutions at temperatures up to 250° C". Geochim Cosmochim Acta 222, 130-145 Geochim Cosmochim Acta 235, 505–508.
[34] Dargent, M., Dubessy, J., Truche, L., Bazarkina, E.F., Nguyen-Trung, C., Robert, P., 2013. Experimental study of uranyl(VI) chloride complex formation in acidic LiCl aqueous solutions under hydrothermal conditions (T 1⁄4 21C–350C, Psat) using Raman spectroscopy. Eur J Mineral 25, 765–775.
[35] Das, A., Ali, S.M., 2019. Molecular dynamics simulation studies on structure, dynamics, and thermodynamics of uranyl nitrate solution at various acid concentrations. J Phys Chem B 123, 4571–4586.
[36] de Jong, W.A., Aprà, E., Windus, T.L., Nichols, J.A., Harrison, R.J., Gutowski, K. E., Dixon, D.A., 2005. Complexation of the carbonate, nitrate, and acetate anions with the uranyl dication: density functional studies with relativistic effective core potentials. J Phys Chem A 109, 11568–11577.
[37] Docrat, T., Mosselmans, J., Charnock, J., Whiteley, M., Collison, D., Livens, F., Jones, C., Edmiston, M., 1999. X-ray absorption spectroscopy of tricarbonatodioxouranate (V),[UO2 (CO_3) 3] 5-, in aqueous solution. Inorg Chem 38, 1879–1882.
[38] Dong, W., Brooks, S.C., 2008. Formation of aqueous MgUO2 (CO_3) 32− complex and uranium anion exchange mechanism onto an exchange resin. Environ Sci Technol 42, 1979–1983.
[39] Dong, W.M., Brooks, S.C., 2006. Determination of the formation constants of ternary complexes of uranyl and carbonate with alkaline earth metals (Mg2+, Ca2+, Sr2+, and Ba2+) using anion exchange method. Environ Sci Technol 40, 4689–4695.
[40] Driesner, T., 2007. The System H2O- NaCl. II. Correlations for molar volume, enthalpy, and isobaric heat capacity from 0 to 1000 degrees C, 1 to 5000 bar, and 0 to 1 XNaCl. Geochim Cosmochim Acta 71, 4902–4919.
[41] Driesner, T., Heinrich, C.A., 2007. The system H2O- NaCl. I. Correlation formulae for phase relations in temperature- pressure-composition space from 0 to 1000°C, 0 to 5000 bar, and 0 to 1 XNaCl. Geochim Cosmochim Acta 71, 4880–4901.
[42] Du, S., Yoo, S., Li, J., 2017. Comparison of the melting temperatures of classical and quantum water potential models. Front Phys 5, 34.
[43] Duvail, M., Dumas, T., Paquet, A., Coste, A., Berthon, L., Guilbaud, P., 2019. UO 2 2+ structure in solvent extraction phases resolved at molecular and supramolecular scales: a combined molecular dynamics, EXAFS and SWAXS approach. Phys Chem Chem Phys 21, 7894–7906.
[44] Eliet, V., Grenthe, I., Bidoglio, G., 2000. Time-resolved laser-induced fluorescence of uranium(VI) hydroxo-complexes at different temperatures. Appl Spectrosc 54, 99–105.
[45] Etschmann, B.E., Mei, Y., Liu, W., Sherman, D., Testemale, D., Müller, H., Rae, N., Kappen, P., Brugger, J., 2018. The role of Pb (II) complexes in hydrothermal mass transfer: An X-ray absorption spectroscopic study. Chem Geol 502, 88–106.
[46] Ewing, R.C., 2015. Long-term storage of spent nuclear fuel. Nat Mater 14, 252–257.
[47] Finch, R., Cooper, M., Hawthorne, F., Ewing, R., 1999. Refinement of the crystal structure of rutherfordine. Can Mineral 37, 929–938.
[48] Fischer, A., 2003. Competitive coordination of the uranyl ion by perchlorate and water-the crystal structures of UO2 (ClO4) 2·3H2O and UO2 (ClO4) 2·5H2O and a redetermination of UO2 (ClO4) 2·7H2O. Z Anorg Allg Chem 629, 1012–1016.
[49] Gagliardi, L., Grenthe, I., Roos, B.O., 2001. A theoretical study of the structure of tricarbonatodioxouranate. Inorg Chem 40, 2976–2978.
[50] Gagliardi, L., Roos, B.O., 2002. Coordination of the neptunyl ion with carbonate ions and water: a theoretical study. Inorg Chem 41, 1315–1319.
[51] Gál, M., Goggin, P.L., Mink, J., 1992. Vibrational spectroscopic studies of uranyl complexes in aqueous and non-aqueous solutions. Spectrochim Acta 48A, 121–132.
[52] Garcia-Hernandez, M., Willnauer, C., Kruger, S., Moskaleva, L.V., Rosch, N., 2006. Systematic DFT study of gas phase and solvated uranyl and neptunyl complexes AnO(2)X(4) (n) (An = U, Np; X = F, Cl, OH, n =-2; X = H2O, n =+2). Inorg Chem 45, 1356–1366.
[53] Gillan, M.J., Alfe, D., Michaelides, A., 2016. Perspective: How good is DFT for water? J Chem Phys 144, 130901.
[54] H. Greenberg J. Wen T. Buscheck Scoping thermal analysis of alternative dual-purpose canister disposal concepts. Lawrence Livermore National Lab.(LLNL), Livermore CA (United States) 2013.
[55] Grenthe, I., Plyasunov, A., Runde, W., Konings, R.J.M., Moore, E.E., Gaona, X., Rao, L., Grambow, B. and Smith, A.L. (2020) Second Update on the Chemical Thermodynamics of Uranium, Neptunium, Plutonium, Americium and Technetium. OECD Nuclear Energy Agency, Data Bank, Boulogne-Billancourt, France.
[56] Gu, J.-F., Lu, C.-H., Chen, W.-K., Chen, Y., Xu, K., Huang, X., Zhang, Y.-F., 2012. Electronic structures of Uranyl (VI) carbonate complexes in the aqueous phase. Acta Phys Chim Sin 28, 792–798.
[57] Guan, Q., Mei, Y., Etschmann, B., Louvel, M., Testemale, D., Bastrakov, E., Brugger, J., 2022. Yttrium speciation in sulfate-rich hydrothermal ore-forming fluids. Geochim Cosmochim Acta.
[58] Guan, Q., Mei, Y., Etschmann, B., Testemale, D., Louvel, M., Brugger, J., 2020. Yttrium complexation and hydration in chloride-rich hydrothermal fluids: a combined ab initio molecular dynamics and in situ X-ray absorption spectroscopy study. Geochim Cosmochim Acta 281, 168–189.
[59] Guckel, K., Rossberg, A., Brendler, V., Foerstendorf, H., 2012. Binary and ternary surface complexes of U(VI) on the gibbsite/water interface studied by vibrational and EXAFS spectroscopy. Chem Geol 326, 27–35.

[60] Guckel, K., Tsushima, S., Foerstendorf, H., 2013. Structural characterization of the aqueous dimeric uranium(VI) species: (UO2)(2)CO_3(OH)(3)(-). Dalton Trans 42, 10172–10178.
[61] Guilbaud, P., Wipff, G., 1996. Force field representation of the UO22+ cation from free energy MD simulations in water. Tests on its 18-crown-6 and NO3− adducts, and on its calix[6]arene6− and CMPO complexes. J Mol Struct: Theochem 366, 55–63.
[62] Guillaumont, R., Fanghänel, T., Neck, V., Fuger, J., Palmer, D., Grenthe, I. and Rand, M.H. (2003) Update on the chemical thermodynamics of uranium, neptunium, plutonium, americium and technetium. OECD Nuclear Energy Agency, Data Bank, Issy-les-Moulineaux, France.
[63] Gutowski, K.E., Dixon, D.A., 2006. Predicting the energy of the water exchange reaction and free energy of solvation for the uranyl ion in aqueous solution. J Phys Chem A 110, 8840–8856.
[64] Hardin, E., Price, L.L., Kalinina, E.A., Hadgu, T., Ilgen, A.G., Bryan, C.R., Scaglione, J.M., Banerjee, K., Clarity, J., Jubin, R., 2015. Summary of investigations on technical feasibility of direct disposal of dual-purpose canisters. Sandia National Lab (SNL-NM). Albuq, NM (U S); Sandia.
[65] Haukwa, C.B., Wu, Y.S., Bodvarsson, G.S., 2003. Modeling thermal–hydrological response of the unsaturated zone at Yucca Mountain, Nevada, to thermal load at a potential repository. J Contam Hydrol 62–63, 529–552.
[66] Heinrich, C., Walshe, J., Harrold, B., 1996. Chemical mass transfer modelling of ore-forming hydrothermal systems: current practise and problems. Ore Geol Rev 10, 319–338.
[67] Helgeson, H.C., Kirkham, D.H., Flowers, G.C., 1981. Theoretical prediction of the thermodynamic behaviour of aqueous electrolytes at high pressures and temperatures IV. Calculation of activity coefficients, osmotic coefficients, and apparent molal and standard and relative partial molal properties to 600°C and 5KB. Am J Sci 281, 1249–1516.
[68] Hennig, C., Ikeda, A., Schmeide, K., Brendler, V., Moll, H., Tsushima, S., Scheinhost, A.C., Skanthakumar, S., Wilson, R., Soderholm, L., Servaes, K., Görrler-Walrand, C., Van Deun, R., 2008. The relationship of monodentate and bidentate coordinated uranium(VI) sulfate in aqueous solution. Radiochim Acta 96, 607–611.
[69] Hennig, C., Schmeide, K., Brendler, V., Moll, H., Tsushima, S., Scheinhost, A.C., 2007. EXAFS investigation of U(VI), U(IV), and Th(IV) sulfato complexes in aqueous solution. Inorg Chem 46, 5882–5892.
[70] Hennig, C., Tutschku, J., Rossberg, A., Bernhard, G., Scheinost, A., 2005. Comparative EXAFS investigation of uranium (VI) and-(IV) aquo chloro complexes in solution using a newly developed spectroelectrochemical cell. Inorg Chem 44, 6655–6661.
[71] Hummel, W., Berner, U., Curti, E., Pearson, F., Thoenen, T., 2002. Nagra/PSI chemical thermodynamic data base 01/01. Radiochim Acta 90, 805–813.
[72] Humphrey, W., Dalke, A., Schulten, K., 1996. VMD: visual molecular dynamics. J Mol Graph 14, 33–38.
[73] Ikeda, A., Hennig, C., Tsushima, S., Takao, K., Ikeda, Y., Scheinost, A.C., Bernhard, G., 2007. Comparative study of uranyl(VI) and -(V) carbonato complexes in an aqueous solution. Inorg Chem 46, 4212–4219.
[74] Ikeda-Ohno, A., Hennig, C., Tsushima, S., Scheinost, A.C., Bernhard, G., Yaita, T., 2009. Speciation and structural study of U (IV) and-(VI) in perchloric and nitric acid solutions. Inorg Chem 48, 7201–7210.
[75] Ikeda-Ohno, A., Tsushima, S., Takao, K., Rossberg, A., Funke, H., Scheinost, A.C., Bernhard, G., Yaita, T., Hennig, C., 2009. Neptunium carbonato complexes in aqueous solution: an electrochemical, spectroscopic, and quantum chemical study. Inorg Chem 48, 11779–11787.
[76] Ingram, K.I., Häller, L.J.L., Kaltsoyannis, N., 2006. Density functional theory investigation of the geometric and electronic structures of [UO 2 (H 2 O) m (OH) n] 2− n (n+ m= 5). Dalton Trans 2403–2414.
[77] Jo, Y., Kim, H.-K., Yun, J.-I., 2019. Complexation of UO 2 (CO 3) 3 4− with Mg 2 + at varying temperatures and its effect on U (vi) speciation in groundwater and seawater. Dalton Trans 48, 14769–14776.
[78] Jo, Y., Kirishima, A., Kimuro, S., Kim, H.-K., Yun, J.-I., 2019. Formation of CaUO 2 (CO 3) 3 2− and Ca 2 UO 2 (CO 3) 3 (aq) complexes at variable temperatures (10–70° C). Dalton Trans, 48, 6942–6950.
[79] Johnson, J.W., Oelkers, E.H., Helgeson, H.C., 1992. SUPCRT92: a software package for calculating the standard molal thermodynamic properties of minerals, gases, aqueous species, and reactions from 1 to 5000 bar and 0 to 1000C. Comput Geosci 18, 899–947.
[80] Johnson, L., Niemeyer, M., Klubertanz, G., Siegel, P. and Gribi, P. (2002) Calculations of the temperature evolution of a repository for spent fuel, vitrified high-level waste and intermediate level waste in Opalinus Clay. National Cooperative for the Disposal of Radioactive Waste (NAGRA).
[81] Kalintsev, A., Migdisov, A., Alcorn, C., Baker, J., Brugger, J., Mayanovic, R.A., Akram, N., Guo, X., Xu, H., Boukhalfa, H., Caporuscio, F.A., Viswanathan, H., Jove-Colon, C., Wang, Y., Matteo, E.N., Roback, R., 2021. Uranium carbonate complexes demonstrate drastic decrease in stability at elevated temperatures. Commun Chem 4, 1–8.
[82] Kalintsev, A., Migdisov, A.A., Xu, H., Roback, R., Brugger, J., 2019. Uranyl speciation in sulfate-bearing hydrothermal solutions up to 250 °C. Geochim Cosmochim Acta 267, 75–91.
[83] Kelly, S., Hesterberg, D., Ravel, B., 2008. Analysis of soils and minerals using X-ray absorption spectroscopy. Methods of soil analysis. Part 5 Mineral Methods 5, 387–464.
[84] Kelly, S.D., Kemner, K.M., Brooks, S.C., 2007. X-ray absorption spectroscopy identifies calcium-uranyl-carbonate complexes at environmental concentrations. Geochim Cosmochim Acta 71, 821–834.
[85] Kelly, S.D., Ravel, B., 2007. EXAFS energy shift and structural parameters. AIP Conference Proceedings. American Institute of Physics, pp. 132–134.
[86] Kerisit, S., Liu, C.X., 2010. Molecular simulation of the diffusion of uranyl carbonate species in aqueous solution. Geochim Cosmochim Acta 74, 4937–4952.
[87] Kimura, T., Nagaishi, R., Ozaki, T., Arisaka, M., Yoshida, Z., 2002. Uranium(VI) speciation at elevated temperatures and pressures by time-resolved laser-induced fluorescence spectroscopy. J Nucl Sci Technol 39, 233–239.
[88] Kirishima, A., Kimura, T., Tochiyama, O., Yoshida, Z., 2004.) Speciation study on uranium (VI) hydrolysis at high temperatures and pressures. J Alloy Compd 374, 277–282.
[89] Knope, K.E., Soderholm, L., 2013. Solution and solid-state structural chemistry of actinide hydrates and their hydrolysis and condensation products. Chem Rev 113, 944–994.
[90] Kohn, W., Sham, L.J., 1965. Self-consistent equations including exchange and correlation effects. Phys Rev 140, A1133.
[91] Kubicki, J.D., Halada, G.P., Jha, P., Phillips, B.L., 2009. Quantum mechanical calculation of aqueuous uranium complexes: carbonate, phosphate, organic and biomolecular species. Chem Cent J 3, 1–29.
[92] Kulik, D.A., Wagner, T., Dmytrieva, S.V., Kosakowski, G., Hingerl, F.F., Chudnenko, K.V., Berner, U.R., 2013. GEM-Selektor geochemical modeling package: revised algorithm and GEMS3K numerical kernel for coupled simulation codes. Comput Geosci 17, 1–24.
[93] Le Naour, C., Trubert, D., Di Giandomenico, M.V., Fillaux, C., Den Auwer, C., Moisy, P., Hennig, C., 2005. First structural characterization of a protactinium (V) single oxo bond in aqueous media. Inorg Chem 44, 9542–9546.
[94] Lee, C., Wang, W., Parr, R.G., 1988. Development of the colle-salvetti correlation energy formula into a functional of the electron density. Phys Rev B: Condens Matter Mater Phys 37, 785.
[95] Lee, J.Y., Vespa, M., Gaona, X., Dardenne, K., Rothe, J., Rabung, T., Altmaier, M., Yun, J.I., 2017. Formation, stability and structural characterization of ternary MgUO2 (CO_3)(3)(2-) and Mg2UO2 (CO_3)(3) (aq) complexes. Radiochim Acta 105, 171–185.
[96] Lee, J.Y., Yun, J.I., 2013. Formation of ternary CaUO2(CO_3)(3)(2-) and Ca2UO2 (CO_3)(3)(aq) complexes under neutral to weakly alkaline conditions. Dalton Trans 42, 9862–9869.
[97] Li, B., Zhou, J.W., Priest, C., Jiang, D.E., 2017. Effect of salt on the uranyl binding with carbonate and calcium ions in aqueous. Solut J Phys Chem B 121, 8171–8178.
[98] Lin, I.-C., Seitsonen, A.P., Tavernelli, I., Rothlisberger, U., 2012. Structure and dynamics of liquid water from ab initio molecular dynamics: comparison of BLYP, PBE, and revPBE density functionals with and without van der Waals corrections. J Chem Theory Comput 8, 3902–3910.
[99] Liu, W., Borg, S.J., Testemale, D., Etschmann, B., Hazemann, J.-L., Brugger, J., 2011. Speciation and thermodynamic properties for cobalt chloride complexes in hydrothermal fluids at 35–440C and 600 bar: an in-situ XAS study. Geochim Cosmochim Acta 75, 1227–1248.
[100] Liu, W., Etschmann, B., Mei, Y., Guan, Q., Testemale, D., Brugger, J., 2020. The role of sulfur in molybdenum transport in hydrothermal fluids: Insight from in situ synchrotron XAS experiments and molecular dynamics simulations. Geochim Cosmochim Acta 290, 162–179.
[101] Liu, X., Sprik, M., Cheng, J., 2013. Hydration, acidity and metal complexing of polysulfide species: a first principles molecular dynamics study. Chem Phys Lett 563, 9–14.
[102] Liu, X.D., Cheng, J., He, M.J., Lu, X.C., Wang, R.C., 2016. Acidity constants and redox potentials of uranyl ions in hydrothermal solutions. Phys Chem Chem Phys 18, 26040–26048.
[103] Löfman, J., 2005. Simulation of hydraulic disturbances caused by the decay heat of the repository in Olkiluoto. Posiva 2005–2007.
[104] Lynes, O., Austin, J., Kerridge, A., 2019. Ab initio molecular dynamics studies of hydroxide coordination of alkaline earth metals and uranyl. Phys Chem Chem Phys 21, 13809–13820.
[105] Majumdar, D., Roszak, S., Balasubramanian, K., Nitsche, H., 2003. Theoretical study of aqueous uranyl carbonate (UO2CO3) and its hydrated complexes: UO2CO3 center dot nH(2)O(n=1-3). Chem Phys Lett 372, 232–241.
[106] Marchenko, A., Truflandier, L.A., Autschbach, J., 2017. Uranyl carbonate complexes in aqueous solution and their ligand NMR chemical shifts and O-17 quadrupolar relaxation studied by ab initio molecular dynamics. Inorg Chem 56, 7384–7396.
[107] Martín, L.B., Rutqvist, J., Birkholzer, J.T., 2015. Long-term modeling of the thermal–hydraulic–mechanical response of a generic salt repository for heat-generating nuclear waste. Eng Geol 193, 198–211.
[108] Mayanovic, R.A., Anderson, A.J., Dharmagunawardhane, H.A., Pascarelli, S., Aquilanti, G., 2012. Monitoring synchrotron X-ray-induced radiolysis effects on metal (Fe, W) ions in high-temperature aqueous fluids. J Synchrotron Radiat 19, 797–805.
[109] Mei, Y., Etschmann, B., Liu, W., Sherman, D.M., Testemale, D., Brugger, J., 2016. Speciation and thermodynamic properties of zinc in sulfur-rich hydrothermal fluids: Insights from ab initio molecular dynamics simulations and X-ray absorption spectroscopy. Geochim Cosmochim Acta 179, 32–52.
[110] Metz, V., Geckeis, H., González-Robles, E., Loida, A., Bube, C., Kienzler, B., 2012. Radionuclide behaviour in the near-field of a geological repository for spent nuclear fuel. Radiochim Acta 100, 699–713.
[111] Migdisov, A., Runde, W., Williams-Jones, A., Boukhalfa, H., Roback, R., Timofeev, A., 2018. Response to the comment "Uranyl-chloride speciation and uranium transport in hydrothermal brines: comment on Migdisov et al.(2018)" by Dargent et al. Geochim Cosmochim Acta 235.

[112] Migdisov, A.A., Boukhalfa, H., Timofeev, A., Runde, W., Roback, R., Williams-Jones, A.E., 2018. A spectroscopic study of uranyl speciation in chloride-bearing solutions at temperatures up to 250 ºC. Geochim Cosmochim Acta 222, 130–145.
[113] Migdisov, A.A., Williams-Jones, A., Van Hinsberg, V., Salvi, S., 2011. An experimental study of the solubility of baddeleyite (ZrO2) in fluoride-bearing solutions at elevated temperature. Geochim Cosmochim Acta 75, 7426–7434.
[114] Miron, G.D., Wagner, T., Kulik, D.A., Heinrich, C.A., 2016. Internally consistent thermodynamic data for aqueous species in the system Na–K–Al–Si–O–H–Cl. Geochim Cosmochim Acta 187, 41–78.
[115] Moll, H., Reich, T., Hennig, C., Rossberg, A., Szabó, Z., Grenthe, I., 2000. Solution coordination chemistry of uranium in the binary UO2+-SO2− and the ternary UO2+-SO2−-OH− system. Radiochim Acta 88, 559–566.
[116] Moll, H., Reich, T., Szabo, Z., 2000. The hydrolysis of dioxouranium (VI) investigated using EXAFS and 17O NMR. Radiochim Acta 88, 411-416.
[117] Moll, H., Rossberg, A., Steudtner, R., Drobot, Br, Müller, K., Tsushima, S., 2014. Uranium (VI) chemistry in strong alkaline solution: speciation and oxygen exchange mechanism. Inorg Chem 53, 1585–1593.
[118] Moreno Martinez, D., Guillaumont, D., Guilbaud, P., 2022. Force field parameterization of actinyl molecular cations using the 12-6-4 model. J Chem Inf Model 62, 2432–2445.
[119] Mosselmans, J., Bailey, E., Schofield, P., 2001. A study of uranium speciation in acetate solutions at temperatures from 25 to 250° C. J Synchrotron Radiat 8, 660–662.
[120] Neuefeind, J., Skanthakumar, S., Soderholm, L., 2004. Structure of the UO22+−SO42- ion pair in aqueous solution. Inorg Chem 43, 2422–2426.
[121] Neuefeind, J., Soderholm, L., Skanthakumar, S., 2004. Experimental coordination environment of uranyl (VI) in aqueous solution. J Phys Chem A 108, 2733–2739.
[122] Nguyen-Trung, C., Begun, G.M., Palmer, D.A., 1992. Aqueous uranium complexes. 2. Raman spectroscopic study of the complex formation of the Dioxouranium(VI) ion with a variety of inorganic and organic ligands. Inorg Chem 31, 5280–5287.
[123] Nichols, P., Bylaska, E.J., Schenter, G.K., de Jong, W., 2008. Equatorial and apical solvent shells of the UO 2 2+ ion. J Chem Phys 128, 124507.
[124] Oelkers, E.H., Helgeson, H.C., 1990. Triple-ion anions and polynuclear complexing in supercritical electrolyte solutions. Geochim Cosmochim Acta 54, 727–738.
[125] Oelkers, E.H., Helgeson, H.C., 1991. Calculation of activity coefficients and degrees of formation of neutral ion pairs in supercritical electrolyte solutions. Geochim Cosmochim Acta 55, 1235–1251.
[126] Ondrejcin, R.S., 1966. Thermal Denitration of Uranyl Nitrate Hexahydrate. J Chem Eng Data 11, 130–133.
[127] Plášil, J., Fejfarová, K., Dušek, M., Škoda, R., Rohlíček, J., 2013. Actinides in geology, energy, and the environment: revision of the symmetry and the crystal structure of čejkaite, Na4 $(UO2)(CO_3)$ 3. Am Miner 98, 549–553.
[128] Plyasunov, A.V., Grenthe, I., 1994. The temperature dependence of stability constants for the formation of polynuclear cationic complexes. Geochim Cosmochim Acta 58, 3561–3582.
[129] Quiles, F., Nguyen-Trung, C., Carteret, C., Humbert, B., 2011. Hydrolysis of Uranyl(VI) in acidic and basic aqueous solutions using a noncomplexing organic base: a multivariate spectroscopic and statistical study. Inorg Chem 50, 2811.
[130] Rao, L., Tian, G., Xia, Y., Friese, J.I., Zanonato, P., Di Bernardo, P., 2010. Bridging the gap in the chemical thermodynamic database for nuclear waste repository: studies of the effect of temperature on actinide complexation. Nuclear Energy and the Environment. ACS Publications,, pp. 299–318.
[131] Ravel, B., Newville, M., 2005. ATHENA, ARTEMIS, HEPHAESTUS: data analysis for X-ray absorption spectroscopy using IFEFFIT. J Synchrotron Radiat 12, 537–541.
[132] Runde, W., 2000. The chemical interactions of actinides in the environment. Los Alamos Sci 26, 392–411.
[133] Ryzhenko, B.N., Bryzgalin, O.V., Artamkina, I.Y., Spasennykh, M., Shapkin, A.I., 1985. An electrostatic model for the electrolytic dissociation of inorganic substances dissolved in water. Geochem Int 22, 138–144.
[134] Schlosser, F., Moskaleva, L.V., Kremleva, A., Kruger, S., Rosch, N., 2010. Comparative density functional study of the complexes $UO2(CO_3)(3)$ (4-) and $(UO2)(3)(CO_3)(6)$ (6-) in aqueous solution. Dalton Trans 39, 5705–5712.
[135] Schofield, P., Bailey, E., Mosselmans, J., 1999. Structure and stability of the solvated (UO2) 2+ uranyl ion: an in situ XAS study. Geochemistry of the Earth's Surface. AA Balkema, Rotterdam, the Netherlands, pp. 465–468.
[136] Schreckenbach, G., Hay, P.J., Martin, R.L., 1999. Density functional calculations on actinide compounds: survey of recent progress and application to UO2X4 (2-) (X = F, Cl, OH) and AnF(6) (An = U, Np, Pu). J Comput Chem 20, 70–90.
[137] Sémon, L., Boehme, C., Billard, I., Hennig, C., Lützenkirchen, K., Reich, T., Roßberg, A., Rossini, I., Wipff, G., 2001. Do perchlorate and triflate anions bind to the uranyl cation in acidic aqueous medium? A combined EXAFS and quantum mechanical investigation. ChemPhysChem 2, 591.
[138] Seward, T.M., Williams-Jones, A.E., Migdisov, A.A., 2013. The chemistry of metal transport and deposition by ore-forming hydrothermal fluids. Treatise Geochem 2nd Ed.
[139] Shamov, G.A., Schreckenbach, G., 2008. Theoretical study of the oxygen exchange in uranyl hydroxide. An old riddle solved? J Am Chem Soc 130, 13735–13744.
[140] Sherman, D.M., 2010. Metal complexation and ion association in hydrothermal fluids: insights from quantum chemistry and molecular dynamics. Geofluids.
[141] Shock, E.L., Sassani, D.C., Betz, H., 1997. Uranium in geologic fluids: estimates of standard partial molal properties, oxidation potentials, and hydrolysis constants at high temperatures and pressures. Geochim Cosmochim Acta 61, 4245–4266.
[142] Shock, E.L., Sassani, D.C., Willis, M., Sverjensky, D.A., 1997. Inorganic species in geologic fluids: correlations among standard molal thermodynamic properties of aqueous ions and hydroxide complexes. Geochim Cosmochim Acta 61, 907–950.
[143] Shvarov, Y.V., Bastrakov, E.N., 1999. HCh, A software package for geochemical equilibrium modeling: user's guide. Record 1999/2 5.
[144] Skála, R., Ondruš, P., Veselovský, F., Císařová, I., Hloušek, J., 2011. Agricolaite, a new mineral of uranium from Jáchymov, Czech Republic. Mineral Petrol 103, 169–175.
[145] Skirrow, R.G., Jaireth, S., Huston, D.L., Bastrakov, E., Schofield, A., Van der Wielen, S., Barnicoat, A., 2009. Uranium mineral systems: processes, exploration criteria and a new deposit framework. Geosci Aust Rec 20, 44.
[146] Soderholm, L., Skanthakumar, S., Neuefeind, J., 2005. Determination of actinide speciation in solution using high-energy X-ray scattering. Anal Bioanal Chem 383, 48–55.
[147] Soderholm, L., Skanthakumar, S., Wilson, R.E., 2011. Structural correspondence between uranyl chloride complexes in solution and their stability constants. J Phys Chem A 115, 4959–4967.
[148] Sonnenberg, J.L., Hay, P.J., Martin, R.L., Bursten, B.E., 2005. Theoretical investigations of uranyl-ligand bonding: four- and five-coordinate uranyl cyanide, isocyanide, carbonyl, and hydroxide complexes. Inorg Chem 44, 2255–2262.
[149] Stern, E.A., Newville, M., Ravel, B., Yacoby, Y., Haskel, D., 1995. The UWXAFS analysis package: philosophy and details. Phys B: Condens Matter 208–209, 117–120.
[150] Sverjensky, D.A., Shock, E.L., Helgeson, H.C., 1997. Prediction of the thermodynamic properties of aqueous metal complexes to 1000C and 5 kb. Geochim Cosmochim Acta 61, 1359–1412.
[151] Tagirov, B.R., Zotov, A., Akinfiev, N., 1997. Experimental study of dissociation of HCl from 350 to 500C and from 500 to 2500 bars: thermodynamic properties of HCl (aq). Geochim Cosmochim Acta 61.
[152] Taylor, J., Hurst, H., 1971. The hydrogen-atom locations in the α and β forms of uranyl hydroxide. Acta Crystallogr Sect B: Struct Crystallogr Cryst Chem 27, 2018–2022.
[153] Testemale, D., 2003. Structures locales en solutio aqueuse supercritique. Grenoble 1.
[154] Testemale, D., Brugger, J., Liu, W., Etschmann, B., Hazemann, J.-L., 2009. In-situ X-ray absorption study of iron (II) speciation in brines up to supercritical conditions. Chem Geol 264, 295–310.
[155] Tian, Y., Brugger, J., Liu, W., Borg, S., Etschmann, B., O'Neill, B., Testemale, D., Hazemann, J.-L., Glover, C. and Ngothai, Y. (2010) High-temperature and pressure spectroscopic cell for in-situ XAS study of supercritical fluids at the Australian Synchrotron. Chemeca 2010: Engineering at the Edge; 26–29 September 2010, Hilton Adelaide, South Australia, 3425.
[156] Tian, Y., Etschmann, B., Liu, W., Borg, S., Mei, Y., Testemale, D., O'Neill, B., Rae, N., Sherman, D.M., Ngothai, Y., Johannessen, B., Glover, C., Brugger, J., 2012. Speciation of nickel (II) chloride complexes in hydrothermal fluids: In situ XAS study. Chem Geol 334, 345–363.
[157] Tian, Y., Etschmann, B., Mei, Y., Grundler, P.V., Testemale, D., Hazemann, J.-L., Elliott, P., Ngothai, Y., Brugger, J., 2014. Speciation and thermodynamic properties of manganese (II) chloride complexes in hydrothermal fluids: in situ XAS study. Geochim Cosmochim Acta 129, 77–95.
[158] Tirler, A.O., Hofer, T.S., 2014. Structure and dynamics of the uranyl tricarbonate complex in aqueous solution: Insights from quantum mechanical charge field molecular dynamics. The. J Phys Chem B 118, 12938–12951.
[159] Tsushima, S., Rossberg, A., Ikeda, A., Mueller, K., Scheinost, A.C., 2007. Stoichiometry and structure of uranyl (VI) hydroxo dimer and trimer complexes in aqueous solution. Inorg Chem 46, 10819–10826.
[160] Tsushima, S., Uchida, Y., Reich, T., 2002. A theoretical study on the structures of $UO2(CO_3)(3)(4-)$, $Ca2UO2(CO_3)(3)(0)$, and $Ba2UO2(CO_3)(3)(0)$. Chem Phys Lett 357, 73–77.
[161] Vallet, V., Grenthe, I., 2007. On the structure and relative stability of uranyl(VI) sulfate complexes in solution. Comptes Rendus Chim 10, 905–915.
[162] Vallet, V., Wahlgren, U., Schimmelpfennig, B., Moll, H., Szabo, Z., Grenthe, I., 2001. Solvent effects on uranium (VI) fluoride and hydroxide complexes studied by EXAFS and quantum chemistry. Inorg Chem 40, 3516–3525.
[163] Vochten, R., Vanhaverbeke, L., Vanspringel, K., Blaton, N., Peeters, O., 1995. The structure and physicochemical characteristics of synthetic zippeite. Can Mineral 33, 1091–1101.
[164] Wahlgren, U., Moll, H., Grenthe, I., Schimmelpfennig, B., Maron, L., Vallet, V., Gropen, O., 1999.) Structure of uranium(VI) in strong alkaline solutions. A combined theoretical and experimental investigation. J Phys Chem A 103, 8257–8264.
[165] Yamamura, T., Kitamura, A., Fukui, A., Nishikawa, S., Yamamoto, T., Moriyama, H., 1998. Solubility of U (VI) in highly basic solutions. Radiochim Acta 83, 139–146.
[166] Zabinsky, S., Rehr, J., Ankudinov, A., Albers, R., Eller, M., 1995. Multiple-scattering calculations of X-ray-absorption spectra. Phys Rev B 52, 2995.
[167] Zanonato, P., Bernardo, P.D., Bismondo, A., Liu, G., Chen, X., Rao, L., 2004. Hydrolysis of Uranium(VI) at variable temperatures (10–85 °C). J Am Chem Soc 126, 5515–5522.
[168] Zhou, W., Apted, M.J., Kessler, J.H., 2010. The thermal-hydrological impact on increased spent-fuel storage capacity in Yucca mountain repository. Nucl Technol 170, 336–352.